Uncovering novel ShcA signaling networks and their impacts on breast cancer growth and therapeutic resistance

Kathryn Hunt, Division of Experimental Medicine

McGill University, Montreal

MARCH 2023

A thesis submitted to McGill University in partial fulfillment of the requirements of the degree of Masters of Experimental Medicine.

TABLE OF CONTENTS

ABSTRACT

ENGLISH

Breast cancer is the most prevalent cancer in Canadian women, and although many advances have been made, all subtypes of breast cancer can develop therapeutic resistance. One such method of therapeutic resistance can be due to abnormal, or hyperactive receptor tyrosine kinase (RTK) signaling, as seen in HER2+ and basal breast cancers. ShcA is an adaptor protein which facilitates downstream RTK signaling cascades, including the MAPK and PI3K/AKT pathways. When ShcA Y313 cannot be phosphorylated, the resulting tumours demonstrated delayed tumour onset and delayed tumour outgrowth. To understand the mechanisms by which this occurs, BioID was performed on both wildtype and mutant ShcA cell populations. With numerous potential interactors identified, an shRNA screen was conducted to narrow down the most probable interactors. In this thesis, I identify potential novel interactors, including PPP6C and eIF4G2, which may be interacting with ShcA to facilitate these phenotypes. As recurrent disease becomes an ever-increasing concern, the identification of novel protein interactions may highlight new druggable targets to overcome these challenges and provide further insight into the complexities of intracellular signalling.

FRENCH

Le cancer du sein est le cancer le plus répandu chez les Canadiennes. Bien que nous ayons pu progresser dans le traitement du cancer du sein, tous les sous-types peuvent développer une résistance thérapeutique. L'une des façons dont la résistance thérapeutique peut survenir est la signalisation anormale ou hyperactive du récepteur tyrosine kinase (RTK), comme on le voit dans les cancers du sein HER2+ et basaux. ShcA est une protéine adaptatrice qui facilite la signalisation RTK en aval via les voies MAPK et PI3K/AKT. Lorsque ShcA Y313 ne peut pas être phosphorylé, les tumeurs résultantes ont montré un retard d'apparition et de développement.

Pour comprendre comment cela se produit, BioID a été utilisé pour comparer les interactions protéiques de ShcA et du mutant ShcA Y313F. Avec de nombreux interacteurs potentiels identifiés, un écran fonctionnel a été réalisé à l'aide de shRNA pour affiner les interacteurs les plus probables. Dans cette thèse, j'identifie de nouveaux interacteurs potentiels, PPP6C et eIF4G2, qui peuvent interagir avec ShcA pour faciliter ces phénotypes. Alors que l'incidence du cancer du sein récurrent et résistant monte, l'identification de nouvelles interactions protéiques pourrait révéler de nouvelles voies pour vaincre la résistance, et fournir plus d'informations sur les complexités de la signalisation intracellulaire.

ACKNOWLEDGEMENTS

I am extremely grateful to my supervisor, Dr. Josie Ursini-Siegel for her ongoing and continuous support, excellent mentorship, and patience during my studies. Her deep caring for the success of her students has encouraged me throughout this entire thesis, and for that, I couldn't thank her enough. I would also like to thank Dr. Sonia Del Rincon, Dr. Mike Witcher, and Dr. François Mercier for serving as my committee members and providing helpful feedback and suggestions to help build my project.

I am greatly thankful for the members in the JUS lab who have helped me when I struggled and rejoiced when I was met with success. They made moving to a new city in the middle of a pandemic much less isolating and lonely.

Many thanks to my friends and the members of Biocord who have offered their support, advice, and wisdom throughout this time. I would also like to extend my sincere thanks to my Nana, Leona, who has been in constant support of my pursuit for higher education.

Finally, I would like to express my gratitude to my parents, my sister, and my partner. Without their tremendous understanding and encouragement over the last few years, it would be impossible for me to complete my study.

CONTRIBUTION OF AUTHORS

Chapters 1-6
J.U.S. devised the project, developed the theoretical framework and proof outline. K.H wrote the manuscript.

Chapter 4
K.H wrote the manuscript. J.U.S. devised the project, developed the theoretical framework and proof outline. S.H. from the Department of Biochemistry at McGill designed the shRNA library. N.B. and K.J. from the University of Laval, along with R.A. performed AP-MS and BioID experiments. K.H. worked out the shRNA experiment parameters with assistance from S.T. K.H. performed the shRNA screen, with help from E.M. and C.M. V.S. performed MFP injections. K.H. performed genomic DNA isolation and performed PCR1 using the protocol developed by J.S. and S.H. J.H. from IRIC performed PCR2 for the shRNA screen. S.H. and J.J. analysed shRNA screen results with MAGeCK. K.H. performed individual shRNA infection with protocol developed by S.H. K.H. performed co-immunoprecipitation with help from K.L. and E.M. K.H. performed RTK inhibitor experiments, and imaged results with assistance from P.J. and E.C.C. K.H. performed western blots with assistance from E.C.C. and P.J.

LIST OF TABLES

LIST OF FIGURES

LIST OF ABBREVIATIONS

Abbreviation	Meaning
4PL curve	Four parameter logistic curve
AGO2	Argonaute 2
AKT	Akt serine/threonine kinase
AMPK	AMP-activated protein kinase
ANOVA	Analysis of variance
AO-PI	Acridine Orange-Propidium Iodide
AP-MS	Affinity purification-mass spectrometry
BCA assay	Bicinchoninic acid assay
BSA	Bovine serum albumin
co-IP	Co-immunoprecipitation
CRISPR	Clustered Regularly Interspaced Short Palindromic Repeats
DMEM	Dulbecco's modified Eagle's medium
DMSO	Dimethyl sulfoxide
dNTP	Deoxynucleoside triphosphates
dsRNA	Double-stranded RNA
DTT	Dithiothreitol
EDTA	Ethylenediaminetetraacetic acid
EGF	Epidermal growth factor
EGFR	Epidermal growth factor receptor
EGTA	Egtazic acid
ER	Estrogen receptor
ERK	Extracellular-signal-regulated kinase
FBS	Fetal Bovine Serum
FGFR	Fibroblast growth factor receptors
FVB	Transgenic mouse line FVB/NJ
GDP	Guanosine diphosphate
GTP	Guanosine-5'-triphosphate
HBS	HEPES-Buffered Saline
HR	Hormone receptor
IC30	30% inhibitory concentration
IC50	half maximal inhibitory concentration
IGFR	Insulin-like growth factor receptor
IHC	Immunohistochemistry
MAGeCK	Model-based Analysis of Genome-wide CRISPR/Cas9 Knockout
MAPK	Mitogen-activated protein kinase
MEGS	Mammary epithelial growth supplement
MEK	Mitogen-activated protein kinase kinase

MEK	ERK kinase
MFP	Mammary fat pad
miRNA	microRNA
MLDP	Membrane-linked docking proteins
MMTV/MT	Mouse mammary tumor virus
MOI	Multiplicity of infection
mTOR	Mammalian target of rapamycin
mTORC1	Mammalian target of rapamycin complex 1
mTORC2	Mammalian target of rapamycin complex 2
NMuMG	Nontransformed mouse mammary gland epithelial cell line
NT	Transformed NMuMG cells
NT313F	Transformed NMuMG cells with ShcA Y313F mutation
NTA	Wildtype transformed NMuMG cells
ORF	Open reading frame
PAM	Protospacer adjacent motif
PBS	Phosphate-buffered saline
PCR	Polymerase chain reaction
PDK1	Pyruvate dehydrogenase kinase 1
PFS	Protospacer flanking sequence
PI3K	Phosphoinositide-3-kinase
PIK3CA	p110α protein-coding gene
PIP2	Phosphatidylinositol 4,5-bisphosphate
PIP3	Phosphatidylinositol-3, 4, 5-triphosphate
PLC	Phospholipase C gamma 1
PR	Progesterone receptor
pre-miRNA	Precursor miRNA
pri-miRNA	Primary miRNA
PTB	Phosphotyrosine-binding domain
R^2	Coefficient of determination
RIPA buffer	Radioimmunoprecipitation assay buffer
RISC	RNA-induced silencing complex
RNAi	RNA interference
RTK	Receptor tyrosine kinase
SDS	Sodium dodecyl sulfate
SDS-PAGE	Sodium dodecyl-sulfate polyacrylamide gel electrophoresis
SH2	Src homolog 2
SH3	Src homology 3
shRNA	Short hairpin RNA
siRNA	Small interfering RNA
SOS	Son of sevenless homolog

TBS	Tris Buffered Saline
TBST	Tris Buffered Saline with Tween 20
TGF-β	Transforming growth factor beta
TKI	Tyrosine kinase inhibitor
TβRI	TGF-β receptor 1
TβRII	TGF-β receptor 2
VEGFR	Vascular endothelial growth factor receptors
WT	Wildtype
Y313	Tyrosine 313 on ShcA
Y313F	ShcA Y313F mutant

1. INTRODUCTION

Breast cancer is one of the four most diagnosed cancers in Canada and the most prevalent cancer in Canadian women (Bryan et al., 2018). Approximately 70-80% of cases are invasive ductal carcinoma, where tumours arise in the milk ducts, while around 10% originate in the breast lobule, known as invasive lobular carcinoma (Tsang & Tse, 2020). There are different ways to categorize and describe breast cancer, but the mode predominant methods of classification include molecular subtyping and histological staining. Molecular subtyping evaluates the gene expression profiles of tumours, and can test for mutation in genes such as TP53 and PIK3CA (Pernas & Tolaney, 2020) and define five subtypes: luminal A, luminal B, HER2+, basal and normal-like breast cancers. However, the most common method for classifying breast cancers is through histological staining due to accessibility in the clinic and close approximation to intrinsic subtyping (Goldhirsch et al., 2011). This method uses immunohistochemical staining to observe the presence or absence of estrogen receptor (ER), progesterone receptor (PR), HER2 receptor, and the proliferative marker Ki-67 to separate tumours into either ER+ and/or PR+/HER2-, ER- and/or PR-/HER2+ and triple negative (ER-/PR-/HER2-) subtypes (Goldhirsch et al., 2011).

The primary treatment for breast cancer is surgery to remove as much cancerous tissue, and any surrounding lymph nodes which may be affected. Afterwards, breast cancer subtyping helps oncologists determine the treatment plan, as treatments vary between the subtypes. ER+ breast cancers are treated with hormone therapy, such as aromatase inhibitors and estrogen receptor inhibitors, with no preferred chemotherapeutics as these tumours tend to respond poorly to chemotherapy (Barzaman et al., 2020; Goldhirsch et al., 2011). ER+/ HER2- cancers are treated with hormone therapy and cytotoxic chemotherapeutics such as topoisomerase II inhibitors and

mitotic inhibitors, while ER+/HER2+ cancers are given additional anti-HER2 receptor drugs (Goldhirsch et al., 2011). HER2+ cancers are treated with anti-HER2 receptor drugs, such as lapatinib and trastuzumab, in combination with chemotherapy (Barzaman et al., 2020; Goldhirsch et al., 2011). Triple negative cancers are treated with chemotherapeutics, in combination with alkylating agents such as cyclophosphamides, which inhibit protein synthesis through DNA crosslinking (Goldhirsch et al., 2011; Morales-Ramírez, Vallarino-Kelly, & Cruz-Vallejo, 2014).

Although many advances have been made in the fields of diagnostics and therapeutics, all subtypes of breast cancer have demonstrated drug resistance (Chun, Park, & Fan, 2017). There have been many proposed mechanisms to explain the development of therapeutic resistance in breast cancer, however, no exact mechanism has been identified. Central themes include abnormal activation of receptor tyrosine kinases (RTKs) resulting in increased proliferative signaling and metabolic flexibility to overcome therapeutic stress (Im et al., 2018; Miricescu et al., 2020; Tomas, Futter, & Eden, 2014; Xuhong, Qi, Zhang, & Jiang, 2019).

1.1. Receptor tyrosine kinase signaling

Currently, 58 different receptor tyrosine kinases have been identified and grouped into 20 different subfamilies based on their structure, interactions, and other class-specific traits (Butti et al., 2018). Some of the RTK subfamilies include epidermal growth factor receptors (EGFRs), vascular endothelial growth factor receptors (VEGFRs), fibroblast growth factor receptors (FGFRs), insulin-like growth factor receptor (IGFR) and many more (Regad, 2015). HER2 is part of a larger subfamily called the EGFR/HER family, consisting of EGFR/HER1/ERBB1,

HER2/ERBB2/Neu, HER3/ERBB3, and HER4/ERBB4 (Zhang, 2021). Of the four EGFR family receptors, only HER2 has no known ligand (Weinberg, Peckys, & de Jonge, 2020). Additionally, studies have shown that HER2 preferentially heterodimerizes with either HER3 or EGFR, both of which have documented ligands (Weinberg et al., 2020; Zhang, 2021). Overexpression of EGFR is seen in 15-30% of breast tumours, while overexpression of HER2 is seen in 15-20% of breast cancers (Hsu & Hung, 2016; Wolff et al., 2013). Overexpression of either EGFR or HER2 is correlated with worse clinical outcome (Hsu & Hung, 2016).

Activation of the receptor begins with receptor-ligand binding, which results in conformational change to the RTK, allowing dimerization to occur (Wang, 2017). Once dimerized, tyrosine residues on the cytoplasmic portion of the receptor are autophosphorylated, allowing proteins with Src homolog 2 (SH2) or phosphotyrosine-binding (PTB) domains to bind and facilitate downstream signaling, shown in the figure below (Fig.1) (Ullah, Yin, Snell, & Wan, 2022). Two such proteins, Grb2 and Gab1, facilitate downstream signaling of two important pathways: ERK/MAPK and PI3K/AKT. Grb2 can interact with son of sevenless homolog (SOS) which then catalyzes the exchange of GDP for GTP on RAS, which then activates Raf to continue the ERK/MAPK signaling cascade (Tomas et al., 2014; Ullah et al., 2022). Alternatively, Grb2 can interact with Gab1, which recruits PI3K upon phosphorylation (Belov & Mohammadi, 2012; Gotoh, 2008). The adaptor protein ShcA can help facilitate Grb2 and Gab1 interaction with phosphorylated tyrosine kinases, aiding RTK signal transduction (Ravichandran, 2001).

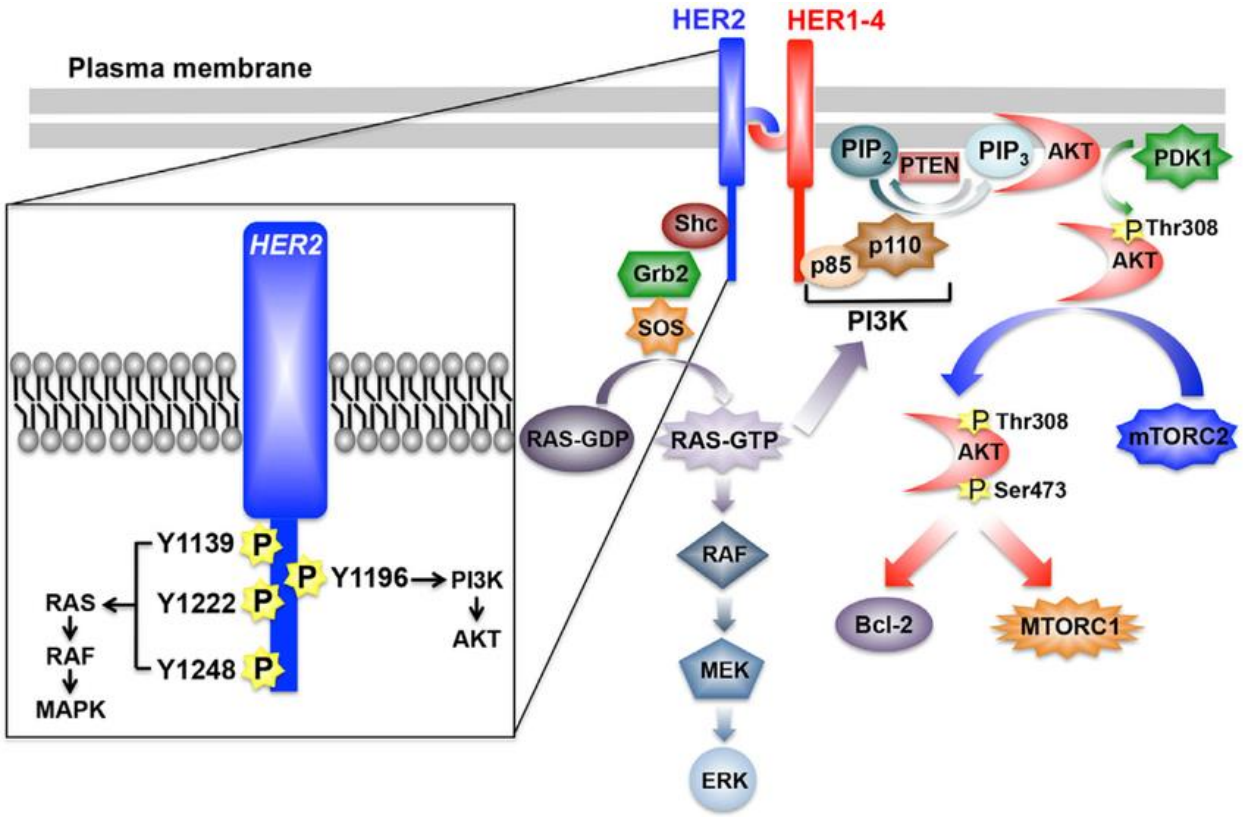

Figure 1. An overview of the HER2 signaling cascade.
Sourced from (Schiemann, Gollamudi, Parvani, & Vinayak, 2016). License CC BY-NC 4.0. No alterations were made to the original image.

Grb2 binds to activated RTKs via its Src homolog 2 (SH2) domain, resulting in the phosphorylation of Grb2, which then recruits son of sevenless homolog (SOS) (Batzer, Rotin, Ureña, Skolnik, & Schlessinger, 1994; Chardin et al., 1993). This mediates the exchange of guanine diphosphate (GDP) to guanine triphosphate (GTP) on Ras, which binds the serine/threonine kinase Raf, relieving its auto-inhibition and allowing dimerization of Raf family members. This, in turn, perpetuates the ERK/MAPK signaling cascade (Belov & Mohammadi, 2012; Tomas et al., 2014; Ullah et al., 2022) by phosphorylating MEK1 at S218 and S222, allowing it to subsequently phosphorylate ERK1 at Thr202/204 (Ullah et al., 2022). Phosphorylated ERK is then able to enter the nucleus and facilitate expression of various transcription factors including ETS1/2, ELK-1, and JUN, or it can or it can phosphorylate cytoplasmic substrates including SOS, MEK, MNK1, and eIF4E (Rocca, Braga, Volpe,

Maiocchi, & Generali, 2022; Ullah et al., 2022). Activation of this signaling cascade results in cell proliferation, migration, differentiation, and drug resistance (Rocca et al., 2022; Xuhong et al., 2019).

Gab1 can interact with activated RTKs directly, through its PTB domain, or indirectly with Grb2 or ShcA/Grb2 (Belov & Mohammadi, 2012; Ravichandran, 2001). Phosphorylation of Gab1 recruits phosphoinositide-3-kinase (PI3K) which then catalyzes the phosphorylation of phosphatidylinositol 4,5-bisphosphate (PIP2) to phosphatidylinositol-3, 4, 5-triphosphate (PIP3) (Miricescu et al., 2020). This phosphorylation event results in the translocation of AKT and pyruvate dehydrogenase kinase 1 (PDK1) to the cell membrane. After AKT and PDK1 localize to the membrane, PDK1 phosphorylates AKT at Thr308, while mTORC2 phosphorylates AKT at Ser473 (Miricescu et al., 2020). This active form of AKT is then able to translocate from the membrane and phosphorylate various targets including TSC1/2, FOXO, and BAD (Wang, 2017). This results in inhibition of apoptosis, increased cell growth, and increased cell proliferation (Mattoon, Lamothe, Lax, & Schlessinger, 2004; Wang, 2017).

One adaptor protein which facilitates RTK signal transduction through binding Gab1 and Grb2 to phosphorylated RTKs is ShcA. ShcA has three isoforms: p66, p52, and p46. The p66 isoform can relocate to the mitochondria upon phosphorylation of serine 36, whereas the p52 and p46 isoforms stay within the cytosol (Ursini-Siegel et al., 2008). In the presence of an activated RTK, the PTB domain of p46/52 ShcA translocate to the plasma membrane and bind to the RTK (Ursini-Siegel et al., 2008). This allows for the phosphorylation of residues Y239, Y240, and Y317 (Y313 in mice) on ShcA, creating a docking site for Gab1 or Grb2 (Tomas et al., 2014). ShcA has been shown to be elevated in HER2+ and basal breast cancers, which correlates with

worse clinical outcome (Cheang et al., 2008; Davol, Bagdasaryan, Elfenbein, Maizel, & Frackelton, 2003). It is possible that elevation of PI3K/AKT and ERK/MAPK signaling is due to ShcA facilitating the recruitment of Gab1 and Grb2 to active RTKs.

1.2. Research objectives

Up until now, many studies have focused on the pro-tumorigenic properties of ShcA upon tyrosine phosphorylation. Previous studies have demonstrated that RTKs require an intact Y313 phosphorylation site to potentiate breast tumor growth (Ursini-Siegel et al., 2008). Loss of Y313 phosphorylation, through Y313F mutation, dramatically impairs mammary tumorigenesis in pre-clinical breast cancer mouse models (Ursini-Siegel et al., 2008). To explore the possibilities behind these phenotypes, two methods of examining protein interactions were conducted: affinity purification-mass spectrometry (AP-MS) and BioID. Both techniques were able to identify expected interactors with ShcA, however, they also showed that ShcA Y313F uniquely binds to several proteins which cannot bind ShcA with an intact Y313 phosphorylation site. This suggests that non-phosphorylated Y313 may be interacting with proteins which may mediate crucial pathways associated with tumorigenesis and drug interactions.

The purpose of this project is to identify possible proteins or pathways that non-phosphorylated ShcA interacts with. As a result of these findings from BioID, we created a shRNA library that includes the unique pY313 interactors identified, in addition to other potential ShcA interactors, to stably reduce the expression levels of each protein. I examined how the absence of 313 phosphorylation impacts tumour growth, biguanide sensitivity, and response to the tyrosine kinase inhibitor lapatinib. Additionally, I investigated if loss of Y313 phosphorylation alters cell response solely to tyrosine kinase inhibitors or if this trend is also

observed downstream of the RTK pathway. Due to previous research showing that abnormal RTK signaling is a potential mechanism of therapeutic resistance in breast cancer, I wished to examine if ShcA Y313F mutants would respond the same to the tyrosine kinase inhibitor lapatinib. Since ShcA Y313F mutants demonstrate altered interaction with downstream RTK signal proteins, it was proposed that these mutants would respond differently compared to their wildtype counterparts. Additionally, I wished to examine if ShcA Y313F mutants would respond differently to other downstream RTK inhibitors including MEK, AKT, and mTOR.

In this thesis, readers will learn more about the current gaps in knowledge allowing me to explore this topic. I will highlight key literature which helped frame the theoretical background and how I was able to identify potential novel interactors of ShcA. I have identified potential novel interactors, including PPP6C and eIF4G2, which may be interacting with ShcA to facilitate the aforementioned phenotypes. I also demonstrate the different responses in WT ShcA and ShcA Y313F mutants to RTK inhibitors downstream of HER2. This research may identify novel targetable vulnerabilities to eradicate therapy-resistant breast cancers and expand our knowledge of how tyrosine kinase signaling is dynamically regulated in these tumors.

2. REVIEW OF LITERATURE

Previously, I discussed etiology of breast cancer and receptor tyrosine kinase signaling. In this chapter, I will explore the classification of breast cancer subtypes, therapies, and therapeutic resistance. Additionally, I will discuss adaptor proteins and their expansive roles in cell signaling. I will also explain current methods used to identify protein interaction networks. Lastly, I will explain the purpose of functional screens to reveal interactors which are invoking the most impact, and subsequently highlighting proteins with the most potential to serve as therapeutic targets. Using this information, I will reveal the current gaps in knowledge and how my project aims to fill those gaps to give us a better understanding of the complex signaling networks mediated by ShcA.

2.1. CLASSIFICATION OF BREAST CANCER

There are many ways to categorize and describe breast cancer, but the most predominant methods used include molecular subtyping and histological staining. Molecular breast cancer subtypes include Luminal A, Luminal B, HER2+, and basal breast cancers. Most luminal A tumours show high expression of ERα, GATA binding protein 3, and often have low mutational burden (Sørlie et al., 2001; Tsang & Tse, 2020). Luminal B cancers often display high expression of ER and PR, high expression of the proliferative marker Ki-67, and either low expression of HER2 (Luminal B HER2-) or overexpression of HER2 (Luminal B HER2+) (Gomes do Nascimento, 2020). Molecular subtyping identifies HER2+ as tumours which have high expression of ERBB2-amplicon genes, FGF4 genes, EGFR genes, and have increased ERBB2 mRNA (Pernas & Tolaney, 2020). ERBB2+ tumours are also more likely to have mutations in TP53 (Sørlie et al., 2001). Lastly, basal tumours are often triple negative and have

high expression of keratin 5, keratin 17, and fatty acid binding protein 7 while also having the highest incidence of TP53 mutation (Sørlie et al., 2001).

However, the most common method for classifying breast cancers is through histological staining, as it is often more accessible than gene expression profiling (Goldhirsch et al., 2011). These subtypes are divided into ER/PR+/HER2-, ER/PR+/HER2+, ER/PR-/HER2+, and ER/PR-/HER2-. This uses immunohistochemical staining to observe the presence or absence of estrogen receptor (ER), progesterone receptor (PR), HER2 receptor, and Ki-67 (Goldhirsch et al., 2011). ER/PR+/HER2- breast cancers are hormone receptor positive, HER2 receptor negative, and have low levels of Ki-67 (Goldhirsch et al., 2011; Tsang & Tse, 2020). Alternatively, ER/PR+/HER2+ cancers stain positive for both hormone and HER2 receptors, while Ki-67 can vary (Goldhirsch et al., 2011). ER/PR-/HER2+ tumours display minimal staining for hormone receptors and show strong staining for HER2 along the cell membrane or have a HER2:CEP17 ratio ≥2 (Tsang & Tse, 2020). Lastly, ER/PR-/HER2- breast cancers stain negative for both hormone receptors and HER2 receptor (Tsang & Tse, 2020).

Approximately 15-20% of breast cancers stain positive for HER2 receptor (Wolff et al., 2013). HER2+ cancers have mutational profiles reflective of HER2 gene amplification, whereas Luminal B HER2+ cancers have a mutational profile more similar to luminal breast cancers (Pernas & Tolaney, 2020; Tsang & Tse, 2020). HER2 is a receptor tyrosine kinase (RTK) which, when active, facilitates cell proliferation and survival (Miricescu et al., 2020; Wang, 2017). HER2+ tumours also have increased levels of other RTKs including EGFR and FGFR4, as well as the highest amount of EGFR/HER2 activation (Pernas & Tolaney, 2020). Increased levels of

HER2 are correlated with worse clinical outcome due to the overactivation of the MAPK and PI3K/AKT signaling pathways. Overactivation of these pathways increases proliferation rates, increases invasion of local tissues, and increases the risk of developing metastasis (Barzaman et al., 2020; Marti, Hyder, Nasrazadani, & Brufsky, 2020).

2.2. HER2-LUMINAL AND HER2-ENRICHED BREAST CANCER THERAPIES

The first step for breast cancer treatment is tumour resection, followed by drug therapy, which is dependent on the tumour subtype. Since the majority of breast cancers are hormone receptor positive, the most common targeted therapy includes tamoxifen, to block estrogen receptor activity in breast tissue, as well as letrozole or anastrozole, which prevent the conversion of testosterone into estradiol through inhibition of aromatase (Barzaman et al., 2020). For HER2+ breast cancers, there are numerous HER2 receptor inhibitors such as trastuzumab, lapatinib, pertuzumab, neratinib, and trastuzumab-emtansine (Barzaman et al., 2020). These drugs vary in their methods of inhibiting HER2, preventing dimerization by binding to the dimerization domain, inhibiting tyrosine kinase activity, or delivery of a cytotoxic drug through receptor-mediated endocytosis (Fig. 2) (Barok, Joensuu, & Isola, 2014; Gajria & Chandarlapaty, 2011; Marti et al., 2020).

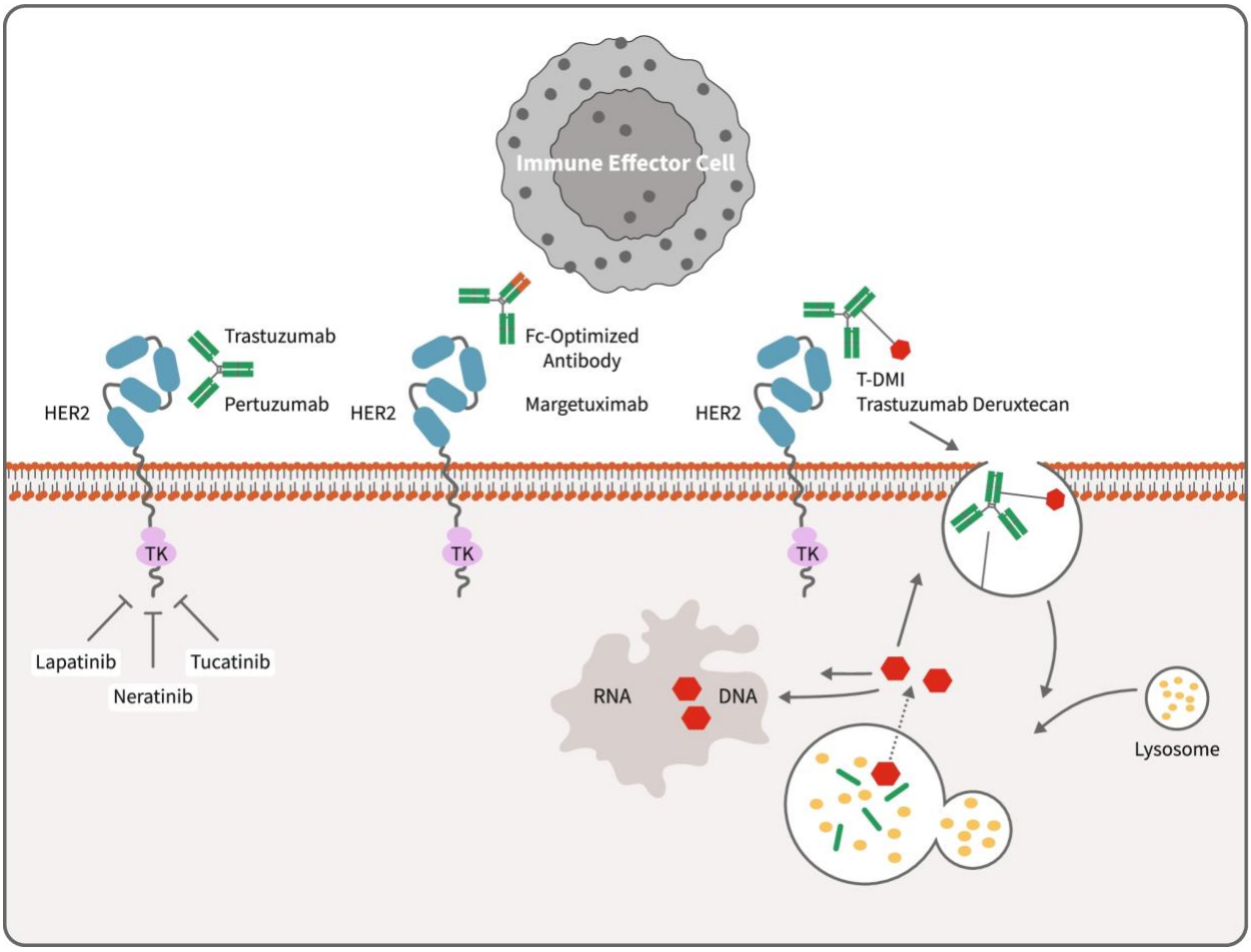

Figure 2. Anti-cancer mechanisms of action targeting HER2 receptor.
Sourced from (Wynn & Tang, 2022). License CC BY 4.0. No alterations were made to the original image.

In comparison, triple negative cancers are treated with chemotherapeutics, such as topoisomerase II inhibitors and mitotic inhibitors, in combination with alkylating agents such as cyclophosphamides, which inhibit protein synthesis through DNA crosslinking (Goldhirsch et al., 2011; Morales-Ramírez et al., 2014). Although there are many targeted therapies available for luminal and HER2+ breast cancers, tumours can become resistant to these therapies (Marti et al., 2020; Miricescu et al., 2020). Additionally, while they are rather effective to treat primary tumours, metastatic cancers seem to be largely unaffected (Marti et al., 2020). Clinical trials are being conducted to evaluate tolerability of various combination therapies, including combination therapy with MEK and AKT inhibitors for metastatic triple-negative breast cancer, combination AKT and RTK inhibitors in patients with advanced breast cancer, and combination AKT

inhibitor and paclitaxel chemotherapy in patients with advanced breast cancer (Institute, 2010, 2011b; Institute & GlaxoSmithKline, 2013). Since breast cancer is known to metastasize early in tumour development, it has become increasingly urgent to develop treatments which can overcome resistance and treat metastatic tumours (Mittal, Brown, & Holen, 2018).

2.3. Therapeutic resistance in HER2-luminal and HER2-enriched breast cancers

While luminal cancers can be treated with aromatase inhibitors and estrogen receptor inhibitors, these tumours can develop resistance over time. One of the methods by which these cancers develop resistance is through the overexpression of other RTKs including EGFR, HER2, IGFR, and FGFR (Rocca et al., 2022). As a result of the overexpression of other RTKs, hyperactive MEK/ERK and PI3K/AKT can increase phosphorylation of estrogen receptor, leading to ligand-independent activation and signaling (Rocca et al., 2022). For example, in the ER+/PR- tamoxifen-resistant breast cancer line MCF7/TAMR1, it has been shown to have increased levels of HER2 and increased activation of the AKT/mTOR pathway (Gandhi & Das, 2019). Other hormone-positive cancers can develop resistance to anti-cancer drugs including aromatase inhibitors through de novo mutations in estrogen receptor, PI3K, and PTEN (Miricescu et al., 2020). For example, mutations in ERα D538G causes a conformational change which mimics receptor activation, allowing for ligand-independent signaling (Merenbakh-Lamin et al., 2013).

Therapeutic resistance has also been documented in HER2+ breast cancers. Studies have demonstrated resistance to lapatinib, as well as other tyrosine kinase inhibitors in these tumours (Escrivá-de-Romaní, Arumí, Bellet, & Saura, 2018; X. Li, Zhang, Hu, & Luo, 2020; L. Liu et al., 2009; Xuhong et al., 2019). Resistance to lapatinib has been shown to be mediated by RTK-

associated pathways, such as PI3K/AKT/mTOR, ERK/MAPK, and other RTK subfamilies (Xuhong et al., 2019). Additional interaction of Gab1 with Grb2 further potentiates PI3K activation, resulting in a positive-feedback loop which targets Gab1 to the plasma membrane to further potentiate cell proliferation and cell survival (Tomas et al., 2014). Alternatively, loss of PTEN, the negative regulator of the PI3K/AKT pathway, has also been shown to affect hormone negative breast cancers (Miricescu et al., 2020). The loss of pathway regulation results in overactive signaling through AKT/mTOR, ultimately leading to tyrosine kinase inhibitor (TKI) resistance.

Another method by which HER2+ breast cancers confer drug resistance is through metabolic reprogramming (Xuhong et al., 2019). Previously, my colleagues have shown that the adaptor protein ShcA promotes metabolic flexibility in breast cancer cells, and that tyrosine phosphorylation allows for the flexibility between using glycolysis and oxidative phosphorylation for energy (Im et al., 2018). Specifically, Y313 is crucial for mediating this metabolic flexibility, and loss of Y313 phosphorylation forces the tumour to rely on mitochondrial metabolism, which can be exploited with the mitochondrial complex I inhibitor phenformin (Totten et al., 2021).

2.4. Adaptor proteins

Adaptor proteins are a class of proteins which facilitate downstream signaling pathways. These proteins have a vast interaction network and can contribute to many signaling networks within the cell. Adaptor proteins can interact with many proteins, depending on the domains they contain. They can have a combination of phosphotyrosine binding domains (PTB), Src homology 2 domains (SH2), Src homology 3 domains (SH3), or pleckstrin homology (PH) domains. PTB

domains bind to phosphotyrosine (pY) residues on proteins which have a NPXpY/NXXpY sequence motif (Sain, Tiwari, & Mohanty, 2016). The SH2 domain also has a phosphotyrosine binding site as well as a specificity pocket at the +3 position from the pY site (Jaber Chehayeb & Boggon, 2020). SH3 domains contain a WPY triad to bind to proteins with proline-rich regions (Alfaidi, Scott, & Orr, 2021). While PH domains can bind to phospholipids such as PIP2 and PIP3 (Diggins & Webb, 2017).

One example of a docking adaptor protein is ShcA. ShcA has three isoforms: p66, p52, and p46 (Fig. 3) (Mir, Ali, Mushtaq, & Khanday, 2020). The p66 isoform can relocate to the mitochondria upon phosphorylation of serine 36, whereas the p52 and p46 isoforms stay within the cytosol (Ursini-Siegel et al., 2008). ShcA has been shown to be elevated in HER2+ and basal breast cancers, which correlates with worse clinical outcome (Cheang et al., 2008; Davol et al., 2003). In a small cohort of various cancerous and non-cancerous tissue samples, expression of p52 ShcA was more than doubled in 5 of the 9 breast cancer samples (Wright et al., 2019). Meanwhile, pre-clinical models have shown that ErbB2-mediated transformation is significantly impaired if Grb2- or ShcA-binding sites on ErbB2 are mutated (Dankort, Jeyabalan, Jones, Dumont, & Muller, 2001). Additionally, selective deletion of ShcA in the mammary epithelium inhibits tumour formation in a pre-clinical model of ErbB2+ breast cancer (Ursini-Siegel et al., 2008).

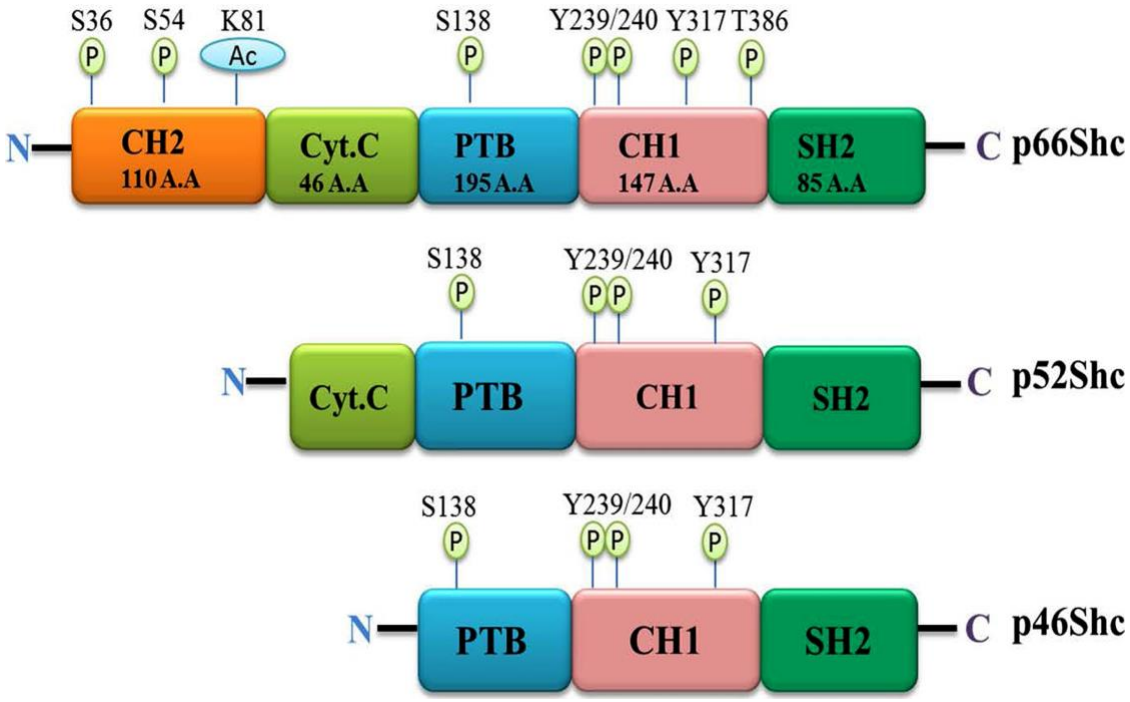

Figure 3. Isoforms of ShcA and its domains.
p52Shc and p46Shc remain in the cytosol while phosphorylation of Ser36 of p66Shc relocates it to the mitochondria. Reprinted from Ageing Research Reviews, 63, Hilal Ahmad Mir, Roshia Ali, Umar Mushtaq, and Firdous A. Khanday, Structure-functional implications of longevity protein p66Shc in health and disease. Copyright (2020), with permission from Elsevier.

ShcA contains a PTB domain, an SH2 domain, and a CH1 domain (Fig. 3). The PTB domain of p52ShcA is from residues 46-207 while the SH2 domain is located at the C-terminus (Fig. 3) (Ravichandran, 2001). The SH2 domain on ShcA has a specificity pocket for leucine or isoleucine at the +3 position from the phosphotyrosine (Ravichandran, 2001). The CH1 domain of ShcA falls between the PTB and SH2 domains and contains three important phosphotyrosine residues: Y239/240 and Y317 (313 in mice) (Ravichandran, 2001). In the presence of an activated RTK, the PTB domain of p52 ShcA binds to the RTK (Ursini-Siegel et al., 2008). This allows for the phosphorylation of residues Y239, Y240, and Y317 (Y313 in mice) on ShcA, creating a docking site for Gab1 or Grb2 (Tomas et al., 2014). Conditional knockout of p52 ShcA results in delayed tumour onset, and additional studies have shown that phosphorylation of tyrosines 239/240 and 313 facilitate tumour growth (Ursini-Siegel et al., 2008; Wright et al., 2019). Furthermore, p52 ShcA has been shown to facilitate the invasion of breast cancer through

the mediation of both ERBB2 and TGF-β pathways in a phosphorylation-dependent manner (Northey et al., 2008).

ShcA can interact with many proteins, including Gab1 and Grb2, however there are still many more proteins ShcA interacts with which are not well understood. For example, knockout of ShcA in murine embryonic fibroblasts results in defective cell spreading, and mutation in Y239/240/317 has dominant negative effects on cells (Ravichandran, 2001). Additionally, hyperactivation of ShcA can lead to the development of tyrosine kinase inhibitor resistance in pre-clinical models of ErbB2 breast cancer (Ha et al., 2018).

The ShcA adaptor protein interacts with a large number of proteins across many different pathways. Since adaptor proteins do not contain enzymatic domains, it is rather difficult to target these molecules with therapeutic drugs (Luo & Hahn, 2015). Additionally, targeting an adaptor protein with a large network of interactors may lead to unwanted side effects which could be avoided if the treatment targeted a downstream signaling protein. To get a better understanding of the role p52ShcA plays in tumorigenesis, tumour invasion, and overall prognosis, we turn to protein-protein interaction networks. These interaction networks can then be used to identify potential therapeutic targets. There are many methods used to identify protein-protein interaction networks including affinity purification mass spectrometry (AP-MS) and BioID.

2.5. Identifying protein-protein interaction networks

AP-MS is a high throughput method to identify protein interactions. In this assay, the protein of interest is purified from cell lysate, resulting in the pull down of both the bait and

interactors (Gingras, Gstaiger, Raught, & Aebersold, 2007). After purification, protein interaction complexes undergo proteolytic digestion, and samples are run through mass spectrometry (Gingras et al., 2007). This allows for the identification of proteins bound to ShcA.

Since ShcA is an adaptor protein with multiple phosphorylation sites, it can be regulated by phosphatases. It is possible that phosphatases could dephosphorylate ShcA during the experiment, which could weaken interactions of ShcA with other proteins if they are dependent on ShcA phosphorylation. To overcome this, samples are treated with pervanadate, a tyrosine phosphatase inhibitor, or a vehicle control 20 minutes prior to purification.

While AP-MS can identify many protein interactions, there are some shortcomings. As previously mentioned, AP-MS is performed on whole cell lysates. This can pose an issue if interactions are found between proteins located in separate cellular compartments (Roux, Kim, Burke, & May, 2018). Additionally, there is a chance that some interactions are missed. If the protein interactions are quite weak, or are sensitive to the lysis buffers used in pulldown, they may be lost (X. Liu, Salokas, Weldatsadik, Gawriyski, & Varjosalo, 2020). AP-MS is generally performed in a short period of time, for example, pulldown of Flag-tagged ShcA was completed after 20 minutes of treatment with pervanadate or a vehicle control. There is a possibility that there are low frequency or rare protein interactions which would not be captured in that time frame (X. Liu et al., 2020).

In the past decade, BioID emerged as an additional method to identify protein-protein interactions within living cells (Roux et al., 2018). This is unique because other methods are

performed following whole cell lysis. This technique requires the fusion of a mutant biotin ligase (BirA) to the protein of interest (bait), allowing for the biotinylation of proteins within 10-15nm to the bait (Roux et al., 2018). Since biotinylation is a rare post-translational modification, it is quite easy to identify tagged proteins with mass spectrometry (Roux et al., 2018).

BioID captures protein interactions over a 12 to 24-hour period while the cells are alive (Roux et al., 2018). This allows for the identification of rare or infrequent interactions as they occur within the cell. Other advantages include identification of weak protein interactions, identification of transient or short-term protein interactions, and identification of low frequency protein interactions (X. Liu et al., 2020). This can include enzyme-substrate interactions, kinase and protease interactions, and interactions which may have been impacted by lysis buffers used in AP-MS (X. Liu et al., 2020). However, BioID identifies proteins in proximity to the bait, meaning that proteins tagged may not directly interact with the protein of interest (Roux et al., 2018). To elucidate true protein interactors and discern which targets have the greatest potential for therapeutic targeting, functional screens are conducted.

2.6. Functional screens

Functional, or phenotypic, screens are those which examine the effects of gene knockout, gene knockdown, gene overexpression, or drug treatment on various cell lines (Moffat, Rudolph, & Bailey, 2014; Molendijk et al., 2022). These screens examine the phenotypic differences in response to various conditions, which includes alterations to cell viability, cell proliferation, and cell cycle arrest. There are many methods used for functional screens including RNA

interference, CRISPR-Cas9 gene silencing, and phenotypic drug screening (Grissenberger et al., 2022; Molendijk et al., 2022).

RNA interference, commonly referred to as RNAi, is a method to repress gene expression through mRNA translation inhibition or mRNA degradation (Sheng, Flood, & Xie, 2020). This results in reduced expression of target genes without altering DNA. There are different mechanisms to repress target gene activity: microRNA (miRNA) and small interfering RNA (siRNA). miRNA genes are transcribed and undergo post-transcriptional modification in the nucleus, forming a double-stranded primary miRNA (pri-miRNA) with a 5' cap, 3' polyadenylated tail, and a stem-loop (Lam, Chow, Zhang, & Leung, 2015). The pri-miRNA is cleaved by Drosha, resulting in precursor miRNA (pre-miRNA), which is then exported from the nucleus into the cytoplasm (Lam et al., 2015). Dicer then cleaves the pre-miRNA, allowing miRNA to interact with the RNA-induced silencing complex (RISC), release the sense strand, and guide RISC to target mRNAs (Lam et al., 2015).

Alternatively, siRNAs are derived from double-stranded RNAs (dsRNAs) or short hairpin RNAs (shRNAs) using endogenous cell machinery (Lam et al., 2015). dsRNA is either transcribed in the cell or introduced to the cell through viral infection, while shRNA is solely introduced to the cell through viral infection (Lam et al., 2015). Once in the cytoplasm, the dsRNA or shRNA is then cleaved by Dicer to form siRNA (Lam et al., 2015). The siRNA can then interact with RISC, allowing a portion of the complex called argonaute 2 (AGO2) to cleave the sense strand of the siRNA, leaving a single-stranded siRNA to guide RISC (Lam et al., 2015).

miRNA and siRNA vary greatly in the number of mRNA they can regulate. miRNA does not require a perfect match target mRNA for inactivation (Lam et al., 2015). As a result, one miRNA can target multiple mRNAs. Alternatively, siRNA exclusively binds to mRNA that fully complement the antisense strand, allowing for highly specific targeting (Lam et al., 2015). While miRNA is advantageous in some circumstances, due to the nature of the screen, it was best to use siRNA-mediated repression to reduce the likelihood of off-target mRNA repression (Lam et al., 2015).

RNAi is a common method to regulate gene expression, recently emerging CRISPR-Cas technology has begun to dominate the field. CRISPR-Cas was discovered as a protective response against bacteriophage infection in bacteria and archaea (Ishino, Krupovic, & Forterre, 2018). The CRISPR RNA identifies targets through homologous sequence targeting, and trans-activating CRISPR RNA recruits Cas9 to the target site, cleaving the target DNA (Ishino et al., 2018). Researchers have been able to exploit the CRISR-Cas9 system by creating guide RNA to influence CRISPR targets (Pickar-Oliver & Gersbach, 2019). However, for cleavage to occur, the target sequence must be positioned near a protospacer adjacent motif (PAM) sequence (Pickar-Oliver & Gersbach, 2019). The guide RNAs must include PAM sequences for proper site-specific cleavage (Pickar-Oliver & Gersbach, 2019). CRISPR-Cas9 has many applications including gene deletion, gene insertion, single-base editing, translocations, and high-throughput loss-of-function screens (Pickar-Oliver & Gersbach, 2019).

There is a new group of Cas proteins called Cas13a which targets RNA and mediates RNA degradation (Granados-Riveron & Aquino-Jarquin, 2018; Pickar-Oliver & Gersbach, 2019). Like Cas9, many Cas13a endonucleases require a nearby spacer sequence, called a protospacer flanking sequence (PFS) in order to function (Pickar-Oliver & Gersbach, 2019). Cas13a then cleaves at any uracil bases nearby, which can also include non-targeted RNAs, dubbed "collateral" cleavage (Pickar-Oliver & Gersbach, 2019). Cas13a has been used to target specific mRNAs in both bacteria and eukaryotes, and although off-target cleavage was not seen in eukaryotic cells, it's unknown how eukaryotic cells do not have off-target collateral cleavage (Pickar-Oliver & Gersbach, 2019). While Cas13 is capable of RNAi, and has many advantages, the majority of researched using CRISPR technology has been performed with the CRISPR-Cas9 system, leaving many gaps in knowledge (Granados-Riveron & Aquino-Jarquin, 2018).

2.7. Using functional screening to identify p52ShcA interactors

HER2-enriched and HER2+ luminal breast cancers demonstrate therapeutic resistance which is often correlated with increased RTK activity. The adaptor protein ShcA plays an important role in facilitating downstream RTK signaling, interacting with Gab1 and Grb2 to mediate ERK/MAPK and PI3K/AKT pathway activation. However, ShcA has been shown to have other effects on cell structure when knocked out, and mutation of residues Y239, Y240, and/or Y317 have dominant negative effects on cells. Not much is known about other ShcA interactors, which is where my project comes in.

Prior to my arrival, AP-MS and BioID were used to reveal protein interactors between WT ShcA and ShcA Y313F mutants. AP-MS was able to identify many interactors which were expected, such as Gab1 and Grb2. Interestingly, Grb2 was able to bind to wildtype ShcA as well

as 313F mutants; however, Gab1 did not bind to the 313F mutant. Using BioID, my colleagues previously made the novel observation that ShcA Y313F uniquely binds to several proteins that cannot bind ShcA with an intact Y313 phosphorylation site. This finding suggests that non-phosphorylated Y313 may be interacting with proteins which may mediate crucial pathways associated with tumorigenesis and drug interactions. To learn more about the recently identified ShcA interactors, I conducted a functional screen using RNAi to explore the consequences of gene silencing without altering the genome directly. For the purposes of this project, it was best to use RNA interference as a screening tool since ShcA Y313F mutant cells already exhibit one mutation. If another method of functional screen was employed, such as CRISPR-Cas9 knockout, this would run the risk of synthetic lethality in my mutant cell line.

It is crucial to identify therapeutic targets which can overcome hard-to-treat and recurring breast cancers, as risk of recurrence rises years following treatment. This project may identify novel targetable vulnerabilities to eradicate breast cancer cells and expand our knowledge of how tyrosine kinase signaling is dynamically regulated in breast tumors.

3. METHODOLOGY

3.1. MATERIALS

Cell culture

- Wisent BioProducts Dulbecco's modified Eagle's medium (DMEM) Cat#319-005-CL
- Wisent BioProducts Penicillin-Streptomycin Solution Cat#450-201-EL
- Wisent BioProducts Gentamycin Sulfate Solution Cat#450-135-XL
- Wisent BioProducts Fetal Bovine Serum Cat#080-150
- Mammary epithelial growth supplement (MEGS): 5 mg/mL insulin, 3 ng/mL human epidermal growth factor (Invitrogen Cat#PHG0311), 0.5 mg/mL hydrocortisone (Stem Cell Cat#74142), and 0.4% v/v bovine pituitary extract (Wisent BioProducts Cat#002-011-IL)
- Wisent BioProducts 10X Phosphate Buffered Saline diluted to 1X Cat#311-012-CL
- Wisent BioProducts Trypsin Cat#325-043-EL
- Wisent BioProducts Trypan blue Cat#609-130-EL
- Lonza MycoAlert Mycoplasma Detection Kit Cat#LT07-318
- Millipore Sigma Polybrene Cat#TR-1003-G
- Acridine Orange-Propidium Iodide (AO-PI)
- 2.3% Crystal violet solution

Western Blot

- PLCγ buffer: 50 mM HEPES [pH 7.5], 150 mM NaCl, 10% glycerol, 1% Triton X-100, 1 mM EGTA [pH 8.0], 1.5 mM $MgCl_2$
- RIPA buffer: 10 mM Na phosphate [pH 7.0], NaCl 150 mM, NP-40 1.0%, sodium dodecyl sulfate (SDS) 0.1%, Na deoxycholate 1.0%, EDTA 2 mM
- 50mM $Na3VO_4$
- 0.5M NaF
- 1000X PIN: 1µg/mL chymostatin, 2µg/mL antipain, 2µg/mL leupeptin, 1µg/mL pepstatin, 2µg/mL aprotinin
- 10X Tris-Glycine SDS Running Buffer: 25 mM Tris Base, 192 mM Glycine, 0.1% SDS, pH 8.3 diluted to 1X with ddH_2O

- 10X Tris-Glycine Transfer Buffer: 12 mM Tris Base, 96 mM Glycine, pH 8.3 diluted to 1X with ddH_2O
- 10X Tris Buffered Saline (TBS): 24g Tris Base, 88g NaCl, 900mL ddH2O, pH 7.6 with HCl
- 1X Tris-buffered saline with Tween 20 (TBST): 10% 10X TBS, 1% Tween 20, ddH_2O
- 5% Bovine serum albumin (BSA): 1X TBST, 5% BSA BioShop Cat#ALB001.500
- EMD Millipore Re-blot Plus Strong Solution

Polymerase chain reaction (PCR)

- Invitrogen UltraPure™ DNase/RNase-Free Distilled Water Cat#10977-015
- Roche High Pure PCR Product Purification Kit Cat#11732668001
- Roche PCR Nucleotide Mix Cat#11581295001
- NEB Q5 Hot Start High-Fidelity DNA Polymerase Cat#M0493
- NEB 5x Q5 Reaction Buffer
- NEB 5x Q5 High GC Enhancer
- IDT 20 nmole Ultramer DNA oligos:

PCR1 pZIP Nextera F primer:

TCGTCGGCAGCGTCAGATGTGTATAAGAGACAGTAGTGAAGCCACAGATGTA

PCR1 pZIP Nextera R primer:

GTCTCGTGGGCTCGGAGATGTGTATAAGAGACAGCCAGAGGTTGATTGTTCCAG

Individual shRNA infection

- HBS buffer (pH 6.95 to 7.05)
- 2.5M $CaCl_2$
- psPAX2 (Packaging plasmid all in one: Gag, Pol, Rev, Tat)
- pMD2.G (Envelope plasmid: VSV-G)
- Sarstedt Inc 0.45μm syringe filter unit Cat#83.1826

Mammary fat pad injection

- Charles River Laboratories female FVB mice
- Corning Matrigel Mix
- Dufort & Lavigne LTEE U-100 BD Micro-Fine IV Insulin Syringes 1 ml Cat#BEC329424

- Dufort & Lavigne LTEE U-100 BD Micro-Fine IV Lo-Dose Insulin Syringes 0.5cc Cat#BEC329461
- Digital caliper

Antibodies

- Cell Signaling AKT Cat#9272
- Cell Signaling AKT pS473 Cat#9271
- Cell Signaling AMPK Cat#5831
- Cell Signaling AMPKα pT172 Cat#50081
- Cell Signaling RS6 Cat#2217
- Cell Signaling RS6 pS240/244 Cat#2215
- Cell Signaling S6K Cat#2708
- Cell Signaling S6K pT389 Cat#9205
- Cell Signaling 4EBP1 Cat#9452
- Cell Signaling 4EBP1 pT37/46 Cat#9456
- Sigma Aldrich FLAG Cat#F1804
- Bethyl Labs PPP6C Cat#A300-844A
- Sigma Aldrich Tubulin Cat#T5168

Drugs

- Phenformin hydrochloride
- Lapatinib (GW-572016)
- Trametinib (GSK1120212)
- MK-2206 2HCl
- Torin-1
- EST-001

Kits

- High Pure PCR Template Preparation Kit Roche (REF 11 796 828 001)
- RNAse A 675.250 BioShop (20mg/mL)
- EZ-10 DNAaway RNA Miniprep Kit BioBasic
- Bio-Rad Bradford Protein Assay
- ThermoFisher Bicinchoninic Acid (BCA) Assay

Equipment

- Agilent BioTek Take3
- Take3 Trio Micro-Volume Microplates
- CellDrop FL Fluorescence Cell Counter DeNovix
- Azure 300 Imaging System
- Image J Version 1.53
- Prism 9 for macOS Version 9.5.0 (525)
- Microsoft Excel Version 16.67

3.2. METHODS

Cell lines

Wildtype MT cells were derived from transgenic mice carrying the mouse mammary tumour virus-polyoma middle T virus (MMTV/MT) fusion gene (Guy, Cardiff, & Muller, 1992). As previously described, mutant ShcA knock in mice were interbred with MMTV/MT mice to generate offspring expressing both MMTV/MT and homozygous ShcA Y313F mutation (Ursini-Siegel et al., 2008). The NT cell lines used were NMuMG cells transformed with a Neu/ErbB2 overexpression vector, and ShcA Y313F mutant was ectopically expressed as previously described (Ursini-Siegel et al., 2008).

MT ShcA and MT ShcA Y313F cells were grown in DMEM supplemented with 2.5% FBS, 0.5% MEGS, and penicillin/streptomycin and gentamicin. NT ShcA and NT ShcA313F cells were grown in DMEM supplemented with 10% FBS, 10μg/mL insulin, 10 mmol/L HEPES, and penicillin/streptomycin and gentamicin. 293T cells were grown in DMEM supplemented with 10% FBS, and penicillin/streptomycin and gentamicin. All cell lines were grown at 37 °C, with

5% CO_2. Cells were screened for mycoplasma upon thawing new vials and prior to *in vivo* injection with the MycoAlert mycoplasma detection kit by Lonza.

Affinity purification mass spectrometry (AP-MS)

Cell lines used for AP-MS were infected with FLAG-tagged WT ShcA, FLAG-tagged ShcA Y313F, or FLAG-tagged MYC as negative control. Cells were treated with the tyrosine phosphatase inhibitor pervanadate or a vehicle control 20 minutes prior to affinity purification. Cells were lysed and treated with Anti-FLAG antibody. Recovery was performed using beads to pull down FLAG antibody. Proteins were dissociated from the beads and separated using SDS-PAGE electrophoresis. Lanes were then cut and digested. Mass spectrometry was used to identify proteins present in the final product.

BioID

Cell lines used for BioID were infected with either BioID-ShcA, BioID-ShcA Y313F, or BirA alone. After selection, cells were plated. Biotin was added to cell media to allow for BirA to biotinylate proteins in proximity to ShcA or ShcA Y313F. After 24 hours, cells were lysed, and were purified using streptavidin beads to pull down any biotinylated proteins. Proteins were dissociated from the beads and proteins present were identified with mass spectrometry.

shRNA screen generation

BioID was able to identify many proteins in proximity to ShcA within living cells. However, the large number of proteins identified would take far too long to test individually. To narrow down the field, an shRNA library was generated with aid from the lab of Dr. Sid Huang to repress the

synthesis of proteins identified in the BioID assay. To ensure the results were due to repression of the specific target gene, 3-5 shRNAs were generated for each target. This pooling of shRNAs is advantageous not only to validate results, but also because it requires lower concentrations of each shRNA to repress gene expression (Lam et al., 2015).

Viral titration

The target multiplicity of infection (MOI) was 0.3 for this screen to maximize infectivity of one shRNA per cell, while minimizing the chances of 2 or more shRNA infecting a single cell. 6 well plates were plated with either MT ShcA or MT ShcAY313F cells so that they reached 70%-80% confluency the next day. Cells were treated with increasing concentrations of viral media or no viral media and 1.6uL polybrene per well. Cells were then centrifuged at 2100 RPM for 30 minutes and then left to incubate at 37°C overnight. After incubation, the viral media was aspirated and replaced with regular media. The cells were then trypsinized and separated into two 60mm plates per well and treated with puromycin or no selection marker for 48 hours. After 48 hours, plates were counted using trypan blue exclusion. The ratio of live cells in puromycin-treated plates compared to untreated plates was used to determine the number of cells that survived following selection.

$IC30_{Phenformin/Lapatinib}$

MT ShcA and MT ShcA Y313F cells were plated in 24 well plates and seeded so that they would not exceed confluency before completion of the experiment. Cells were treated with either 100-200μM phenformin or 50-400nM lapatinib. PBS was used as a vehicle control for phenformin treated cells, while DMSO served as a vehicle control for lapatinib treated cells. Both media and

drug treatment or vehicle control were refreshed after 48 hours. After 72 hours, cells were trypsinized and resuspended with media into individual microtubes. Cell viability was determined with acridine orange-propidium iodide (AO-PI) staining. A 1:1 ratio of cells: AO-PI was used, and samples were counted using the CellDrop FL Fluorescence Cell Counter.

shRNA screen

To reduce noise and increase signal, 1000X coverage of each shRNA was used. For a library of 798 shRNAs, this would mean a minimum of 798,000 shRNA-infected cells per condition. MT ShcA and MT ShcA Y313F cells were plated in 6 well plates and infected with 50uL viral media containing the shRNA library and 1.6uL polybrene per well. Cells were then centrifuged at 2100 RPM for 30 minutes and then left to incubate at 37 °C overnight. After incubation, the viral media was aspirated and replaced with regular media. The cells were then trypsinized and separated into two 60mm plates per well and treated with puromycin or no selection marker for 48 hours.

Following puromycin selection, 2 million cells from each cell line were pelleted and frozen as input control. 1 million cells were plated into 15cm plates and cultured in DMEM for 14 days to assess *in vitro* growth. Following puromycin selection, 1 million cells were plated into 15cm plates and cultured in DMEM. The following day, cells were treated 150μM phenformin for WT ShcA cells or 100μM phenformin for ShcA Y313F cells. Media and drug treatments were refreshed every 48 hours. Cells were trypsinized and split when necessary. Cells were cultured for 14 days to assess response to phenformin. Following puromycin selection, 1 million cells were plated into 15cm plates and cultured in DMEM. The following day, cells were treated

100nM lapatinib for WT ShcA cells or 300nM lapatinib for ShcA Y313F cells. Media and drug treatments were refreshed every 48 hours. Cells were trypsinized and split when necessary. Cells were cultured for 14 days to assess response to lapatinib.

Mammary fat pad (MFP) injection

After the 48-hour puromycin selection period, infected MT ShcA or MT ShcA Y313F cells were washed twice with PBS and counted with trypan blue exclusion. 5 million cells were aliquoted and centrifuged to pellet. Cells were resuspended in a 1:1 ratio of PBS and Matrigel so that 50μL of solution would contain approximately 500,000 cells.

Female FVB mice aged 6-8 weeks were injected into the fourth mammary fat pads with 500,000 cells per injection. A total of 3 mice were used per cell line. 7 days following MFP injection, staples were removed. Tumours were palped and measured with a digital caliper every 48 hours following the removal of staples. Tumour volume was calculated using the following equation: $4/3 \times (3.14159) \times (\text{length}/2) \times (\text{width}/2)^2$. And endpoint approximately 500mm^3 was selected for *in vivo* conditions to allow tumours time to develop without becoming necrotic.

DNA extraction

Upon conclusion of the screen, all cell cultures were centrifuged and frozen as pellets while tumours were harvested and frozen. Frozen tumours were then crushed to make DNA extraction easier. DNA was extracted from pellets and crushed tumours using a modified High Pure PCR Template Preparation Kit from Roche. The protocol was modified in the following way:

10uL of RNAseA (20mg/ml stock) was added to samples along with the Binding Buffer and incubated at 37°C for 30 minutes. After DNA was extracted using the modified Roche protocol, the quality of samples was examined using Take3. Additionally, samples were run on a 2% agarose gel to confirm there was no contamination in the samples prior to PCR amplification.

PCR amplification

The first PCR amplification was then performed on samples to amplify the shRNA region and add Nextera overhangs for identification of the shRNA isolated. A master mix of 5x Q5 Reaction Buffer, 5x Q5 High GC Enhancer, dNTPs, Nextera F primer, Nextera R primer, and Q5 enzyme polymerase was used. 1μg genomic DNA was added to PCR reaction tube along with 26.5μL master mix. Samples were topped up to 50μL with DNAse/RNAse free water. The minimum number of PCR reactions required for this screen was determined by the amount of coverage required per shRNA, the amount of shRNAs in the screen, and the amount of DNA per cell. For 1000X coverage in this screen, 5.2 PCR reactions was required. Therefore, multiple individual PCR reactions were performed for each sample, and final PCR products were pooled together.

PCR amplified samples were run through 1% agarose gel to confirm the final PCR product was the correct size and to check for primer dimers and other sources of contamination. The final PCR product following amplification and addition of Nextera overhangs is estimated to be 271 nucleotides. Samples were sent to IRIC to perform the second PCR reaction to add the P5 and P7 sequences. Results from the second PCR reaction were sent to the Huang lab for analysis.

MAGeCK analysis

Data received from the final PCR readout was analyzed using MAGeCK by the Dr. Sig Huang laboratory. MAGeCK is capable of identifying both positively and negatively selected genes at the same time (W. Li et al., 2014). Additionally, MAGeCK can take into account the knockdown efficiency of numerous different shRNAs per target (W. Li et al., 2014). Negatively selected shRNA were those which had shRNA for the target protein present in the Input Control but little to no shRNA following treatment condition. This is interpreted as that protein being essential for cell viability, since knockdown decreased the final number of cells with that shRNA. Alternatively, shRNA which were more abundant following treatment were described as positively selected. This implies that cells with decreased target protein was beneficial for cell survival. Numerous proteins had significant differences between input and condition treatment, so to narrow the proteins of interest, only those proteins which had significant differences in two or more conditions were selected for further analysis.

Individual shRNA knockdown

Five shRNAs per target were selected and purchased from Dr. Sid Huang. Bacterial cultures received from the Huang lab were made into glycerol stocks. Bacterial shRNA cultures were grown in 10mL LB media overnight at 37°C. Plasmid DNA was extracted from bacterial cultures using the EZ-10 DNAaway RNA Miniprep Kit by BioBasic. Quantity and quality of plasmid DNA was examined using Take3.

Plasmids were transfected into 293T cells using the Calcium Phosphate Transfection method provided by Dr. Huang. 293T cells were plated in a 6-well dish and left for 8 hours. The

transfection mix comprised of 2μg shRNA, 1μg packaging plasmid psPAX2, and 1μg envelope plasmid pMD2.G, HBS buffer, and $CaCl_2$ was prepared and left in the dark for 30 minutes prior to transfection. Transfection mixture was added drop wise to avoid direct contact with cells. Cells were incubated overnight, and media was refreshed in the morning. Viral media was harvested at both 24 hours and 36 hours following infection with a 0.45μm syringe filter and then frozen at -80°C.

MT ShcA or MT ShcAY313F cells were plated to reach 70%-80% confluency the next day. Cells were treated with 100-200μL viral media and 1.6μL polybrene per well. Cells were then centrifuged at 2100 RPM for 30 minutes and then left to incubate at 37°C overnight. Cells were split into 10cm plates and treated with puromycin for 48 hours.

Western blot

Following puromycin selection, plates were either frozen to perform Western Blot analysis to confirm target knockdown or expanded and frozen for future use. Lysates were made by lysing cells with 300-500μL of PLCγ buffer supplemented with 5mM Na3VO4, 5mM NaF, and PIN. Following lysis treatment for 10 minutes on ice, cells were scraped and transferred to a microtube. Lysates were centrifuged at 16,000 × *g*, 4 °C for 10 minutes and supernatant was transferred to a new microtube. Protein concentration was measured using the Bio-Rad Protein assay. Samples were prepared into ready to load stocks with lysate, DTT, protein loading dye, and water to equalize the total protein concentration per sample. Samples were separated by SDS-PAGE and transferred onto polyvinylidene difluoride membranes. Membranes were blocked in 2.5% bovine serum albumin (BSA) and probed with antibodies overnight.

Cell culture drug treatments

Phenformin hydrochloride was resuspended in PBS and filtered to a stock concentration of 100μM. Stock solution was stored for up to 4 weeks at 4°C. MT ShcA and MT ShcA Y313F cells were plated in 24 well plates and seeded so that they would not exceed confluency before completion of the experiment. Cells were treated with 50-250 μM phenformin or with PBS as vehicle control. Both media and drug treatment were refreshed after 48 hours.

Lapatinib (GW-572016) was resuspended in dimethyl sulfoxide (DMSO) at a concentration of 1μM and frozen at −20 °C. MT ShcA and MT ShcA Y313F cells were plated in 24 well plates and seeded so that they would not exceed confluency before completion of the experiment. Cells were treated with 100-500nM lapatinib or with DMSO as vehicle control. Both media and drug treatment were refreshed after 48 hours.

Trametinib was resuspended in dimethyl sulfoxide (DMSO) at a concentration of 1μM and stored at −80 °C. MT ShcA and MT ShcA Y313F cells were plated in 24 well plates and seeded so that they would not exceed confluency before completion of the experiment. Cells were treated with 5-25nM trametinib or with DMSO as vehicle control. Both media and drug treatment were refreshed after 48 hours.

MK-2206 2HCl was resuspended in dimethyl sulfoxide (DMSO) at a concentration of 100μM and stored at −80 °C. MT ShcA and MT ShcA Y313F cells were plated in 24 well plates and seeded so that they would not exceed confluency before completion of the experiment. Cells

were treated with 1-3μM MK-2206 or with DMSO as vehicle control. Both media and drug treatment were refreshed after 48 hours.

Torin-1 was resuspended in dimethyl sulfoxide (DMSO) at a concentration of 100nM and stored at −20 °C for up to 4 months. MT ShcA and MT ShcA Y313F cells were plated in 24 well plates and seeded so that they would not exceed confluency before completion of the experiment. Cells were treated with 50-250nM Torin-1 or with DMSO as vehicle control. Both media and drug were refreshed every 48 hours.

An aliquot of EST-001 was kindly donated by the lab of Dr. Ivan Topisirovic. EST-001 was resuspended in dimethyl sulfoxide (DMSO) at a concentration of 100nM and kept at −80 °C. MT ShcA and MT ShcA Y313F cells were plated in 24 well plates and seeded so that they would not exceed confluency before completion of the experiment. Cells were treated with 0.5-10nM EST-001 or with DMSO as vehicle control. Both media and drug were refreshed every 48 hours.

Western blot for drug treatment validation

MT ShcA and MT ShcA Y313F cells were plated so they would reach 70% confluency the following day. Cells were treated with either 50-250 μM phenformin, 100-500nM lapatinib, 5-25nM trametinib, 1-3μM MK-2206, 50-250nM Torin-1, or 0.5-10nM EST-001 for 24 hours. Vehicle controls were PBS for phenformin-treated plates and DMSO for all other drug treatments.

Cell viability assay

Drug response between WT ShcA and ShcA Y313F were examined using crystal violet. Cells were plated on 24 well plates and treated with increasing doses of one drug. Cells treated with phenformin, lapatinib, trametinib, or MK-2206 were treated for 72 hours with drug and media refreshed at 48 hours. Cells drugged with either Torin-1 and EST-001 were treated for 7 days, with drug and media refreshed every 48 hours. Media was aspirated and cells were washed with PBS. 2.3% Crystal violet stock solution was diluted to a final concentration of 0.5% with water and methanol. Crystal violet solution was added to the wells and plates were placed on a rocker for 10-15 minutes. Crystal violet solution was aspirated, and wells were rinsed with PBS three times. Plates were turned over and dried overnight.

Plates were imaged using a plate reader and raw images were saved. Well confluency was quantified using ImageJ. High density threshold was set at 5-100. Medium density threshold was set at 101-180. Low density threshold was set at 181-220. Confluency was then normalized to control wells to determine overall viability. Sample calculations for well confluency and overall viability have been included below. Statistical analyses were performed using GraphPad Prism 9.

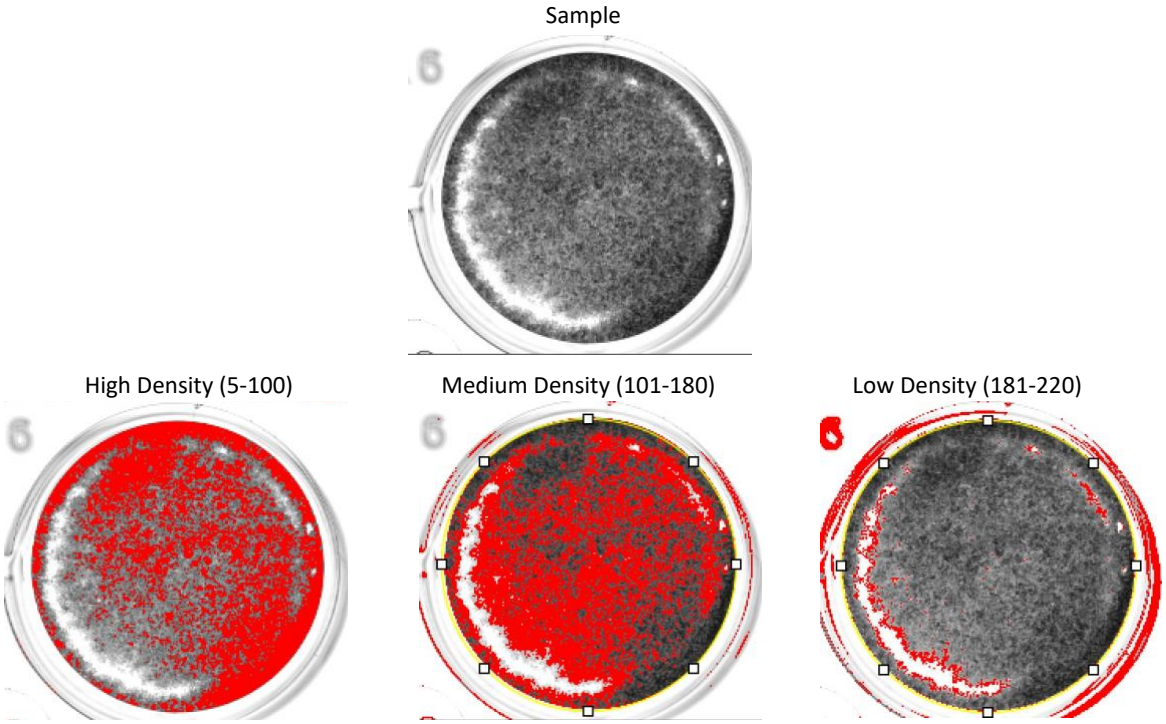

Figure 4. Sample of image processing using ImageJ.
High density signal threshold was set from 5-100. Medium density signal threshold was set from 101-180. Low density signal threshold was set from 181-220.

Table 1. Sample calculation of well confluency and normalization to control wells.

	Raw % Coverage		
Well	**High Density (5-100)**	**Medium Density (101-180)**	**Low Density (181-220)**
Sample	42.828	47.721	4.132

	Relative % Coverage			
Well	**High Density**	**Medium Density**	**Low Density**	**Total Confluency (%)**
Sample	42.828	23.861	1.033	67.722

Well	**Confluency (%)**	**Average**	**Normalized**	**Survival (%)**
Control 1	88.92	89.3975	0.9947	99.47
Control 2	90.34		1.0105	101.05
Control 3	91.15		1.0196	101.96
Control 4	87.18		0.9751	97.51
Sample	67.72		0.7575	75.75

3.3. JUSTIFICATION OF CHOSEN METHODOLOGY

Selection of MT cell lines to model disease

The MMTV/MT model is a well-known model used to study tyrosine kinase-dependent breast cancer due to its ability to reflect human breast cancer progression in a murine system (Ursini-Siegel et al., 2008). One advantage to using the MT mouse model to examine the relationship between ShcA mutation, tumour development, and drug response is that ShcA is expressed at physiological levels (Ursini-Siegel et al., 2008). Other models, such as the transformed NMuMG cell line (NT), use an overexpression vector of Neu/ErbB2 to transform the cells and expression of ShcA Y313F has been shown to be consistently lower compared to wildtype NT cells (Ursini-Siegel et al., 2008). However, to develop MMTV/MT cell lines with mutant ShcA, multiple generations of breeding must occur, which provides the disadvantage that these tumours are not from the same parental line.

Additionally, due to the substitution of tyrosine to phenylalanine, it is possible that this mutation has altered the proteins 3D structure, which could impact other molecular interactions, or create artefactual interactions. Although this is unlikely due to the fact that both tyrosine and phenylalanine are residues with hydrophobic side chains, and the lack of polar -OH group in phenylalanine is more likely to decrease intermolecular interactions than create artefactual interactions (Creixell, Schoof, Tan, & Linding, 2012). Future experiments would be required to evaluate the possibility of artefactual interactions due to this substitution, but at this time the MMTV/MT model is a good model to recapitulate disease and reflect physiological expression of ShcA or the mutant.

Identification of protein-protein interactions using AP-MS and BioID

While AP-MS can identify many protein interactions, there are some shortcomings. As previously mentioned, AP-MS is performed on whole cell lysates. This can pose an issue if interactions are found between proteins located in separate cellular compartments (Roux et al., 2018). Additionally, there is a chance that some interactions are missed. If the protein interactions are quite weak, or are sensitive to the lysis buffers used in pulldown, they may be lost (X. Liu et al., 2020). AP-MS is generally performed in a short period of time, for example, pulldown of Flag-tagged ShcA was completed after 20 minutes of treatment with pervanadate or a vehicle control. There is a possibility that there are low frequency or rare protein interactions which would not be captured in that time frame (X. Liu et al., 2020).

BioID captures protein interactions over a 12 to 24-hour period while the cells are alive (Roux et al., 2018). This allows for the identification of rare or infrequent interactions as they occur within the cell. Other advantages include identification of weak protein interactions, identification of transient or short-term protein interactions, and identification of low frequency protein interactions (X. Liu et al., 2020). This can include enzyme-substrate interactions, kinase and protease interactions, and interactions which may have been impacted by lysis buffers used in AP-MS (X. Liu et al., 2020). However, BioID identifies proteins in proximity to the bait, meaning that proteins tagged may not directly interact with the protein of interest (Roux et al., 2018). To elucidate true ShcA interactors following BioID, validation will be done using co-immunoprecipitation (Co-IP).

Functional screen evaluation with RNAi

RNA interference, commonly referred to as RNAi, is a method to repress gene expression through mRNA translation inhibition or mRNA degradation (Sheng et al., 2020). This results in reduced expression of target genes without altering DNA. There are different mechanisms to repress target gene activity: microRNA (miRNA) and small interfering RNA (siRNA). miRNA genes are transcribed and undergo post-transcriptional modification in the nucleus, forming a double-stranded primary miRNA (pri-miRNA) with a 5' cap, 3' polyadenylated tail, and a stem-loop (Lam et al., 2015). The pri-miRNA is cleaved by Drosha, resulting in precursor miRNA (pre-miRNA), which is then exported from the nucleus into the cytoplasm (Lam et al., 2015). Dicer then cleaves the pre-miRNA, allowing miRNA to interact with the RNA-induced silencing complex (RISC), release the sense strand, and guide RISC to target mRNAs (Lam et al., 2015).

Alternatively, siRNAs are derived from double-stranded RNAs (dsRNAs) or short hairpin RNAs (shRNAs) using endogenous cell machinery (Lam et al., 2015). dsRNA is either transcribed in the cell or introduced to the cell through viral infection, while shRNA is solely introduced to the cell through viral infection (Lam et al., 2015). Once in the cytoplasm, the dsRNA or shRNA is then cleaved by Dicer to form siRNA (Lam et al., 2015). The siRNA can then interact with RISC, allowing a portion of the complex called argonaute 2 (AGO2) to cleave the sense strand of the siRNA, leaving a single-stranded siRNA to guide RISC (Lam et al., 2015).

miRNA and siRNA vary greatly in the number of mRNA they can regulate. miRNA does not require a perfect match target mRNA for inactivation (Lam et al., 2015). As a result, one miRNA can target multiple mRNAs. Alternatively, siRNA exclusively binds to mRNA that fully complement the antisense strand, allowing for highly specific targeting (Lam et al., 2015). While

miRNA is advantageous in some circumstances, due to the nature of the screen, it was best to use siRNA-mediated repression to reduce the likelihood of off-target mRNA repression (Lam et al., 2015).

While siRNA can be derived from both dsRNA and shRNA, dsRNA is not the ideal method to induce synthetic gene repression. dsRNA are long strands of exogenous RNA, whereas shRNA are introduced to the cell through viral vectors and synthesized within the nucleus of the host (Lam et al., 2015). Long dsRNA has been shown to activate the interferon pathway, resulting in nonspecific mRNA degradation due to immune activation (Lam et al., 2015). Therefore, shRNA is an ideal method to ensure the repression of one gene while reducing the chances of off-target effects.

RNAi is a common method to regulate gene expression, recently emerging CRISPR-Cas technology has begun to dominate the field. CRISPR-Cas was discovered as a protective response against bacteriophage infection in bacteria and archaea (Ishino et al., 2018). The CRISPR RNA identifies targets through homologous sequence targeting, and trans-activating CRISPR RNA recruits Cas9 to the target site, cleaving the target DNA (Ishino et al., 2018). Researchers have been able to exploit the CRISR-Cas9 system by creating guide RNA to influence CRISPR targets (Pickar-Oliver & Gersbach, 2019). However, for cleavage to occur, the target sequence must be positioned near a protospacer adjacent motif (PAM) sequence (Pickar-Oliver & Gersbach, 2019). The guide RNAs must include PAM sequences for proper site-specific cleavage (Pickar-Oliver & Gersbach, 2019). CRISPR-Cas9 has many applications

including gene deletion, gene insertion, single-base editing, translocations, and high-throughput loss-of-function screens (Pickar-Oliver & Gersbach, 2019).

There is a new group of Cas proteins called Cas13a which targets RNA and mediates RNA degradation (Granados-Riveron & Aquino-Jarquin, 2018; Pickar-Oliver & Gersbach, 2019). Like Cas9, many Cas13a endonucleases require a nearby spacer sequence, called a protospacer flanking sequence (PFS) in order to function (Pickar-Oliver & Gersbach, 2019). Cas13a then cleaves at any uracil bases nearby, which can also include non-targeted RNAs, dubbed "collateral" cleavage (Pickar-Oliver & Gersbach, 2019). Cas13a has been used to target specific mRNAs in both bacteria and eukaryotes, and although off-target cleavage was not seen in eukaryotic cells, it's unknown how eukaryotic cells do not have off-target collateral cleavage (Pickar-Oliver & Gersbach, 2019). While Cas13 is capable of RNAi, and has many advantages, the majority of researched using CRISPR technology has been performed with the CRISPR-Cas9 system, leaving many gaps in knowledge (Granados-Riveron & Aquino-Jarquin, 2018).

CRISPR-Cas9 is not an ideal method of gene repression because it completely silences genes through gene deletion or DNA mutation (Sheng et al., 2020). This method is not recommended because some targets may be lethal if completely silenced (Sheng et al., 2020). There is also the risk of synthetic lethality in our mutant cell line, which already has mutated ShcA. CRISPR-Cas13, on the other hand, behaves similarly to RNAi, regulating gene expression at the mRNA level (Sheng et al., 2020). However, CRISPR relies on exogenous Cas proteins, which may elicit an immunogenic response and have nonspecific gene inactivation (Sheng et al.,

2020). shRNA is advantageous in this instance since it utilizes endogenous machinery to impact gene expression, making it unlikely to elicit an immunogenic response (Sheng et al., 2020).

With these considerations taken into account, this screen was developed using an shRNA library to knockdown gene expression. To ensure the results were due to repression of the specific target gene, 3-5 shRNAs were generated for each target. This pooling of shRNAs is advantageous not only to validate results, but also because it requires lower concentrations of each shRNA to repress gene expression (Lam et al., 2015).

3.4. Difficulties and challenges

Transformed NMuMG cell lines were not used in the screen

While viral titrations were being performed to determine the volume of viral media required to establish an MOI of 0.3, the NT cell lines were not reacting as expected. Death following puromycin selection was comparable between NT cells that received viral media and those that did not. Later, it was discovered that the immortalized cell line NMuMG was transformed into NT2197 using a puromycin-resistance selection marker. Therefore, NT cell lines being used in this experiment were already puromycin-resistant, and therefore we could not determine the MOI in these cells and did not continue the screen with these cell lines.

4. RESULTS

Previous research has shown that adaptor proteins interact with many proteins and can influence many different processes within the cell. While ShcA protein interactors have been identified, little research has been done outside of the interactions between ShcA, Gab1, and Grb2. In this chapter, I have identified numerous interactors of ShcA both in a fully and partially phosphorylated state. Using the methods previously described, I will explore the dynamic protein interactors of ShcA and evaluate which proteins may facilitate breast tumour growth, promote metabolic flexibility, and contribute to therapeutic resistance. Additionally, I will highlight some potential therapeutic targets which could be exploited in TKI resistant breast cancer cells. This research aims to identify novel vulnerabilities while also expanding our current views on protein signaling networks.

4.1. Identification of potential ShcA interactors

AP-MS was able to identify 59 proteins which interact with WT ShcA or ShcA Y313F. Of these 59 proteins, 13 were found to interact with both wildtype and mutant ShcA. 36 proteins were found to only interact with wildtype ShcA and only 10 were found to exclusively interact with mutant ShcA. BioID identified a total of 175 proteins in proximity to ShcA or ShcA Y313F. Of the 175 proteins identified, 72 were found to interact with both ShcA and ShcA Y313F. 41 of the proteins identified were found to interact with wildtype ShcA and not mutants. Interestingly, BioID identified 62 proteins which interact with ShcA Y313F mutants and not wildtype ShcA. While there were some conflicts in whether the tests agree if the target interacts with one or both forms of ShcA, there was still some overlap between the two assays (Table 2). Both were able to identify that wildtype and mutant ShcA interacts with Asap2, Arhgef5, Grb2, Map4k5, Ptpn12,

and Pstpip2 (Table 2). Proteins identified in both screens but under different conditions include Anks1a, Cct5, Cct8, Gm20390, and Sept7 (Table 2).

Table 2. List of proteins found to interact with WT ShcA, ShcA Y313F, or both forms using affinity purification mass spectrometry (AP-MS) and BioID.

AP-MS			BioID			BioID		
WT ShcA & ShcA Y313F	WT ShcA only	ShcA Y313F only	WT ShcA & ShcA Y313F	WT ShcA only	ShcA Y313F only	WT ShcA & ShcA Y313F	WT ShcA only	ShcA Y313F only
Amd2	Ago3	Acaca	Ahcyl2	Actr1b	Aacs	Hspa4l	Stat3	Phactr4
Anks1a**	Ap2a1	Cct2	Ahnak	Actr2	Ahcyl1	Hsph1	Usp15	Pip4k2b
Arhgef5*	Ap2a2	Cct7	AHNAK	Adsl	Anks1a**	Isyna1	Vangl1	Pla2g4a
Asap2*	Ap2b1	Dnajc10	Ahnak2	Arcn1	Arg1	Kif5b	Vps25	Psmd12
Cct5**	Ap2m1	Hnrnpdl	Arhgef10l	Cap1	Asap1	Map4k5*	Vps45	Psmd6
Cct8**	Atxn2	Hnrnpul1	Arhgef5*	Cct5**	Atp6v1e1	Mapre1		Ptpn11
Ctnnd1	Cdk11b	Rbm3	Arhgef7	Cct7	Aven	Mapre2		Scin
Grb2*	Ctnna1	S100a6	Arpin	ckap5	Bcar1	Mob4		Sec23a
Map4k5*	Ctnnb1	Snd1	Asap2	Copb1	Cct8**	Nudc		Septin5
Prkcd	Egfr	Usp9x	Atp6v1b2	Copb2	Cdv3	Pak2		Sh3gl1
Pstpip2*	Eif1a		Casp3	Cops2	Clint1	Parva		Sh3pxd2b
Ptpn12*	Eif3b		Cast	Cops7a	Cnot9	Pdlim5		Slk
Uba1	Erbb2		Cd2ap	Dctn3	Col9a3	Ppp2r1b		Snx1
	Gab1		Ciapin1	Eif4g2	Cops3	Pstpip1		Snx2
	Gm20390**		Cobll1	Elp6	Cops6	Pstpip2		Stim1
	Inppl1		Copg2	Evpl	Ctnna1	Ptpn12		Stk4
	Khdrbs1		Cops4	Gapvd1	Ctsc	Pxn		Stmn1
	Lrrk1		Coro1b	Gm20390**	Drg2	Scfd1		Strn
	Lsm14b		Crk	Lims1	Dvl2	Sec23b		Strn3
	Mfap1		Cttn	Lpp	Echdc1	Sept10		Strn4
	Msn		Dbnl	Lypla2	Epb41l1	Sept6		Tiprl
	Phgdh		Dctn1	Nme1	Epb41l2	Sept7**		Vta1
	Pik3r1		Dnajb1	Nup107	Gps1	Sept8		Vwa5a
	Pkm		Dnm1l	Paics	Hint1	Serpina3h		Washc1
	Pkp1		Dpysl2	Pex14	Idh1	Sh3kbp1		Washc5
	Prdx2		Elp4	Pip4k2c	Ilk	Shc1		Wasl
	Prrc2c		Elp5	Ppl	Inppl1	Shcbp1		
	Ptpn11		Eps8l2	Ppp2r1a	Jpt2	Shq1		
	Rasal2		Esyt1	Ppp6c	Klc1	Stam		
	Rbm27		Fdps	Prkag1	Klc3	Stam2		
	Sept7**		Fnbp1l	Rab11fip1	Lasp1	Tab1		
	Set		Gmds	Rab11fip5	Nup54	Tln1		
	Snrpb2		Grb2*	Rps6ka1	Pacsin2	Tsn		
	Srsf11		Haus1	S100a10	Pdxdc1	Ugp2		
	Tnrc6a		Hgs	Sept11	Pex5	Vcpip1		
	Try10		Hspa4	Sept2	Pfdn2	Vps33b		

* are proteins identified in both assays with the same form of ShcA. ** are proteins identified in both assays but with different forms of ShcA.

4.2. Aim 1: Identification of genes crucial for mediating tumour development and drug reactions in ShcA and ShcA Y313F mutants

Since a large number of previously unidentified ShcA interactors were revealed with BioID, a functional screen was used to further narrow down the most probable interactors. An

shRNA library was generated with the help of Dr. Huang, which contained 799 shRNAs. Three to five shRNA were used to target each potential interactor. By using multiple shRNA per candidate, we increase the likelihood of each candidate being knocked down in the screen and successfully grafting into in vivo conditions. Prior to the screen being performed, WT ShcA and ShcA Y313F mutants were examined to determine the drug concentrations and viral shRNA dose to be used during the experiment.

To examine the influence of the drugs phenformin and lapatinib on ShcA and ShcA Y313F mutants, an inhibitory concentration of approximately 30% (IC30) was determined using acridine orange-propidium iodide (AO-PI) to assess cell viability. The IC30 of each drug was determined through repeated viability experiments and interpolation from a sigmoidal four parameter logistic curve. $IC30_{WT\ ShcA}$ was determined to be around 138.0μM while $IC30_{ShcA\ Y313F}$ was determined to be around 92.7μM (Fig. 5A). The IC30 for lapatinib for both cell lines was determined as mentioned previously. Using the same parameters, $IC30_{WT\ ShcA}$ was determined to be approximately 89.9nM. Unfortunately, $IC30_{ShcA\ Y313F}$ was unable to be interpolated, however $IC50_{ShcA\ Y313F}$ was calculated at around 238.7nM (Fig. 5B). Rounding to the nearest unit of 50, 150μM phenformin and 100nM lapatinib were used to treat MT WT ShcA cells for the screen. Meanwhile, MT ShcA Y313F cells were treated with 100uM phenformin or 300nM lapatinib during the screen.

A multiplicity of infection (MOI) of 0.3 was selected for this screen to maximize infectivity of one shRNA per cell, while minimizing the chances of 2 or more shRNA infecting a single cell. Viral titration assays were performed on each cell line to determine the average MOI. Cell lines were plated and treated with 25μL-125μL viral media, and puromycin was used as the

selection marker. For both MT ShcA and MT ShcA Y313F cell lines, 50μL of virus was required to obtain an MOI of around 0.3 (Fig. 5C).

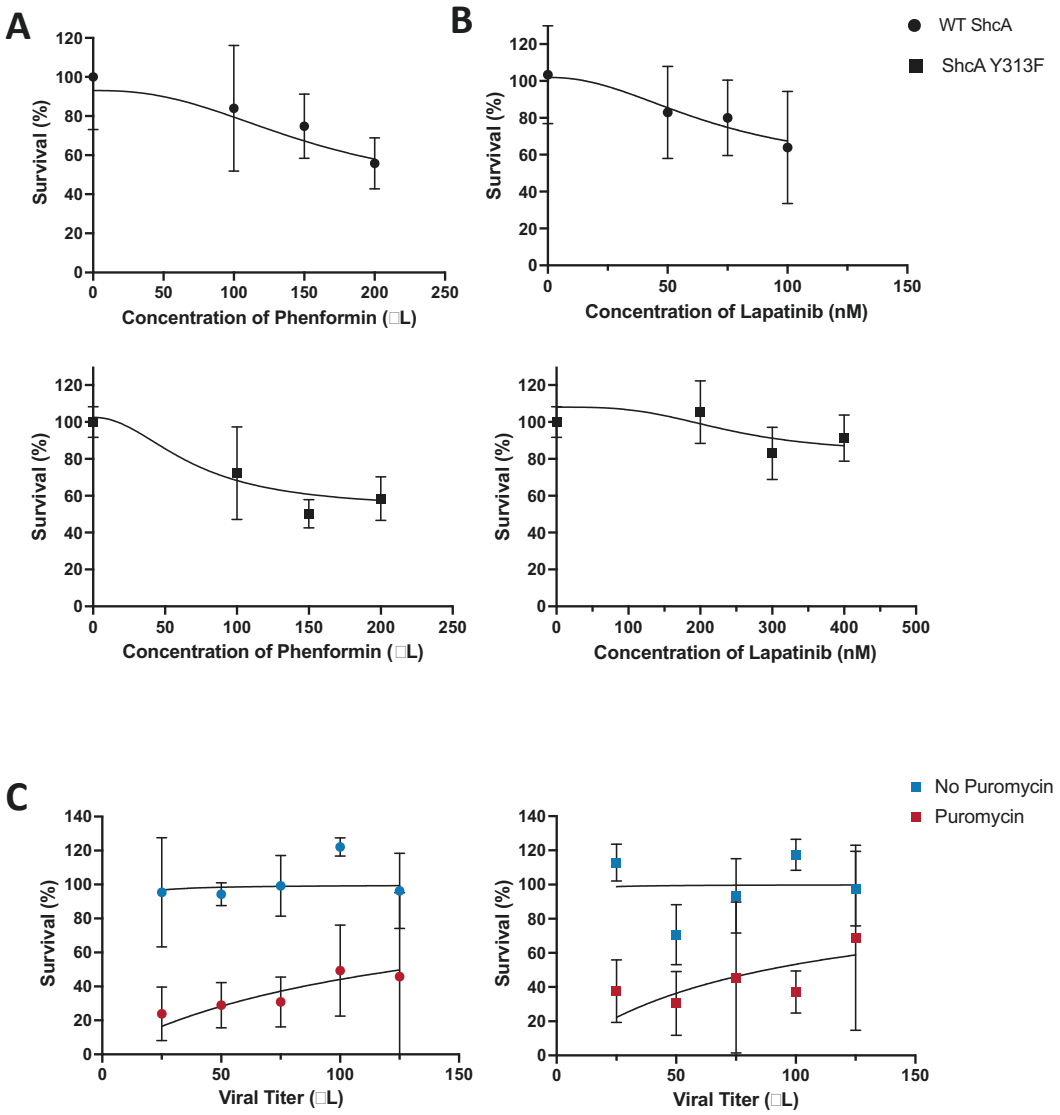

Figure 5. Determining the $IC30_{Phenformin}$, $IC30_{Lapatinib}$, and viral dose required to reach an MOI of 0.3 in WT ShcA and ShcA Y313F cell lines.A) $IC30_{Phenformin}$ for WT ShcA was estimated to be 138.0μM (R^2= 0.3660). $IC30_{Phenformin}$ in ShcA Y313F was estimated to be 92.7μM (R^2= 0.5265). B) $IC30_{Lapatinib}$ for WT ShcA was estimated to be 89.9nM (R^2= 0.2400). ShcA Y313F $IC30_{Lapatinib}$ was unable to be interpolated in Prism due to lack of drug response, however $IC50_{Lapatinib}$ was estimated at 238.7nM (R^2= 0.0741). Statistics performed by interpolation from a sigmoidal 4PL curve.

Upon conclusion of the screen, DNA was extracted from the cells and PCR amplified to identify the shRNAs present in each condition. If an shRNA was not present after the screen but present during the initial infection, this demonstrated that the gene was essential for cell survival in the specific condition, denoted as dropout. Alternatively, increase in an shRNA indicated that

loss of that target protein was beneficial for the cell, denoted as enrichment. Using MAGeCK, RRA scores were compared, and the top 10 genes enriched or dropped out in each condition were graphed.

After 14 days of growth in vitro, many similar dropouts were seen in both cell lines including PSMD6, COPB1, CCT7, COPS3, COPB2, and PSMD12 (Fig. 6). Following treatment with phenformin or lapatinib, there was still overlap in dropouts between the two cell lines (PSMD12 NUP107, COPB1, and CCT7) however, the two cell lines begin to show their differences as translation initiation factor eIF4E drops out in ShcA Y313F mutants but wasn't significant in WT ShcA (Fig. 5B/C). Dropouts from whole tumours were quite different from those seen in vitro. ILK, ELP4, CLINT1, and PPP6C were revealed to be important for survival in WT ShcA tumours, whereas eIF4G2 is the only new dropout not seen in previous ShcA Y313F conditions (Fig. 6).

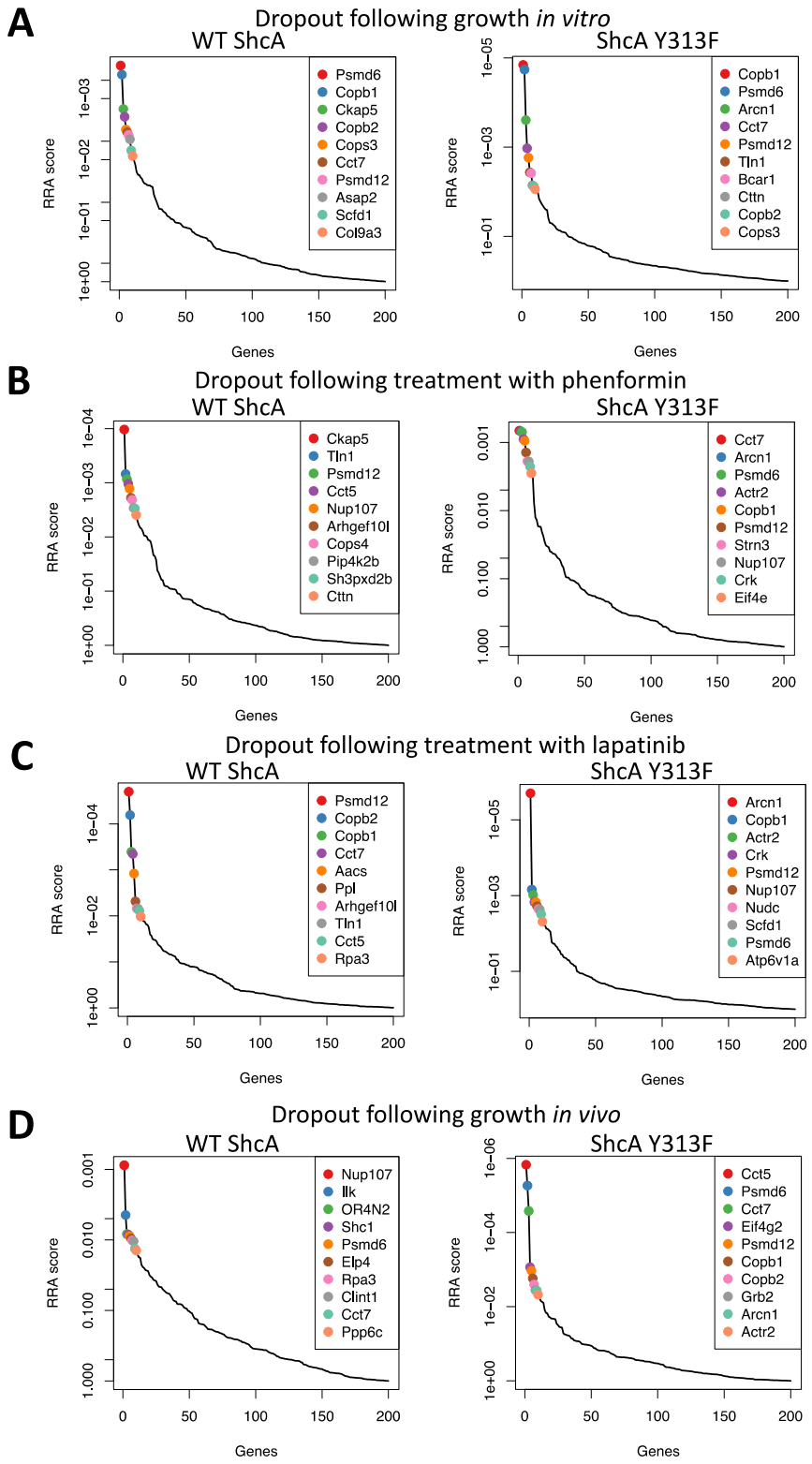

Figure 6. Top 10 gene dropouts in WT ShcA and ShcA Y313F.
Top 10 gene dropouts 14 days of growth in vitro (A), 14 days of growth in vitro with 150µM phenformin for WT ShcA cells and 100µM phenformin for ShcA Y313F cells (B), 14 days of growth in vitro with 100nM lapatinib for W WT ShcA cells and 300nM lapatinib for ShcA Y313F (C), and growth *in vivo* (D) following infection with the shRNA library. All figures were created with MAGeCK software.

There was large variability in the genes enriched upon conclusion of the screen. Overlap did remain between the two cell lines including genes such as SHCBP1, SEPT5, DPYSL2, and SH3KBP1 (Fig. 7). In wildtype cells, there were a few enriched genes which overlapped between conditions including eIF4G2, EPS8L2, PLA2G4A, SCIN, and HN1L (Fig. 7). Alternatively, there are few enriched genes which overlap in ShcA Y313F mutants (PPP6C and DVL2). For a gene to be considered a "hit" for further analysis, the enrichment or loss of the shRNA had to be statistically significant in two or more conditions. These parameters were set due to the numerous shRNA with significant differences in only one condition or cell line.

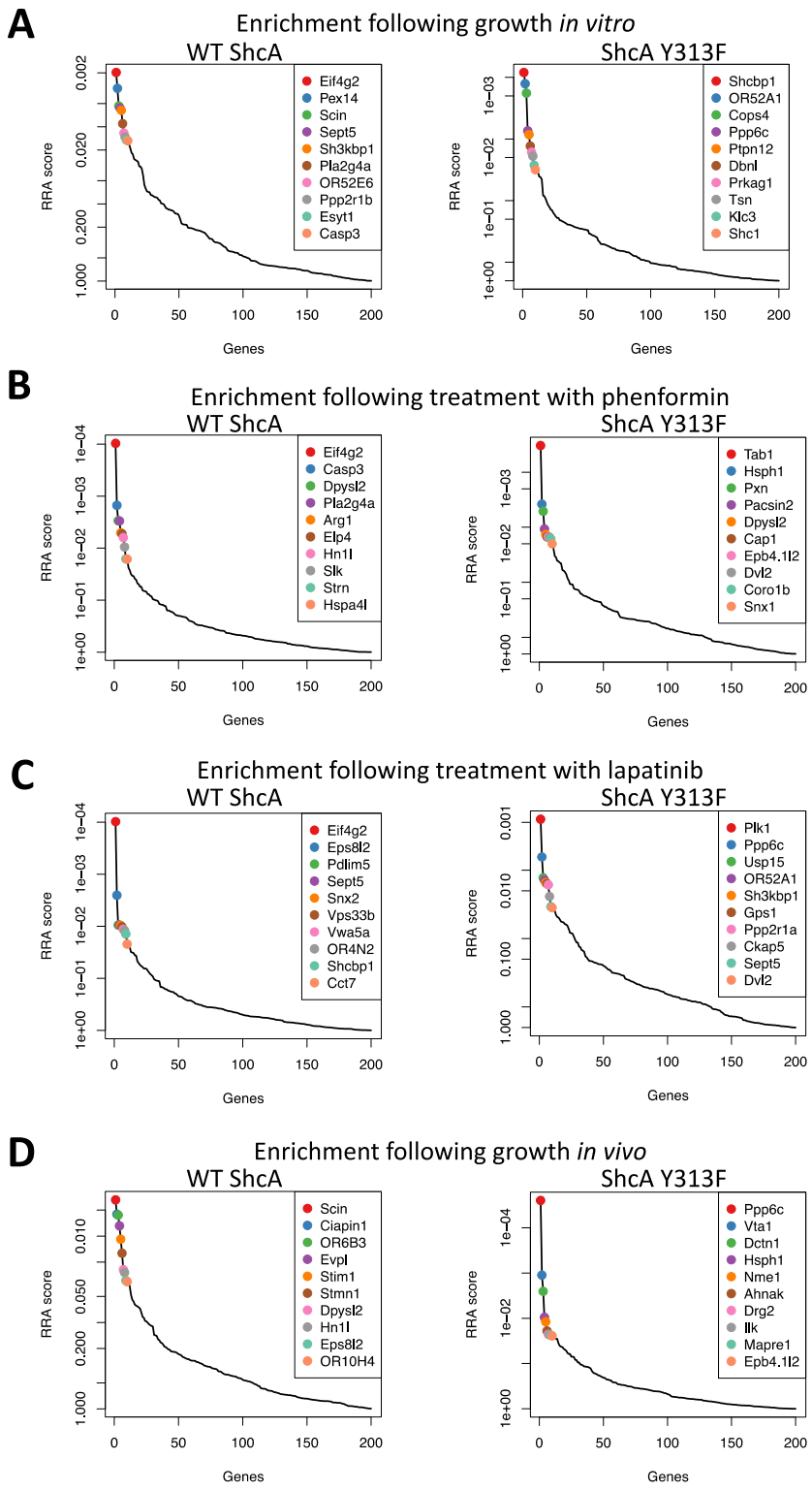

Figure 7. Top 10 gene enrichment in WT ShcA and ShcA Y313F.
Gene enrichment after 14 days of growth in vitro (A), 14 days of growth in vitro with 150μM phenformin for WT ShcA cells and 100μM phenformin for ShcA Y313F cells (B), 14 days of growth in vitro with 100nM lapatinib for WT ShcA cells and 300nM lapatinib for ShcA Y313F (C), and growth *in vivo* (D) following infection with the shRNA library. All figures were created with MAGeCK software.However, there were some interesting patterns revealed when comparing dropout

and enrichment. In the screen, PPP6C shRNA was enriched in mutated ShcA Y313F cells following 14-day growth in vitro, 14-day growth with lapatinib, as well as in vivo tumour growth (Fig. 8B). According to the BioID screen, PPP6C was found to only interact with WT ShcA. eIF4G2 shRNA was enriched in WT ShcA following 14-day growth in vitro, 14-day growth with phenformin treatment, and 14-day growth with lapatinib treatment (Fig. 8A). Conversely, eIF4G2 shRNA was depleted in ShcA Y313F mutant following 14-day phenformin treatment, 14-day lapatinib treatment, and in vivo tumour growth conditions (Fig. 8A). According to BioID, eIF4G2 only bound to WT ShcA.

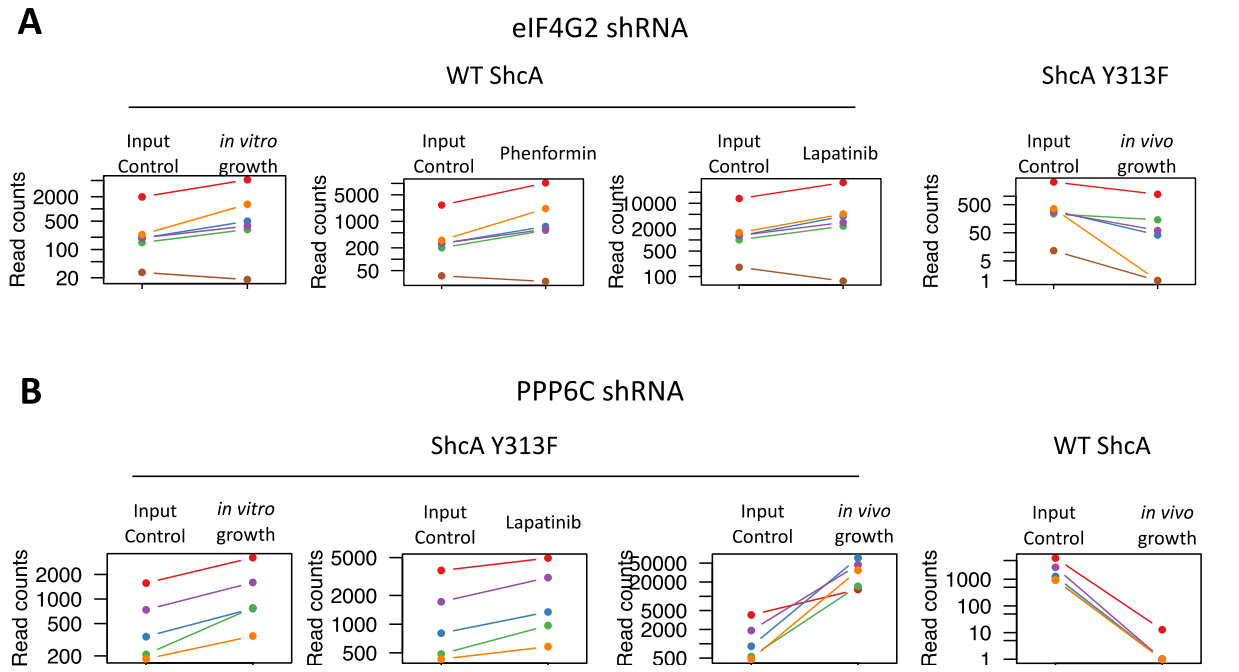

Figure 8. Notable trends following the conclusion of the shRNA screen.
eIF4G2 shows enrichment in numerous WT ShcA conditions, while eIF4G2 drops out in ShcA Y313F. PPP6C is enriched in many ShcA Y313F conditions whereas it drops out in some WT ShcA conditions. A) Individual eIF4G2 shRNA results in WT ShcA *in vitro* growth, WT ShcA with 14 days of treatment with 150μM phenformin, WT ShcA with 14 days of treatment with 100nM lapatinib, and ShcA Y313F *in vivo* growth conditions. B) Individual PPP6C shRNA results after 14 days of growth *in vitro*, 14 days of treatment with 100nM lapatinib in ShcA Y313F mutants, and growth *in vivo* for both cell lines. All figures were created with MAGeCK software.

4.2.1. Phosphatase catalytic subunit PPP6C may interact with ShcA

To examine the relationship between ShcA and PPP6C, five PPP6C shRNAs were purchased from Dr. Huang to perform individual knockdown in wildtype and mutant cell lines. Bacterial shRNA cultures were grown and miniprep DNA extraction was performed. Sample quality was assessed using Take3 to analyze concentration and 260:280 ratio (Fig. 9A). 293T cells were transfected with shRNA and viral media was collected to infect WT ShcA and ShcA Y313F cells. Scramble was used as a vector control to infect both cell lines. Western blot analysis of PPP6C following shRNA knockdown was performed. There appears to be modest knockdown of PPP6C in WT ShcA knockdown cell lines, however it is not clear if knockdown was successful in mutants as ShcA Y313F scramble knockdown had very low PPP6C (Fig. 9B). It is possible that viral media harvested from 293T cells was low in viral content, which would make it difficult to assess potency of each shRNA used. Future experiments are required to validate the efficacy of each shRNA used for PPP6C knockdown. According to the BioID screen previously performed, PPP6C was found in proximity to WT ShcA. Future experiments are required to further examine the relationship between ShcA and PPP6C.

A

shRNA	Concentration (ng/uL)	260:280 Ratio
M3	58.85	1.66
M4	245.5	1.86
M5	203.05	2.005
M6	255.55	1.81
M7	191.95	1.86

B

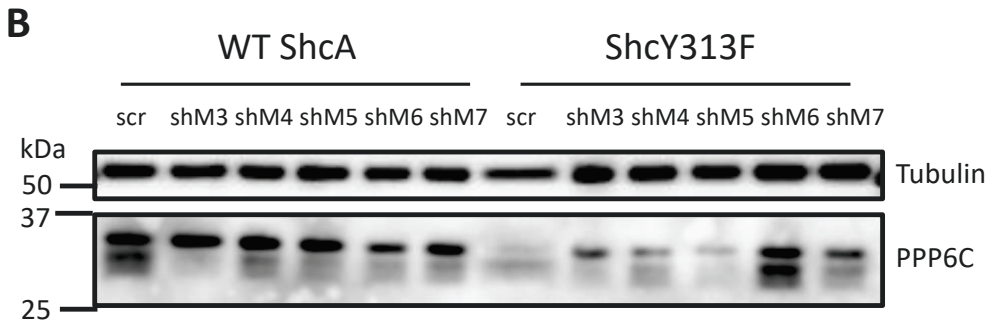

Figure 9. Evaluating the relationship between PPP6C and ShcA through shRNA knockdown in WT ShcA and ShcA Y313F mutant cell lines.
A) Quantification of DNA extracts following bacterial miniprep using the Molecular Biology Kit from BioBasic. Concentration and 260:280 ratio was reported using Take3. B) Evaluation of PPP6C knockdown following individual shRNA infection. Results are currently unclear if knockdown was achieved with the individual shRNAs due to the low levels of PPP6C in ShcA Y313F scramble infected cells.

4.3. Aim 2: Examining the role of ShcA Y313 phosphorylation in response to downstream RTK inhibitors

Due to the ShcA Y313F mutant demonstrating a stunted response to lapatinib during IC30 experiments, we wished to examine if the same trend continued down the signaling cascade by examining the inhibition of various proteins within the RTK pathway including MEK, AKT, and mTOR. The inhibitors chosen were Trametinib, MK-2206, Torin-1, and a novel mTORC1 inhibitor EST-001. To observe how ShcA Y313F mutants respond to various drug treatments compared to their wildtype counterparts, wildtype MT ShcA cells and MT ShcA Y313F mutants

were treated with either phenformin, lapatinib, trametinib, MK-2206, Torin-1, or EST-001. Cells were stained with 0.5% crystal violet, and confluency was quantified using ImageJ. Two-way ANOVA was used to evaluate statistical significance between the cell lines. To confirm the drug effects on cell populations, cell lines were treated with the aforementioned drugs for 24 hours and blotted for their respective downstream targets.

4.3.1. ShcA Y313F mutants display sensitivity to the biguanide phenformin

Wildtype MT ShcA and mutant MT ShcA Y313F cells were treated with 50μM-250μM phenformin or PBS as a vehicle control. Cells were treated for 72 hours, with media and drug treatment being refreshed at 48 hours. After 72 hours, the cells were stained with crystal violet. WT ShcA cells showed modest response to phenformin, with viability being 93.6%, 90.3%, 92.5%, 88.8%, and 78.4% with increased dosing (Fig. 10A). ShcA Y313F mutants demonstrated increased sensitivity to phenformin, with viability being 82.9%, 77.5%, 74.8%, 68.8%, and 62.1% as drug concentration increased. To confirm the drug effects of phenformin, both cell lines were treated with 100μM phenformin or PBS vehicle control for 24 hours and western blot analysis was performed. Lysates were examined for pT172 AMPK and total AMPK to evaluate mitochondrial stress. Experiments were done in parallel with lapatinib treatment, denoted in figure 10B.

According to two-way ANOVA testing, there was no significant difference between cell lines at low doses (50μM and 100μM) of phenformin ($p=0.1484$ and $p=0.0751$, respectively). However, increased doses of phenformin showed significant differences in viability between the cell lines ($p<0.05$) (Fig. 10A). This confirms previous publications which demonstrate that ShcA Y313F mutants have increased sensitivity to the biguanide phenformin (Totten et al., 2021).

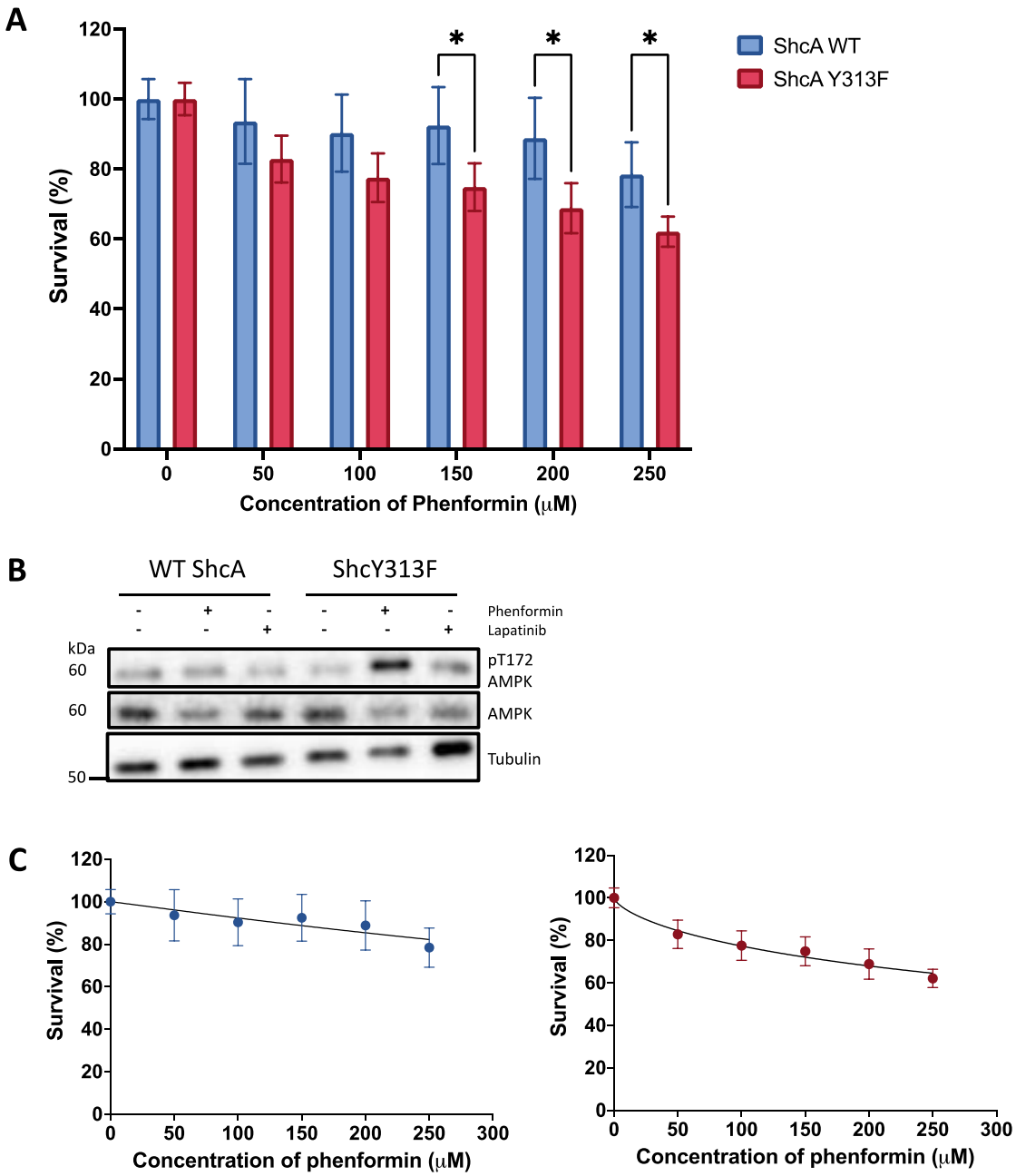

Figure 10. ShcA Y313F mutants show increased sensitivity to the biguanide phenformin.
A) Survival of WT ShcA (blue) and ShcA Y313F (red) following treatment with phenformin or PBS vehicle control for 72 hours. After treatment, cells were fixed and stained with 0.5% crystal violet. Confluency was quantified using ImageJ. Confluency for each repeat was normalized to its respective control condition to show evaluate survival. Three repeats were performed. B) pT172 AMPK and total AMPK protein levels were assessed in WT ShcA and ShcA Y313F mutants following treatment with phenformin or lapatinib for 24 hours. PBS was used as a vehicle control for phenformin and DMSO was used as a vehicle control for lapatinib. Tubulin was used as a loading control. C) Death curves of both WT ShcA (blue) and ShcA Y313F (red) following treatment with phenformin or PBS vehicle control for 72 hours. Statistics performed using two-way ANOVA analysis to compare viability between wildtype and mutant ShcA cells at each dose, *p<0.05.

4.3.2. Tumour cell lines display limited response to tyrosine kinase inhibition

Wildtype MT ShcA and mutant MT ShcA Y313F cells were treated with 100nM-500nM lapatinib or DMSO as a vehicle control. Cells were treated every 48 hours until the 72-hour endpoint, after which they were stained with crystal violet to assess viability. As the concentration of lapatinib increased, viability of WT ShcA decreased from 92.9% to 78.1% (Fig. 11A). Comparatively, ShcA Y313F mutants demonstrated little response to lapatinib. After 72 hours, ShcA Y313F mutants demonstrated 99.4%, 97.2%, 97.4%, 93.5%, and 87.3% viability respectively (Fig. 11A). However, two-way ANOVA only observed significant differences between the two cell lines at 200nM (90.1% & 97.2%, $p<0.01$).

To verify the effects of lapatinib on both cell populations, cells were treated with 100nM lapatinib or DMSO as a vehicle control for 24 hours prior to western blot analysis. To evaluate the drug effects, pS473 AKT, pT202/Y204 ERK 1/2, and total levels of AKT and ERK 1/2 were assessed (Fig. 11B). These experiments were performed in parallel with the phenformin experiments, as seen in figure 10B. While WT ShcA did not seem to indicate decreased pS473 AKT in response to lapatinib, pT202/Y204 ERK 1/2 may appear to decrease. Expected drug effects occur in ShcA Y313F mutants, which may indicate that the concentration of lapatinib used to treat wildtype cells was not enough to elicit a strong response detectable on western blot. Overall, these results indicate that while not statistically significant at most concentrations used in this experiment, ShcA Y313F mutants appear to demonstrate resistance to tyrosine kinase inhibition.

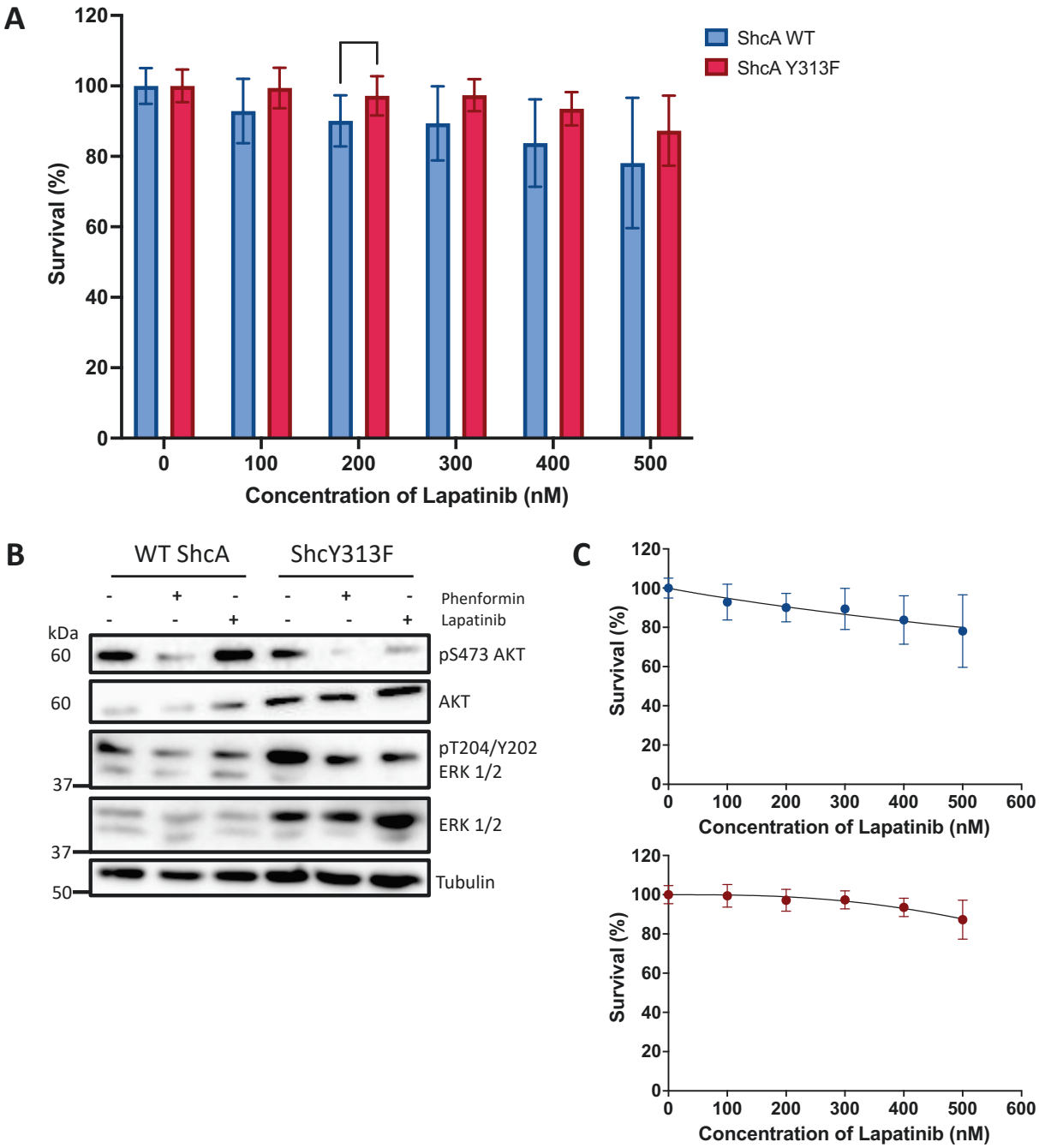

Figure 11. ShcA Y313F mutants show increased sensitivity to the tyrosine kinase inhibitor lapatinib.
A) Survival of WT ShcA (blue) and ShcA Y313F (red) following treatment with lapatinib or DMSO vehicle control for 72 hours. After treatment, cells were fixed and stained with 0.5% crystal violet. Confluency was quantified using ImageJ. Confluency for each repeat was normalized to its respective control condition to show evaluate survival. Three repeats were performed. B) pS473 AKT, pT204/Y202 ERK 1/2, total AKT, and total ERK 1/2 protein levels were assessed in WT ShcA and ShcA Y313F mutants following treatment with phenformin or lapatinib for 24 hours. PBS was used as a vehicle control for phenformin and DMSO was used as a vehicle control for lapatinib. Tubulin was used as a loading control. C) Death curves of both WT ShcA (blue) and ShcA Y313F (red) following treatment with lapatinib or DMSO vehicle control for 72 hours. Statistics performed using two-way ANOVA analysis to compare viability between wildtype and mutant ShcA cells at each dose, **p<0.01.

4.3.3. ShcA Y313F mutants show increased sensitivity to MEK inhibition

Both wildtype MT ShcA and mutant MT ShcA Y313F cells were treated with 5nM-25nM trametinib for 72 hours. DMSO was used as a vehicle control. Media and drug treatment was refreshed at 48 hours. After the 72 hours of treatment, cells were stained with crystal violet to assess viability. At low doses (5nM-15nM), trametinib had minimal effects on WT ShcA viability: 100.3%, 99.5%, and 93.4% respectively (Fig. 12A). 20nM and 25nM trametinib greatly reduced WT ShcA viability to 78.8% and 54.0%. Comparatively, mutants responded well to trametinib, even at the lowest dose. Cell viability decreased from 76.4% to 48.6% in ShcA Y313F mutants (Fig. 12A).

To confirm the drug's effects, both cell lines were treated with 5nM trametinib, 25nM trametinib, or a DMSO vehicle control for 24 hours and western blot analysis was performed to assess pT202/Y204 ERK 1/2 and overall ERK 1/2 levels (Fig. 12B). pT202/Y204 ERK 1/2 levels in wildtype ShcA cells were low, which may be due to the strong signal from ShcA Y313F mutants. Fortunately, the mutant cell line demonstrates that trametinib is working as expected, as increasing concentrations of trametinib decrease phosphorylation of ERK 1/2 (Fig. 12B).

There was a dramatic difference in viability at 5nM to 15nM trametinib ($p<0.0001$). Differences between cell lines decreases at 20nM but is still significant between wildtype and mutant cell lines according to two-way ANOVA testing ($p<0.005$). However, both cell lines responded well to 25nM trametinib, resulting in no significant difference between the cell lines ($p=0.9549$). These findings indicate that ShcA Y313F mutants are sensitive to RTK inhibition downstream of the ERK/MAPK pathway. However, wildtype cells are also sensitive to ERK/MAPK inhibition at a low dose, just not as low as mutants.

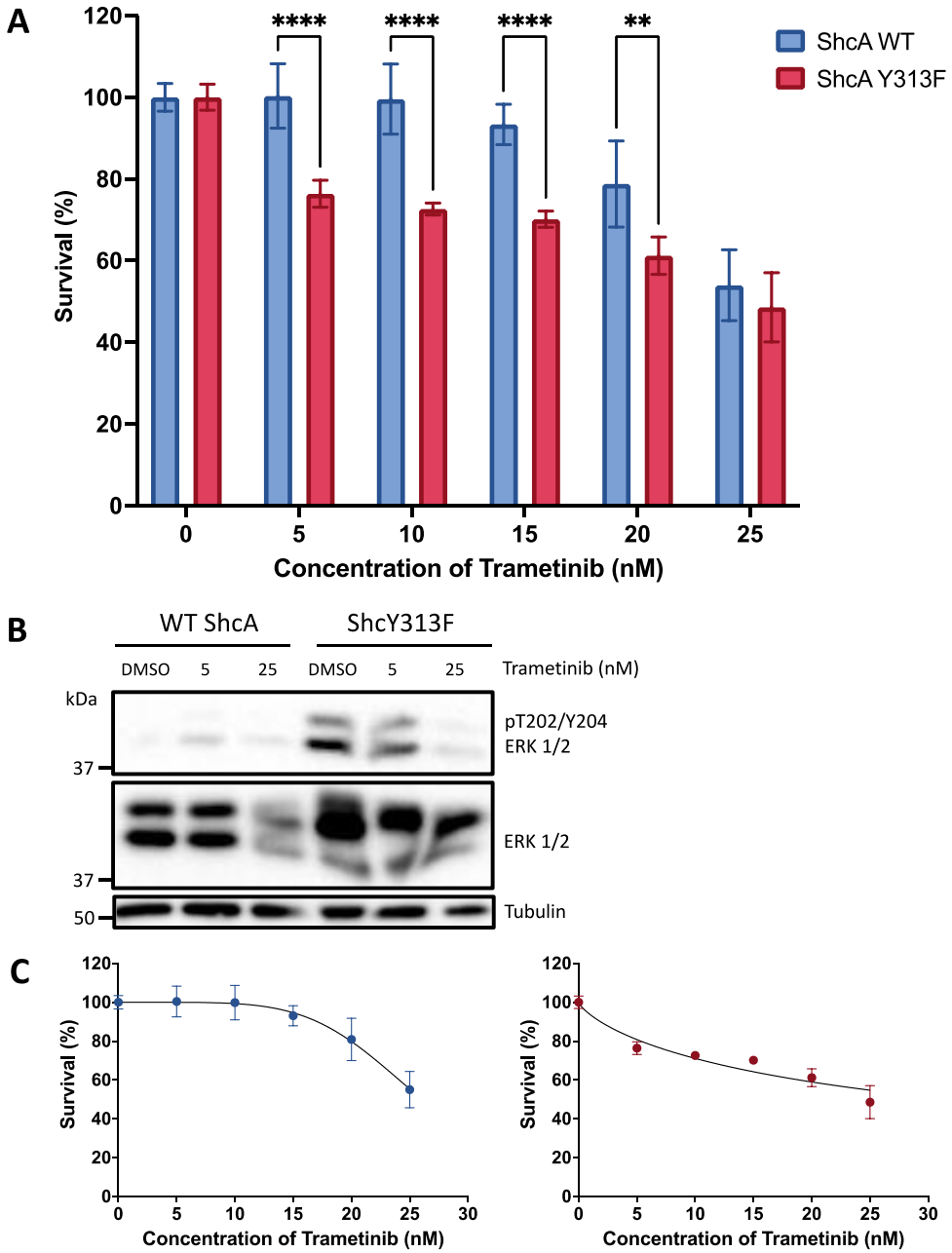

Figure 12. ShcA Y313F mutants show increased sensitivity to the MEK inhibitor trametinib.
A) Survival of WT ShcA (blue) and ShcA Y313F (red) following treatment with trametinib or DMSO vehicle control for 72 hours. After treatment, cells were fixed and stained with 0.5% crystal violet. Confluency was quantified using ImageJ. Confluency for each repeat was normalized to its respective control condition to show evaluate survival. Three repeats were performed. B) pT204/Y202 ERK 1/2 and total ERK 1/2 protein levels were assessed in WT ShcA and ShcA Y313F mutants following treatment with trametinib for 24 hours. DMSO was used as a vehicle control while tubulin was used as a loading control. C) Death curves of both WT ShcA (blue) and ShcA Y313F (red) following treatment with trametinib or DMSO vehicle control for 72 hours. Statistics performed using two-way ANOVA analysis to compare viability between wildtype and mutant ShcA cells at each dose, **p<0.01, ****p<0.0001.*ShcA Y313F mutants are highly sensitive to AKT inhibition*

Wildtype MT ShcA and mutant MT ShcA Y313F cells were treated with the AKT inhibitor MK-2206 at concentrations of 1μM to 3μM for 72 hours. DMSO was used as a vehicle

control. Drug treatments and media were refreshed at 48 hours. After 72 hours, cell viability was assessed using crystal violet. AKT inhibition had minimal impact on wildtype ShcA viability, with the highest dose of MK-2206 resulting in 85.0% viability (Fig. 13A). Comparatively, ShcA Y313F mutants responded incredibly poorly to MK-2206, with viability dropping from 75.1% to 49.4% (Fig. 13A). Two-way ANOVA analysis shows that there was a strong difference between wildtype and mutant ShcA cell lines in response to MK-2206 from 1μM to 2.5μM ($p<0.0001$) (Fig. 13A). Sensitivity to AKT inhibition is still significant between the two cell lines at 3uM, but the statistical significance is lightly less ($p<0.001$).

To confirm the inhibition of AKT, both cell lines were treated with 1μM MK-2206, 3μM MK-2206, or a DMSO vehicle control for 24 hours and western blot analysis was performed to assess pS473 AKT and overall AKT levels (Fig. 13B). As shown, both mutant and wildtype cells demonstrate strong inhibition of AKT, with decreased phosphorylation occurring at the lowest dose of 1uM. Although the loading control shows increased protein concentration in DMSO controls, when compared to total AKT levels, the phosphorylation of S473 is still significantly lower as dosing increases. These findings demonstrate that ShcA Y313F mutants are incredibly sensitive to AKT inhibition, which could be exploited in future research.

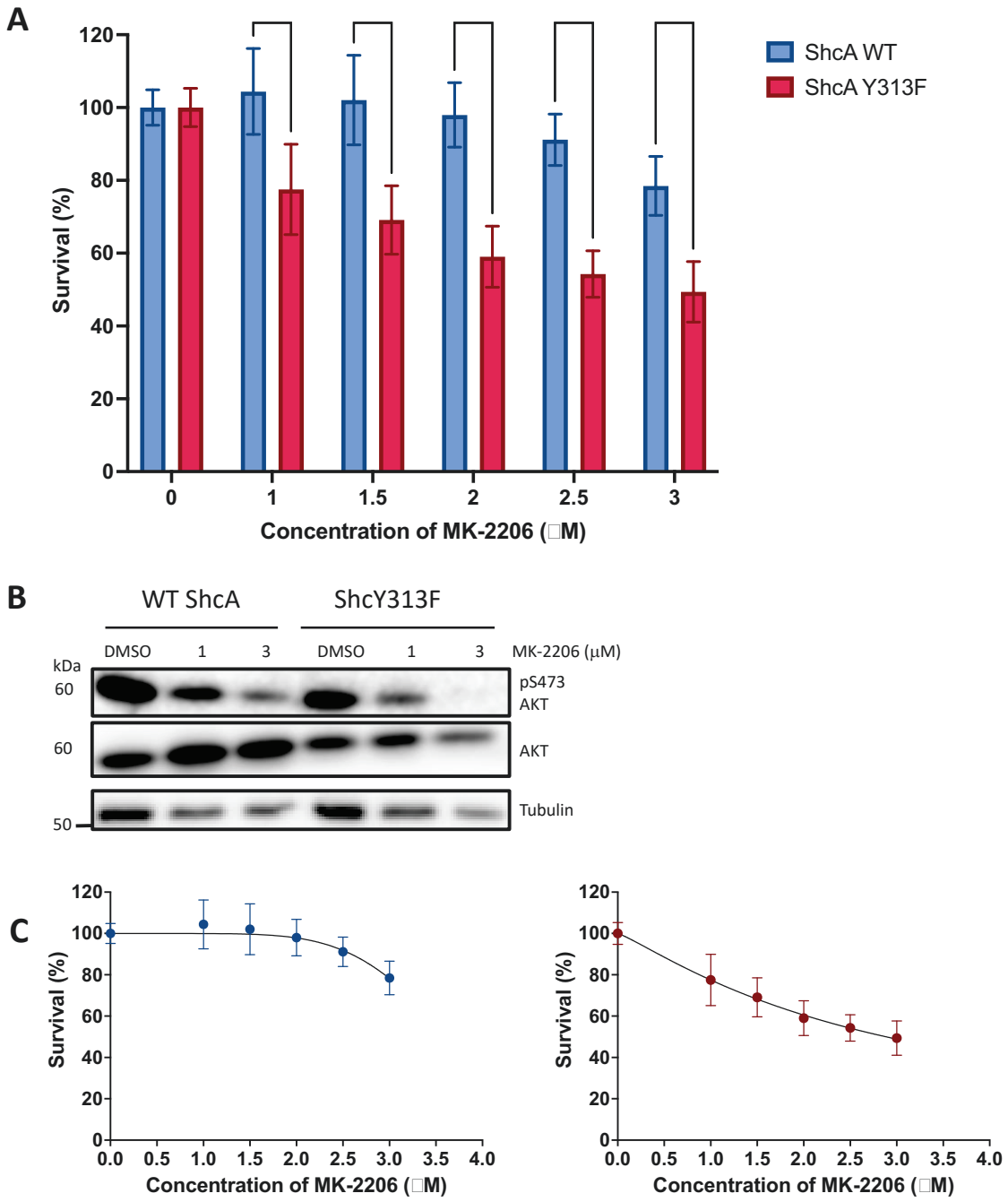

Figure 13. ShcA Y313F mutants show increased sensitivity to the AKT inhibitor MK-2206.
A) Survival of WT ShcA (blue) and ShcA Y313F (red) following treatment with MK-2206 or DMSO vehicle control for 72 hours. After treatment, cells were fixed and stained with 0.5% crystal violet. Confluency was quantified using ImageJ. Confluency for each repeat was normalized to its respective control condition to show evaluate survival. Three repeats were performed. B) pS473 AKT and total AKT protein levels were assessed in WT ShcA and ShcA Y313F mutants following treatment with MK-2206 for 24 hours. DMSO was used as a vehicle control while tubulin was used as a loading control. C) Death curves of both WT ShcA (blue) and ShcA Y313F (red) following treatment with MK-2206 or DMSO vehicle control for 72 hours. Statistics performed using two-way ANOVA analysis to compare viability between wildtype and mutant ShcA cells at each dose, ***p<0.001, ****p<0.0001.

4.3.5. ShcA Y313F mutants are incredibly sensitive to mTOR inhibition

Both wildtype and mutant MT ShcA cells were treated with 50nM-250nM Torin-1, with DMSO serving as a vehicle control. Cells were treated every 48 hours for 7 days, as mTOR inhibition can result in senescence and I wished to observe the effects of Torin-1 on cell viability instead of cell growth rates (Leontieva & Blagosklonny, 2016). After 7 days of treatment, cells were stained with crystal violet to quantify viability. As expected, WT ShcA cell viability dropped steadily as the dose of Torin-1 increased (88.6%, 75.4%, 66.0%, 55.7%, and 48.3% respectively) (Fig. 14A). Surprisingly, ShcA Y313F mutants were incredibly sensitive to Torin-1, with only 26.1% viability at 50nM (Fig. 14A). Two-way ANOVA observed significant differences in response to Torin-1 treatment between the two cell lines ($p<0.001$). Since ShcA Y313F mutants were so sensitive to Torin-1, additional experiments were conducted at lower doses to identify the lowest dose usable before dramatic decreases in viability were observed (Fig. 14B). At this time, only two biological repeats have been conducted, but analysis shows that mutants begin to show increased sensitivity around 30nM.

To verify the effects of Torin-1 on inhibition of mTORC1 and mTORC2, cells were treated 50nM-250nM Torin-1 or DMSO vehicle control for 24 hours prior to western blot analysis. A 0h timepoint was also used as a control. To confirm the inhibition of mTORC1, pT389 S6K, pS240/S244 RS6, pT37/T46 4EBP1total levels of these three proteins were assessed (Fig. 14C). To confirm inhibition of mTORC2, pS473 AKT, and total AKT levels were examined. While pT389 S6K and pS473 AKT were difficult to image in wildtype cells, it may be due to strong signal from the mutants (Fig.14C). Repeated experiments need to be conducted to confirm this, and imaging of these blots may need to be done separately to allow for wildtype signal to appear. Fortunately, pS240/244 RS6 demonstrates that even the lowest dose of Torin-1 used resulted in decreased phosphorylation that was undetectable in both cell lines,

demonstrating its potent inhibitory effects. Overall, these results indicate that ShcA Y313F mutants are incredibly sensitive to dual mTOR inhibition.

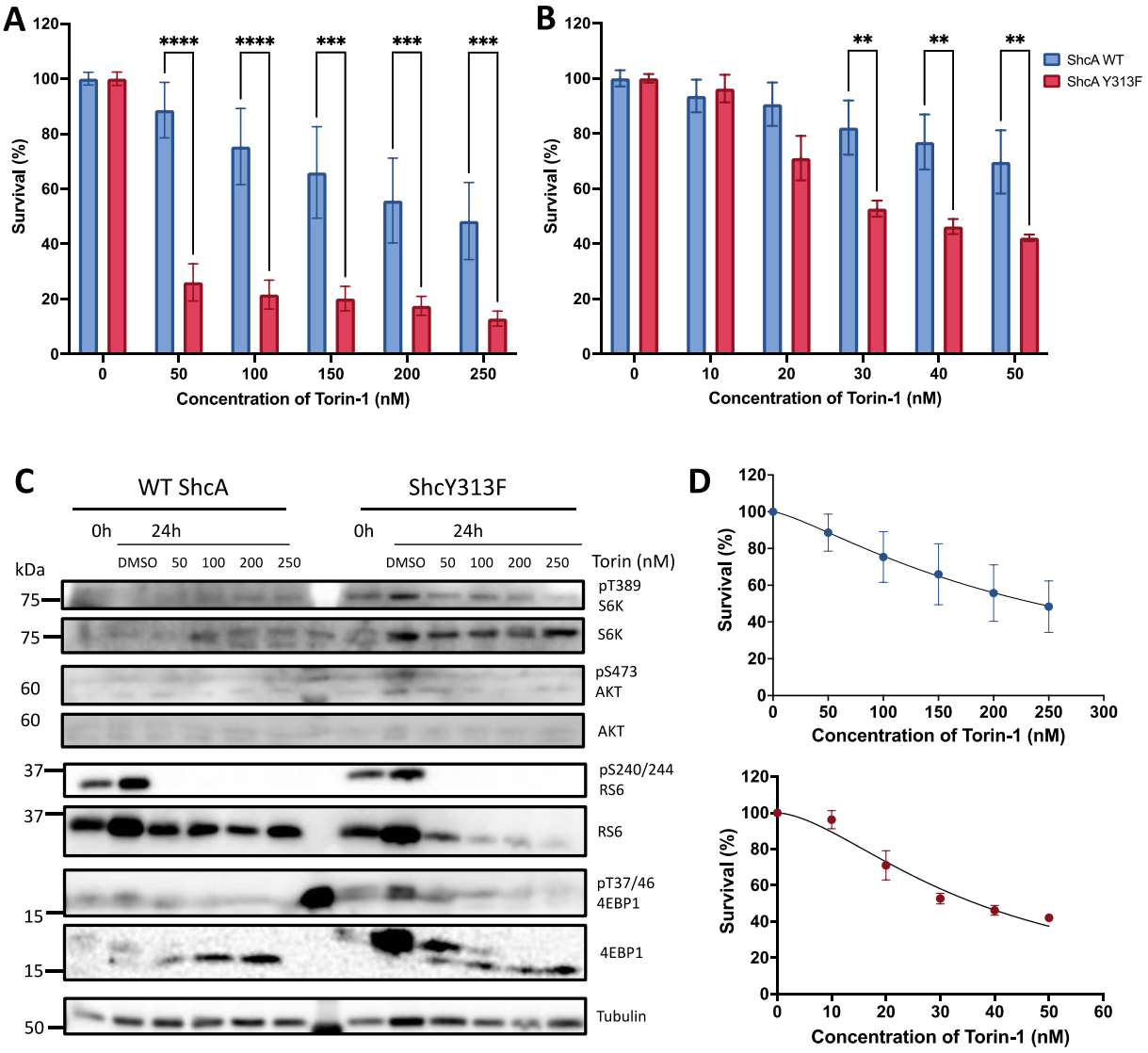

Figure 14. ShcA Y313F mutants show increased sensitivity to the dual-mTOR inhibitor Torin-1.
A) Survival of WT ShcA (blue) and ShcA Y313F (red) following treatment with Torin-1 or DMSO vehicle control for 7 days. After treatment, cells were fixed and stained with 0.5% crystal violet. Confluency was quantified using ImageJ. Confluency for each repeat was normalized to its respective control condition to show evaluate survival. Three repeats were performed. B) Survival of WT ShcA (blue) and ShcA Y313F (red) following treatment with Torin-1 or DMSO vehicle control for 7 days. Two repeats were performed. C) pT389 S6K, pS473 AKT, pS240/244 RS6, pT37/46 4EBP1, total S6K, total AKT, total RS6, and total 4EBP1 protein levels were assessed in WT ShcA and ShcA Y313F mutants following treatment with Torin-1 for 24 hours. DMSO was used as a vehicle control while tubulin served as a loading control. D) Death curves of both WT ShcA (blue) and ShcA Y313F (red) following treatment with Torin-1 or DMSO vehicle control for 7 days. Statistics performed using two-way ANOVA analysis to compare viability between wildtype and mutant ShcA cells at each dose. Statistics performed using two-way ANOVA analysis to compare viability between wildtype and mutant ShcA cells at each dose, **p<0.01, ***p<0.001, ****p<0.0001.

4.3.6. ShcA Y313F mutants show increased sensitivity to mTORC1 inhibition

Both wildtype and mutant MT ShcA cells were treated with 0.5nM-10nM EST-001, with DMSO serving as a vehicle control. Like Torin-1 treated cells, both cell lines were treated for 7 days. Drug treatment and media was refreshed every 48 hours for 7 days, which were subsequently stained with crystal violet to assess viability. Since EST-001 is a relatively new drug synthesized to preferentially inhibit mTORC1 over mTORC2, and almost 80% death was seen in ShcA Y313F cells in response to Torin-1, incredibly low doses were used to compare the two cell lines. WT ShcA cell viability was largely unaffected as the dose of EST-001 increased (99.4%, 99.1%, 97.6%, 97.7%, and 90.0% respectively) (Fig. 15A). Alternatively, ShcA Y313F mutants were sensitive to EST-001, with only viability decreasing from 96.5% to 41.2% (Fig. 15A). Two-way ANOVA testing revealed significant differences in viability between the two cell lines at 5nM ($p<0.05$) and 10nM ($p<0.0001$).

To verify the effects of EST-001 inhibiting mTORC1 and not mTORC2, cells were treated with 0.5nM-10nM EST-001 or DMSO vehicle control for 24 hours prior to western blot analysis. A 0h timepoint was also used as a control. To confirm the inhibition of mTORC1, pT389 S6K, pS240/244 RS6, pT37/46 4EBP1, as well as total levels of these three proteins were assessed (Fig. 15B). To confirm the selectivity of EST-001, mTORC2 activity was used by examining pS473 AKT, and total AKT levels, since mTORC2 phosphorylates AKT at S473 (Miricescu et al., 2020). pS240/244 RS6 decreased steadily as the concentration of EST-001 increased, showing mTORC1 inhibition (Fig. 15B). To confirm there was no inhibition of mTORC2, pS-473 AKT was examined and appears to be relatively steady at all doses of EST-001. Similar to Torin-1, pT-389 S6K was difficult to image in wildtype cells (Fig. 15B). Repeated experiments need to be conducted to confirm the effects of EST-001 on S6K. Overall,

these results indicate that ShcA Y313F mutants are sensitive to not only dual mTOR inhibition, but the mutants are incredibly sensitive to just mTORC1 inhibition.

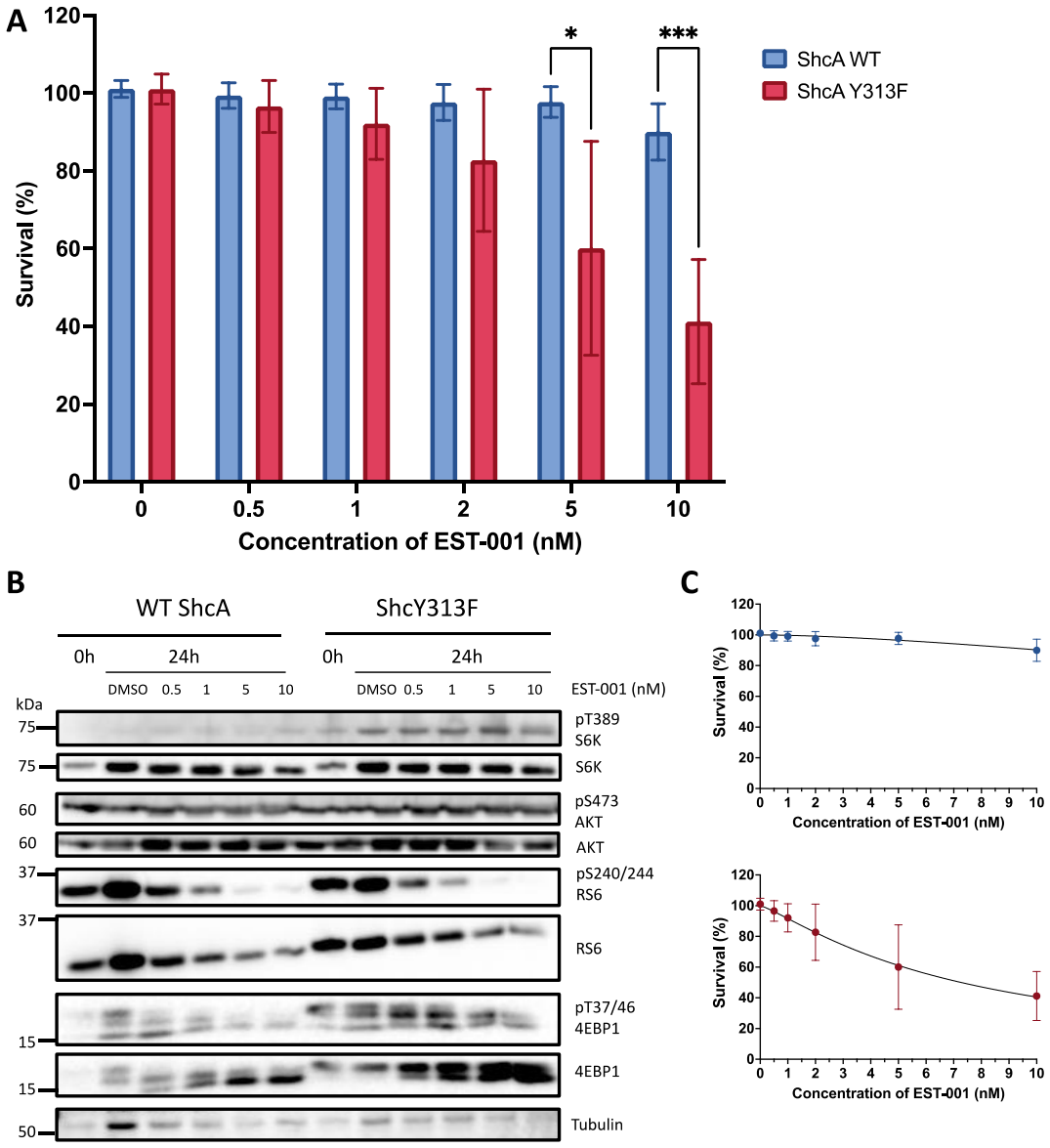

Figure 15. ShcA Y313F mutants show increased sensitivity to the mTORC1 inhibitor EST-001.
A) Survival of WT ShcA (blue) and ShcA Y313F (red) following treatment with EST-001 or DMSO vehicle control for 7 days. After treatment, cells were fixed and stained with 0.5% crystal violet. Confluency was quantified using ImageJ. Confluency for each repeat was normalized to its respective control condition to show evaluate survival. Three repeats were performed. B) pT389 S6K, pS473 AKT, pS240/244 RS6, pT37/46 4EBP1, total S6K, total AKT, total RS6, and total 4EBP1 protein levels were assessed in WT ShcA and ShcA Y313F mutants following treatment with EST-001 for 24 hours. DMSO served as vehicle control while tubulin served as a loading control. C) Death curves of both WT ShcA (blue) and ShcA Y313F (red) following treatment with Torin-1 or DMSO vehicle control for 7 days. Statistics performed using two-way ANOVA analysis to compare viability between wildtype and mutant ShcA cells at each dose. Statistics performed using two-way ANOVA analysis to compare viability between wildtype and mutant ShcA cells at each dose, *p<0.05, ***p<0.001.

Evaluation of drug response in WT ShcA and ShcA Y313F cells reveals numerous differences between the two cell lines. Cells in which ShcA is mutated and unable to be phosphorylated at Y313 demonstrate sensitivity to inhibition of oxidative phosphorylation with the biguanide phenformin. Additionally, mutant cells demonstrate sensitivity to downstream inhibition of the RTK signaling pathway including MEK, AKT, and mTOR. To see if mutants were sensitive to inhibition of one or both mTOR complexes, the recently developed mTORC1 inhibitor EST-001 was used and mutant cells appear to be sensitive to mTORC1 inhibition. Further experiments are required to evaluate wildtype and mutant response in multiple cell lines to validate these findings, however the trends shown above demonstrate therapeutic potential.

5. DISCUSSION

Identification of ShcA interactors using both AP-MS and BioID revealed numerous proteins, however BioID uncovered many potential interactors with ShcA Y313F mutants compared to AP-MS (Table 2). AP-MS identifies protein interactors by pulling down the protein of interest, in this instance WT ShcA or ShcA Y313F, and recovering the protein complexes following whole cell lysis (Gingras et al., 2007). With BioID, proteins in proximity to the protein of interest are biotinylated over a 12-to-24-hour period, after which cells are lysed and the biotinylated proteins are then identified (Roux et al., 2018). Both methods for identifying protein interactions have their strengths and weaknesses. AP-MS can capture high frequency and strong protein interactions, however infrequent or weak protein interactions may be missed due to the short experimental time frame and the buffer used to lyse cells prior to protein pulldown (X. Liu et al., 2020). Alternatively, BioID will biotinylate any proteins found within 10-15nm of the protein of interest and may reveal proteins which do not interact with the bait, but are part of a larger protein complex in which one of the other proteins interacts with the bait (Roux et al., 2018). Therefore, we are left with two methods: one which may miss interactors, and one which may falsely identify interactors. As seen in Table 2, BioID revealed substantially more interactors with ShcA Y313F compared to AP-MS, which suggests that non-phosphorylated ShcA may be interacting with several proteins not previously identified. However, we need to be wary of these findings since BioID may have identified numerous proteins which are part of a complex that interacts with ShcA Y313F but do not interact with ShcA directly.

Since 175 proteins were identified as potential ShcA interactors, we employed a functional shRNA knockdown screen to narrow the list down to those which greatly impact cell

growth and viability in vitro, cell growth and viability in vivo, response to oxidative phosphorylation inhibition, and response to tyrosine kinase inhibition. The screen revealed many proteins essential for survival in multiple conditions including the proteasome 26S subunits PSMD6 and PSMD12, coatomer complex subunits COPB1 and COPB2, molecular chaperone subunit CCT7, and COP9 signalosome complex subunit COPS3 (Fig. 5). Additionally, integrin linked kinase (ILK), histone acetyltransferase complex subunit ELP4, and clathrin interactor CLINT1 were identified as essential for cell survival in WT ShcA tumours (Fig. 5D). Alternatively, decreased Shc-binding protein SHCBP1, collapsin response mediator protein DPYSL2, adaptor protein SH3KBP1, and Septin 5 allowed both cell lines to perform better in many conditions (Fig. 6).

Due to the many proteins identified as significant in the screen, only those which were significant in two or more conditions were considered for further investigation. Of the 41 proteins identified as significant in two or more conditions, two proteins were selected for further analysis: eIF4G2 and PPP6C. eIF4G2 is a homolog of the translation initiating factor eIF4G1, a component of the cap-binding complex which recruits the 43S pre-initiation complex to the 5' cap of mRNA (Smirnova et al., 2022). In acute promyelocytic leukemia (APL) cells, all-*trans*-retinoic acid (ATRA) induces differentiation while arsenic trioxide (ATO) induces apoptosis. Combination treatment has been shown to increase the expression of eIF4G2 while knockdown inhibited differentiation and apoptosis (Ozpolat et al., 2008). Additionally, ATRA-resistant cells were shown to have low expression of eIF4G2, suggesting a link between eIF4G2 expression and treatment response (Ozpolat et al., 2008).

According to BioID, eIF4G2 was found to exclusively interact with WT ShcA (Table 2). In the screen, decreased eIF4G2 was deemed advantageous for WT ShcA in both drug treatment conditions as well as *in vivo* tumour growth (Fig. 7A). A previous study has shown that p53 is a direct target of eIF4G2, and knockdown of eIF4G2 decreased p53 mRNA translation in human lung carcinoma cell lines (Weingarten-Gabbay et al., 2014). Decreased translation of p53 may negatively impact the growth suppressive effects of this tumour suppressor, allowing for tumours to continue to proliferate. Alternatively, eIF4G2 depletion in ShcA Y313F resulted in poor survival following treatment with phenformin (Fig. 7A). These results show a dynamic relationship between eIF4G2 and breast cancer survival, however there are few studies examining this relationship at this time.

PPP6C is a member of the serine/threonine-specific phosphoprotein phosphatase family. This family includes phosphatases crucial for dephosphorylating targets which turn various cellular pathways off or on (Bheri, Mahiwal, Sanyal, & Pandey, 2021). PPP6C is the catalytic subunit of PP6 and is more closely related to PP2Ac and PP4c, making it a PP2A-like phosphatase (Bheri et al., 2021). According to the BioID screen, PPP6C was found to only interact with WT ShcA (Table 2). In the screen, ShcA Y313F cells performed better after PPP6C was knocked down both *in vivo*, *in vitro*, and when cells were treated with lapatinib (Fig. 7B). Conversely, knockdown of PPP6C decreased viability of WT ShcA cells *in vivo* (Fig. 7B).

PPP6C has been shown to be one of the many genes overexpressed in intraductal papillary mucinous neoplasms of the pancreas, and increased PPP6C is correlated with resistance to both chemotherapy and radiation in mesothelioma (Ivanov et al., 2010; Sato et al., 2004). Melanoma cell lines also require PPP6C expression for cell growth and proliferation (Maskin,

Raman, & Houvras, 2022). PPP6C is negatively correlated with melanocyte inducing transcription factor (MITF) and low expression of MITF in melanoma is associated with increased invasion, proliferation, and resistance to MAPK pathway inhibition (Maskin et al., 2022; Müller et al., 2014). DNA-dependent protein kinase is important for mediating double-strand break repair through nonhomologous end joining (Douglas et al., 2010). Work by Douglas et al. has shown that this kinase can interact with this PPP6C, and that silencing of PPP6C increases sensitivity to ionizing radiation in HeLa cells. Additionally, PPP6C-deficient melanocytes with BRAFV600E mutation are less susceptible to UVB-induced tumourigenesis, while melanocytes with semi-deficient PPP6C have increased melanomagenesis (Kanazawa et al., 2021). The combination of BRAFV600E mutation and UVB exposure may increase DNA damage in these cells, and without PPP6C, these cells cannot sufficiently repair the DNA, leading to apoptosis.

Due to time constraints, analysis of ShcA interaction with our hits of interest was only attempted with PPP6C. However, five eIF4G2 shRNA bacterial cultures were purchased, DNA was extracted, and extracts were quantified by Take3. Knockdown of PPP6C using individual shRNAs was attempted in both WT ShcA and ShcA Y313F mutants, however it is difficult to determine if knockdown was successful in both cell lines since mutants infected with scramble control plasmid had incredibly low PPP6C according to western blot analysis (Fig. 8B). Previous research has shown that the p52 isoform of ShcA has a phosphorylation site at Ser29 (Faisal, El-Shemerly, Hess, & Nagamine, 2002). In fact, phosphorylation at Ser29 increases after stimulation with TGF-β (M. K. Lee et al., 2007). In this study they also demonstrate that TGF-β receptors TβRI and TβRII directly phosphorylate ShcA isoform p52 at Ser29, which then

allowed ShcA to interact with Grb2 and SOS. Since PPP6C is the catalytic subunit of the serine/threonine phosphatase PP6, it is possible that PP6 dephosphorylates ShcA.

Since the phosphorylation state of ShcA has been shown to impact tumorigenesis and tumour growth in murine HER2+ breast cancer models, it was hypothesized that mutant ShcA Y313F cells may also respond differently to various therapeutics (Ursini-Siegel et al., 2008). Previous research has shown that HER2+ breast cancers can become resistant to treatment through metabolic reprogramming (Xuhong et al., 2019). Other studies have also shown the ShcA phosphorylation mediates metabolic plasticity in breast cancer cells, allowing them to shift between glycolysis and oxidative phosphorylation when necessary (Im et al., 2018). This flexibility is coordinated by the phosphorylation of Y313, since ShcA Y313F mutants were unable to compensate following the inhibition of mitochondrial complex 1 by phenformin (Totten et al., 2021). WT ShcA and ShcA Y313F mutants were treated with phenformin in this study to demonstrate replicability. As seen in Figure 9A, mutant cells are more sensitive to phenformin as opposed to wildtype ShcA cells. Unfortunately, biguanides alone have not been successful in breast cancer clinical trials, however a phase I clinical trial is currently underway to assess the safety and efficacy of phenformin, trametinib, and BRAF inhibitor triple therapy in metastatic V600E/K-mutated melanoma (Center, Hospital, & University, 2017).

While lapatinib is a standard therapeutic intervention for people with HER2+ breast cancers to counteract the aberrant RTK signaling, many studies have shown that both ER+ and HER2+ breast cancers can acquire resistance to lapatinib and other tyrosine kinase inhibitors (Escrivá-de-Romaní et al., 2018; X. Li et al., 2020; L. Liu et al., 2009; Xuhong et al., 2019). As

seen in Table 1, AP-MS revealed that ShcA Y313F does not interact with Gab1, only WT ShcA, whereas both wildtype and mutant ShcA are found to interact with Grb2. This implies that RTK signaling is reduced in the PI3K/AKT arm in ShcA Y313F mutants. To see if this reduced downstream signaling impacts ShcA Y313F mutant response to tyrosine kinase inhibition, both cell lines were treated with lapatinib for 72 hours. As seen in Figure 10A, the differences between wildtype and mutant ShcA were minimal, however the drug response curve interpolated $IC50_{Lapatinib}$ in WT ShcA cells was around 70.51nM whereas $IC50_{Lapatinib}$ for ShcA Y313F was interpolated to be around 238.7nM. As such, it is possible that ShcA Y313F is somewhat resistant to tyrosine kinase inhibition.

Since ShcA Y313F mutants demonstrated mild resistance to RTK inhibition, we wished to explore if this was true further downstream, or if downstream inhibition could be exploited for therapeutic benefits. Trametinib is a MEK inhibitor already commonly used in combination with BRAF inhibitors to treat melanomas, therefore we wished to examine if this would translate to breast cancer models (Zeiser, Andrlová, & Meiss, 2018). Mutant ShcA cells showed increased sensitivity to MEK inhibition at doses as low as 5nM (Fig. 11A). These findings show that there is potential in treating HER2+ breast cancer with ERK/MAPK inhibitors. However further studies are required to observe if this trend is seen in multiple HER2-overexpressing breast cancer cell lines.

To evaluate the impacts of PI3K/AKT inhibition in a HER2-overexpressing model of breast cancer, the AKT inhibitor MK-2206 was used. Since MK-2206 prevents AKT from localizing to the cell membrane, PI3K cannot phosphorylate AKT, attenuating the signal cascade

(Uko, Güner, Matesic, & Bowen, 2020). Again, mutant ShcA cells showed increased sensitivity to AKT inhibition compared to WT ShcA cells, demonstrating potential for treating HER2+ breast cancers (Fig. 12A). Unfortunately, one clinical trial using MK-2206 as a monotherapy for patients with PIK3CA, AKT, or PTEN-mutated metastatic breast cancer showed no significant effects on tumour burden and was ended early as a result (Xing et al., 2019).

While mutant cells showed sensitivity to AKT inhibition, we also wished to explore if this trend continued further downstream of the PI3K/AKT cascade through the inhibition of both mTOR complexes. While rapamycin is often used to inhibit mTOR, it, along with many other rapalogs, preferentially inhibit mTORC1 over mTORC2 (B. J. Lee et al., 2021; Thoreen et al., 2009). Also, studies have shown that rapamycin doesn't completely inhibit mTORC1, as treatment attenuates downstream S6K activity, but only modestly decreases 4EBP1 activity (B. J. Lee et al., 2021). For these reasons, the bi-specific mTOR inhibitor Torin-1 was chosen to inhibit both mTORC1 and mTORC2. Shockingly, ShcA Y313F mutants were incredibly sensitive to mTOR, with only 26% of cells surviving after treatment with 50nM Torin-1 (Fig. 13A). These findings are encouraging, however further evaluation with multiple breast cancer models and cells lines is required. Within the past decade, clinical trials have been conducted to evaluate the safety and efficacy of various combination therapies targeting multiple proteins within the RTK cascade. One such clinical trial showed that TKI and mTOR inhibitor combination therapy is well tolerated, and can maintain stable disease in patients with TKI-resistant HER2+ metastatic breast cancer (Seiler et al., 2015). While another showed that triple therapy using tyrosine kinase inhibitor, mTOR inhibitor, and chemotherapy is well tolerated in patients with HER2+ breast cancer brain metastases (Hurvitz et al., 2018).

To elucidate whether the sensitivity to mTOR inhibition in mutant cells was a result of mTORC1 inhibition or mTORC2 inhibition, EST-001 was used. Since rapamycin and other rapalogs show inconsistent repression of downstream targets of mTORC1, the third generation mTORC1 inhibitor EST-001 was used, and attenuation of targets downstream from mTORC1 were evaluated with western blot (B. J. Lee et al., 2021). Treatment with EST-001 revealed that ShcA Y313F mutants begin to display noticeable sensitivity at 5nM (Fig. 14A). Evaluation of pS473 AKT reveals stable phosphorylation, indicating that mTORC2 was still capable of phosphorylating AKT (Fig. 14B). pS240/244 RS6 appears to decrease upon treatment, however total levels of RS6 also appear to decrease, making it difficult to confidently interpret. pT389 S6K was difficult to image in WT ShcA cells, however ShcA Y313F cells treated with DMSO vehicle control appear to have slightly elevated S6K phosphorylation compared to cells treated with 10nM EST-001. Reassuringly, EST-001 appears to decrease phosphorylation of 4EBP1, however further experiments are required to confirm these findings. Additional studies are also required to further assess response to EST-001 at higher doses to generate clear response curves in both wildtype and mutant cell lines.

In this thesis, I show that the adaptor protein ShcA has numerous protein interactors that have not been well studied. Interestingly, ShcA Y313F mutants may interact with many proteins, indicating that ShcA may in fact interact with other molecules when it is not fully phosphorylated. With the use of a functional shRNA screen, I show that the phosphorylation of Y313 on ShcA can modulate the interactome, and that this could be the reason for the altered tumour growth and drug response previously seen in ShcA Y313F mutants. With the use of

downstream RTK inhibitors, I also show that ShcA Y313F mutants respond very differently to ERK/MAPK and AKT/mTOR inhibition. These findings suggest that there may be many ShcA interactors which have not been explored yet.

6. CONCLUSION

Breast cancer is the most common cancer diagnosed in Canadian women, and 15-20% of these cases are classified as HER2+ (Bryan et al., 2018; Wolff et al., 2013). Aberrant HER2 receptor tyrosine kinase signaling promotes cell proliferation, tumour invasion, and increases the likelihood of developing metastasis (Barzaman et al., 2020; Marti et al., 2020). Consequently, overexpression of HER2 is correlated with worse clinical outcome. Tumours with high levels of HER2 often have increased amounts of other receptor tyrosine kinases including EGFR and FGFR4 (Pernas & Tolaney, 2020). Although there are many drugs on the market which target HER2+ breast cancer, previous studies have shown that tumours can become resistant to current treatments (Escrivá-de-Romaní et al., 2018; X. Li et al., 2020; L. Liu et al., 2009; Xuhong et al., 2019).

The mechanism by which HER2+ breast cancers develop therapeutic resistance is still unknown, however there are many hypotheses including metabolic reprogramming to overcome stress induced by current treatments, abnormal activation of other RTKs to compensate for the inhibition of HER2, and increased signaling downstream of HER2 (Im et al., 2018; Miricescu et al., 2020; Tomas et al., 2014; Xuhong et al., 2019). The adaptor protein ShcA facilitates the propagation of RTK signaling by acting as a scaffold to recruit Gab1 and Grb2 to active receptor tyrosine kinases for phosphorylation (Tomas et al., 2014). Previous studies have shown that ShcA is upregulated in HER2+ and basal breast cancers and the upregulation of ShcA is correlated with worse clinical outcome (Cheang et al., 2008; Davol et al., 2003).

Adaptor proteins such as ShcA have vast interaction networks, and are difficult to target with therapeutic drugs due in part to their lack of enzymatic domain (Luo & Hahn, 2015). Germline knockout of ShcA is embryonic lethal, and mutation of ShcA at residues Y239/240/317 (Y313 in mice) has rather negative impacts on cells, making it a poor therapeutic target (Mlih et al., 2015; Ravichandran, 2001). Previous research has examined the role of adaptor proteins in cancer; however, many studies have focused on the impacts of phosphorylated adaptor proteins only (Kiepas et al., 2020; Luo & Hahn, 2015). However, protein phosphorylation states are dynamic because of high levels of regulation. By this logic, ShcA must also have dynamic phosphorylation states.

Previous research has shown that mutation of ShcA at Y313 drastically impairs tumour onset and tumour growth in pre-clinical breast cancer models (Ursini-Siegel et al., 2008). Due to these findings, affinity purification mass spectrometry and BioID were used to identify proteins which interact with ShcA both when it can be fully phosphorylated (WT ShcA) and when it cannot (ShcA Y313F). This revealed many proteins which only interact with ShcA when it is not fully phosphorylated. To examine which interactors are most likely contributing to the phenotypes observed, a functional screen was conducted. Upon conclusion of the screen, 41 proteins were shown to have significant impacts in two or more conditions. Of these, the catalytic phosphatase subunit PPP6C and translational protein eIF4G2 were selected for further analysis.

eIF4G2 differs from eIF4G1 in that it does not interact with the 5’ cap-binding protein eIF4E. Therefore, it has been proposed that eIF4G2 mediates cap-independent translation

initiation (Smirnova et al., 2022). Previous research has shown that microRNA-mediated suppression of eIF4G2 slows the development of acute myeloid leukemia, diffuse large B cell lymphoma, and hepatocellular carcinoma (Emmrich et al., 2016; S. Li et al., 2021; Mazan-Mamczarz et al., 2014). Additionally, overexpression of eIF4G2 was able to overcome microRNA-mediated suppression in hepatocellular carcinoma, allowing tumours to thrive (S. Li et al., 2021).

There are conflicting studies regarding PPP6C and cancer. In mesothelioma, PPP6C is associated with both chemotherapy and radiation resistance while repression through microRNA demonstrated anti-tumorigenic effects (Ivanov et al., 2010). Another study showed that PPP6C is one of many genes overexpressed in intraductal papillary mucinous neoplasms of the pancreas (Sato et al., 2004). Additionally, knockdown of PPP6C increased radiation sensitivity in glioblastoma (Shen et al., 2011). Conversely, IHC staining has shown that PPP6C is lower in various breast cancer tumours compared benign breast tumours (Zhong et al., 2011). Another study has shown that knockdown of PPP6C promotes tumour growth in hepatocellular carcinoma, while overexpression induced cell cycle arrest (Wu et al., 2011). Previous research has shown that the p52 isoform of ShcA has a phosphorylation site at Ser29 (Faisal et al., 2002). In fact, phosphorylation at Ser29 increases after stimulation with TGF-β (M. K. Lee et al., 2007). In this study they also demonstrate that TGF-β receptors TβRI and TβRII directly phosphorylate ShcA isoform p52 at Ser29, which then allowed ShcA to interact with Grb2 and Sos. Since PPP6C is the catalytic subunit of the serine/threonine phosphatase PP6, it is possible that PP6 dephosphorylates ShcA.

Additionally, a previous study showed that mutation at ShcA Y313 impairs metabolic flexibility in pre-clinical breast cancer models (Im et al., 2018). Using the mitochondrial complex I inhibitor phenformin, I confirmed a previous study which showed that ShcA Y313F mutants are unable to compensate for the loss of oxidative phosphorylation (Totten et al., 2021). Since AP-MS revealed that ShcA Y313F did not interact with Gab1, it was hypothesized that mutant cells would respond differently to tyrosine kinase inhibitors and other inhibitors downstream of HER2. Interestingly, mutant ShcA cells respond minimally to lapatinib, however they were sensitive to MEK, AKT, mTOR, and mTORC1 inhibition.

While ShcA is not a viable druggable target, it could potentially be used as a biomarker to better aid oncologists in developing treatment plans for patients with HER2+ and HER2-overexpressing breast cancer. As mentioned previously, ShcA Y313F mutants appear to have decreased sensitivity to the HER2 inhibitor lapatinib compared to their wildtype counterparts. Alternatively, these mutants were highly sensitive to downstream inhibition of AKT, mTORC1/2, and mTORC1. Through genetic testing, tumour samples could be identified as carrying the mutant alleles and the patient could be a candidate for combination therapy, while patients with wildtype ShcA tumours would be encouraged to continue with the current standard of care. The use of ShcA as a biomarker could potentially increase the successful treatment of HER2+ and HER2-overexpressing breast cancers.

In the past decade, there have been clinical trials examining the safety and efficacy of mTOR inhibitors in combination with HER2-receptor inhibitors. In one phase IIb clinical trial, the mTOR inhibitor ridaforolimus was given in combination with HER2 inhibitor trastuzumab to

patients with HER2+ trastuzumab-resistant metastatic breast cancer to evaluate the efficacy and safety of combination therapy (Seiler et al., 2015). Of the 34 participants, 41% had stable disease and 21% of patients maintained stable disease for over 24 weeks. Dual therapy was well tolerated shows therapeutic potential for therapy resistant metastatic HER2+ breast cancer. Another phase 1b/2 study showed that triple combination therapy consisting of lapatinib, mTOR inhibitor everolimus, and the chemotherapeutic capecitabine was well tolerated in patients with HER2+ breast cancer brain metastasis (Hurvitz et al., 2018). Of the 19 patients in the trial, 3 had partial response and 7 had stable disease after 12 weeks. These studies reinforce the concept that dual inhibition of the RTK pathway shows therapeutic potential for HER2+ breast cancer.

There have been several clinical trials exploring the safety and efficacy of therapies targeting multiple proteins involved in the RTK signaling cascade. One clinical trial was conducted to determine the best dose of MK-2006 in combination with lapatinib in patients with advanced breast cancer, while another aimed to assess the safety of MK-2206 in combination with paclitaxel chemotherapy (Institute, 2011a, 2011b). A third clinical trial was conducted around the same time to assess the safety of triple therapy consisting of MK-2206, tyrosine kinase inhibitor, and paclitaxel in HER2+ breast cancers (University of California, Sharp, & LLC, 2011). Combination therapy has also been evaluated in many other types of cancer, such as the mTOR and AKT inhibitor dual therapy in patients with advanced prostate cancer, combination MEK and AKT inhibitors for metastatic triple-negative breast cancer, or the triple therapy phenformin, MEK inhibitor, and BRAF inhibitor in patients with melanoma (Center et al., 2017; Institute & GlaxoSmithKline, 2013; Sharp & LLC, 2011).

In conclusion, protein phosphorylation does not necessarily work like a light switch turning pathways off and on. Adaptor proteins such as ShcA have vast interactomes which may interact with a subset of targets when phosphorylated and a different subset of targets when not. To only observe and analyze phosphorylated protein interactions may hide important interactions contributing to cell growth, proliferation, and drug response. Protein phosphorylation may show only a small fraction of these interactions, as seen with ShcA. Since phosphorylation is a highly dynamic post-translational modification, it is important to consider the possibility that proteins may interact with when in an unphosphorylated or partially phosphorylated state.

REFERENCES

Alfaidi, M., Scott, M. L., & Orr, A. W. (2021). Sinner or Saint?: Nck Adaptor Proteins in Vascular Biology. *Front Cell Dev Biol, 9*, 688388. doi:10.3389/fcell.2021.688388

Barok, M., Joensuu, H., & Isola, J. (2014). Trastuzumab emtansine: mechanisms of action and drug resistance. *Breast Cancer Research, 16*(2), 209. doi:10.1186/bcr3621

Barzaman, K., Karami, J., Zarei, Z., Hosseinzadeh, A., Kazemi, M. H., Moradi-Kalbolandi, S., . . . Farahmand, L. (2020). Breast cancer: Biology, biomarkers, and treatments. *International Immunopharmacology, 84*, 106535. doi:https://doi.org/10.1016/j.intimp.2020.106535

Batzer, A. G., Rotin, D., Ureña, J. M., Skolnik, E. Y., & Schlessinger, J. (1994). Hierarchy of binding sites for Grb2 and Shc on the epidermal growth factor receptor. *Mol Cell Biol, 14*(8), 5192-5201. doi:10.1128/mcb.14.8.5192-5201.1994

Belov, A. A., & Mohammadi, M. (2012). Grb2, a double-edged sword of receptor tyrosine kinase signaling. *Sci Signal, 5*(249), pe49. doi:10.1126/scisignal.2003576

Bheri, M., Mahiwal, S., Sanyal, S. K., & Pandey, G. K. (2021). Plant protein phosphatases: What do we know about their mechanism of action? *Febs j, 288*(3), 756-785. doi:10.1111/febs.15454

Bryan, S., Masoud, H., Weir, H. K., Woods, R., Lockwood, G., Smith, L., . . . Badets, N. (2018). Cancer in Canada: Stage at diagnosis. *Health Rep, 29*(12), 21-25.

Butti, R., Das, S., Gunasekaran, V. P., Yadav, A. S., Kumar, D., & Kundu, G. C. (2018). Receptor tyrosine kinases (RTKs) in breast cancer: signaling, therapeutic implications and challenges. *Mol Cancer, 17*(1), 34. doi:10.1186/s12943-018-0797-x

Center, M. S. K. C., Hospital, M. G., & University, W. M. C. o. C. (2017). Clinical Trial of Phenformin in Combination With BRAF Inhibitor + MEK Inhibitor for Patients With BRAF-mutated Melanoma. In: https://ClinicalTrials.gov/show/NCT03026517.

Chardin, P., Camonis, J. H., Gale, N. W., van Aelst, L., Schlessinger, J., Wigler, M. H., & Bar-Sagi, D. (1993). Human Sos1: a guanine nucleotide exchange factor for Ras that binds to GRB2. *Science, 260*(5112), 1338-1343. doi:10.1126/science.8493579

Cheang, M. C. U., Voduc, D., Bajdik, C., Leung, S., McKinney, S., Chia, S. K., . . . Nielsen, T. O. (2008). Basal-like breast cancer defined by five biomarkers has superior prognostic value than triple-negative phenotype. *Clinical cancer research : an official journal of the American Association for Cancer Research, 14*(5), 1368-1376. doi:10.1158/1078-0432.ccr-07-1658

Chun, K. H., Park, J. H., & Fan, S. (2017). Predicting and Overcoming Chemotherapeutic Resistance in Breast Cancer. *Adv Exp Med Biol, 1026*, 59-104. doi:10.1007/978-981-10-6020-5_4

Creixell, P., Schoof, E. M., Tan, C. S., & Linding, R. (2012). Mutational properties of amino acid residues: implications for evolvability of phosphorylatable residues. *Philos Trans R Soc Lond B Biol Sci, 367*(1602), 2584-2593. doi:10.1098/rstb.2012.0076

Dankort, D., Jeyabalan, N., Jones, N., Dumont, D. J., & Muller, W. J. (2001). Multiple ErbB-2/Neu Phosphorylation Sites Mediate Transformation through Distinct Effector Proteins *. *Journal of Biological Chemistry, 276*(42), 38921-38928. doi:10.1074/jbc.M106239200

Davol, P. A., Bagdasaryan, R., Elfenbein, G. J., Maizel, A. L., & Frackelton, A. R., Jr. (2003). Shc proteins are strong, independent prognostic markers for both node-negative and node-positive primary breast cancer. *Cancer Res, 63*(20), 6772-6783.

Diggins, N. L., & Webb, D. J. (2017). APPL1 is a multifunctional endosomal signaling adaptor protein. *Biochem Soc Trans, 45*(3), 771-779. doi:10.1042/bst20160191
Douglas, P., Zhong, J., Ye, R., Moorhead, G. B. G., Xu, X., & Lees-Miller, S. P. (2010). Protein Phosphatase 6 Interacts with the DNA-Dependent Protein Kinase Catalytic Subunit and Dephosphorylates γ-H2AX. *Molecular and Cellular Biology, 30*(6), 1368-1381. doi:doi:10.1128/MCB.00741-09
Emmrich, S., Engeland, F., El-Khatib, M., Henke, K., Obulkasim, A., Schöning, J., . . . Klusmann, J. H. (2016). miR-139-5p controls translation in myeloid leukemia through EIF4G2. *Oncogene, 35*(14), 1822-1831. doi:10.1038/onc.2015.247
Escrivá-de-Romaní, S., Arumí, M., Bellet, M., & Saura, C. (2018). HER2-positive breast cancer: Current and new therapeutic strategies. *Breast, 39*, 80-88. doi:10.1016/j.breast.2018.03.006
Faisal, A., El-Shemerly, M., Hess, D., & Nagamine, Y. (2002). Serine/Threonine Phosphorylation of ShcA: REGULATION OF PROTEIN-TYROSINE PHOSPHATASE-PEST BINDING AND INVOLVEMENT IN INSULIN SIGNALING *. *Journal of Biological Chemistry, 277*(33), 30144-30152. doi:10.1074/jbc.M203229200
Gajria, D., & Chandarlapaty, S. (2011). HER2-amplified breast cancer: mechanisms of trastuzumab resistance and novel targeted therapies. *Expert Rev Anticancer Ther, 11*(2), 263-275. doi:10.1586/era.10.226
Gandhi, N., & Das, G. M. (2019). Metabolic Reprogramming in Breast Cancer and Its Therapeutic Implications. *Cells, 8*(2). doi:10.3390/cells8020089
Gingras, A. C., Gstaiger, M., Raught, B., & Aebersold, R. (2007). Analysis of protein complexes using mass spectrometry. *Nat Rev Mol Cell Biol, 8*(8), 645-654. doi:10.1038/nrm2208
Goldhirsch, A., Wood, W. C., Coates, A. S., Gelber, R. D., Thürlimann, B., & Senn, H. J. (2011). Strategies for subtypes--dealing with the diversity of breast cancer: highlights of the St. Gallen International Expert Consensus on the Primary Therapy of Early Breast Cancer 2011. *Ann Oncol, 22*(8), 1736-1747. doi:10.1093/annonc/mdr304
Gomes do Nascimento, R. M. O., K. (2020). Histological and molecular classification of breast cancer: what do we know? *Mastology, 30*, 137-144. doi:http://doi.org/10.29289/25945394202020200024
Gotoh, N. (2008). Regulation of growth factor signaling by FRS2 family docking/scaffold adaptor proteins. *Cancer Science, 99*(7), 1319-1325. doi:https://doi.org/10.1111/j.1349-7006.2008.00840.x
Granados-Riveron, J. T., & Aquino-Jarquin, G. (2018). CRISPR–Cas13 Precision Transcriptome Engineering in Cancer. *Cancer Research, 78*(15), 4107-4113. doi:10.1158/0008-5472.Can-18-0785
Grissenberger, S., Sturtzel, C., Wenninger-Weinzierl, A., Radic-Sarikas, B., Scheuringer, E., Bierbaumer, L., . . . Distel, M. (2022). High-content drug screening in zebrafish xenografts reveals high efficacy of dual MCL-1/BCL-X(L) inhibition against Ewing sarcoma. *Cancer Lett*, 216028. doi:10.1016/j.canlet.2022.216028
Guy, C. T., Cardiff, R. D., & Muller, W. J. (1992). Induction of mammary tumors by expression of polyomavirus middle T oncogene: a transgenic mouse model for metastatic disease. *Mol Cell Biol, 12*(3), 954-961. doi:10.1128/mcb.12.3.954-961.1992
Ha, J. R., Ahn, R., Smith, H. W., Sabourin, V., Hébert, S., Cepeda Cañedo, E., . . . Ursini-Siegel, J. (2018). Integration of Distinct ShcA Signaling Complexes Promotes Breast Tumor

Growth and Tyrosine Kinase Inhibitor Resistance. *Molecular Cancer Research, 16*(5), 894-908. doi:10.1158/1541-7786.Mcr-17-0623
Hsu, J. L., & Hung, M. C. (2016). The role of HER2, EGFR, and other receptor tyrosine kinases in breast cancer. *Cancer Metastasis Rev, 35*(4), 575-588. doi:10.1007/s10555-016-9649-6
Hurvitz, S., Singh, R., Adams, B., Taguchi, J. A., Chan, D., Dichmann, R. A., . . . Slamon, D. J. (2018). Phase Ib/II single-arm trial evaluating the combination of everolimus, lapatinib and capecitabine for the treatment of HER2-positive breast cancer with brain metastases (TRIO-US B-09). *Ther Adv Med Oncol, 10*, 1758835918807339. doi:10.1177/1758835918807339
Im, Y. K., Najyb, O., Gravel, S.-P., McGuirk, S., Ahn, R., Avizonis, D. Z., . . . Ursini-Siegel, J. (2018). Interplay between ShcA Signaling and PGC-1α Triggers Targetable Metabolic Vulnerabilities in Breast Cancer. *Cancer Research, 78*(17), 4826-4838. doi:10.1158/0008-5472.can-17-3696
Institute, N. C. (2010). Akt Inhibitor MK2206 in Combination With Lapatinib Ditosylate in Patients With Advanced or Metastatic Solid Tumors or Breast Cancer. In: https://ClinicalTrials.gov/show/NCT01245205.
Institute, N. C. (2011a). Akt Inhibitor MK2206 in Treating Patients With Advanced Breast Cancer. In: https://ClinicalTrials.gov/show/NCT01277757.
Institute, N. C. (2011b). MK2206 and Paclitaxel in Treating Patients With Locally Advanced or Metastatic Solid Tumors or Metastatic Breast Cancer. In: https://ClinicalTrials.gov/show/NCT01263145.
Institute, N. C., & GlaxoSmithKline. (2013). Trametinib and Akt Inhibitor GSK2141795 in Treating Patients With Metastatic Triple-Negative Breast Cancer. In: https://ClinicalTrials.gov/show/NCT01964924.
Ishino, Y., Krupovic, M., & Forterre, P. (2018). History of CRISPR-Cas from Encounter with a Mysterious Repeated Sequence to Genome Editing Technology. *J Bacteriol, 200*(7). doi:10.1128/jb.00580-17
Ivanov, S. V., Goparaju, C. M. V., Lopez, P., Zavadil, J., Toren-Haritan, G., Rosenwald, S., . . . Pass, H. I. (2010). Pro-tumorigenic Effects of miR-31 Loss in Mesothelioma *. *Journal of Biological Chemistry, 285*(30), 22809-22817. doi:10.1074/jbc.M110.100354
Jaber Chehayeb, R., & Boggon, T. J. (2020). SH2 Domain Binding: Diverse FLVRs of Partnership. *Frontiers in Endocrinology, 11*. doi:10.3389/fendo.2020.575220
Kanazawa, K., Kishimoto, K., Nomura, M., Kurosawa, K., Kato, H., Inoue, Y., . . . Shima, H. (2021). Ppp6c haploinsufficiency accelerates UV-induced BRAF(V600E)-initiated melanomagenesis. *Cancer Sci, 112*(6), 2233-2244. doi:10.1111/cas.14895
Kiepas, A., Voorand, E., Senecal, J., Ahn, R., Annis, M. G., Jacquet, K., . . . Brown, C. M. (2020). The SHCA adapter protein cooperates with lipoma-preferred partner in the regulation of adhesion dynamics and invadopodia formation. *J Biol Chem, 295*(31), 10535-10559. doi:10.1074/jbc.RA119.011903
Lam, J. K. W., Chow, M. Y. T., Zhang, Y., & Leung, S. W. S. (2015). siRNA Versus miRNA as Therapeutics for Gene Silencing. *Molecular Therapy - Nucleic Acids, 4*. doi:10.1038/mtna.2015.23
Lee, B. J., Boyer, J. A., Burnett, G. L., Thottumkara, A. P., Tibrewal, N., Wilson, S. L., . . . Rosen, N. (2021). Selective inhibitors of mTORC1 activate 4EBP1 and suppress tumor growth. *Nat Chem Biol, 17*(10), 1065-1074. doi:10.1038/s41589-021-00813-7

Lee, M. K., Pardoux, C., Hall, M. C., Lee, P. S., Warburton, D., Qing, J., . . . Derynck, R. (2007). TGF-beta activates Erk MAP kinase signalling through direct phosphorylation of ShcA. *Embo j, 26*(17), 3957-3967. doi:10.1038/sj.emboj.7601818

Leontieva, O. V., & Blagosklonny, M. V. (2016). Gerosuppression by pan-mTOR inhibitors. *Aging (Albany NY), 8*(12), 3535-3551. doi:10.18632/aging.101155

Li, S., Shao, J., Lou, G., Wu, C., Liu, Y., & Zheng, M. (2021). MiR-144-3p-mediated dysregulation of EIF4G2 contributes to the development of hepatocellular carcinoma through the ERK pathway. *Journal of Experimental & Clinical Cancer Research, 40*(1), 53. doi:10.1186/s13046-021-01853-6

Li, W., Xu, H., Xiao, T., Cong, L., Love, M. I., Zhang, F., . . . Liu, X. S. (2014). MAGeCK enables robust identification of essential genes from genome-scale CRISPR/Cas9 knockout screens. *Genome Biology, 15*(12), 554. doi:10.1186/s13059-014-0554-4

Li, X., Zhang, K., Hu, Y., & Luo, N. (2020). ERRα activates SHMT2 transcription to enhance the resistance of breast cancer to lapatinib via modulating the mitochondrial metabolic adaption. *Biosci Rep, 40*(1). doi:10.1042/bsr20192465

Liu, L., Greger, J., Shi, H., Liu, Y., Greshock, J., Annan, R., . . . Gilmer, T. M. (2009). Novel mechanism of lapatinib resistance in HER2-positive breast tumor cells: activation of AXL. *Cancer Res, 69*(17), 6871-6878. doi:10.1158/0008-5472.Can-08-4490

Liu, X., Salokas, K., Weldatsadik, R. G., Gawriyski, L., & Varjosalo, M. (2020). Combined proximity labeling and affinity purification−mass spectrometry workflow for mapping and visualizing protein interaction networks. *Nature Protocols, 15*(10), 3182-3211. doi:10.1038/s41596-020-0365-x

Luo, L. Y., & Hahn, W. C. (2015). Oncogenic Signaling Adaptor Proteins. *J Genet Genomics, 42*(10), 521-529. doi:10.1016/j.jgg.2015.09.001

Marti, J. L. G., Hyder, T., Nasrazadani, A., & Brufsky, A. M. (2020). The Evolving Landscape of HER2-Directed Breast Cancer Therapy. *Current Treatment Options in Oncology, 21*(10), 82. doi:10.1007/s11864-020-00780-6

Maskin, C. R., Raman, R., & Houvras, Y. (2022). PPP6C, a serine-threonine phosphatase, regulates melanocyte differentiation and contributes to melanoma tumorigenesis through modulation of MITF activity. *Sci Rep, 12*(1), 5573. doi:10.1038/s41598-022-08936-0

Mattoon, D. R., Lamothe, B., Lax, I., & Schlessinger, J. (2004). The docking protein Gab1 is the primary mediator of EGF-stimulated activation of the PI-3K/Akt cell survival pathway. *BMC Biol, 2*, 24. doi:10.1186/1741-7007-2-24

Mazan-Mamczarz, K., Zhao, X. F., Dai, B., Steinhardt, J. J., Peroutka, R. J., Berk, K. L., . . . Gartenhaus, R. B. (2014). Down-Regulation of eIF4GII by miR-520c-3p Represses Diffuse Large B Cell Lymphoma Development. *PLOS Genetics, 10*(1), e1004105. doi:10.1371/journal.pgen.1004105

Merenbakh-Lamin, K., Ben-Baruch, N., Yeheskel, A., Dvir, A., Soussan-Gutman, L., Jeselsohn, R., . . . Wolf, I. (2013). D538G Mutation in Estrogen Receptor-α: A Novel Mechanism for Acquired Endocrine Resistance in Breast Cancer. *Cancer Research, 73*(23), 6856-6864. doi:10.1158/0008-5472.Can-13-1197

Mir, H. A., Ali, R., Mushtaq, U., & Khanday, F. A. (2020). Structure-functional implications of longevity protein p66Shc in health and disease. *Ageing Research Reviews, 63*, 101139. doi:https://doi.org/10.1016/j.arr.2020.101139

Miricescu, D., Totan, A., Stanescu, S., II, Badoiu, S. C., Stefani, C., & Greabu, M. (2020). PI3K/AKT/mTOR Signaling Pathway in Breast Cancer: From Molecular Landscape to Clinical Aspects. *Int J Mol Sci, 22*(1). doi:10.3390/ijms22010173

Mittal, S., Brown, N. J., & Holen, I. (2018). The breast tumor microenvironment: role in cancer development, progression and response to therapy. *Expert Review of Molecular Diagnostics, 18*(3), 227-243. doi:10.1080/14737159.2018.1439382

Mlih, M., Host, L., Martin, S., Niederhoffer, N., Monassier, L., Terrand, J., . . . Matz, R. L. (2015). The Src homology and collagen A (ShcA) adaptor protein is required for the spatial organization of the costamere/Z-disk network during heart development. *J Biol Chem, 290*(4), 2419-2430. doi:10.1074/jbc.M114.597377

Moffat, J. G., Rudolph, J., & Bailey, D. (2014). Phenotypic screening in cancer drug discovery — past, present and future. *Nature Reviews Drug Discovery, 13*(8), 588-602. doi:10.1038/nrd4366

Molendijk, J., Blazev, R., Mills, R. J., Ng, Y. K., Watt, K. I., Chau, D., . . . Parker, B. L. (2022). Proteome-wide systems genetics identifies UFMylation as a regulator of skeletal muscle function. *Elife, 11*. doi:10.7554/eLife.82951

Morales-Ramírez, P., Vallarino-Kelly, T., & Cruz-Vallejo, V. (2014). Kinetics of micronucleus induction and cytotoxicity caused by distinct antineoplastics and alkylating agents in vivo. *Toxicol Lett, 224*(3), 319-325. doi:10.1016/j.toxlet.2013.11.012

Müller, J., Krijgsman, O., Tsoi, J., Robert, L., Hugo, W., Song, C., . . . Peeper, D. S. (2014). Low MITF/AXL ratio predicts early resistance to multiple targeted drugs in melanoma. *Nat Commun, 5*, 5712. doi:10.1038/ncomms6712

Northey, J. J., Chmielecki, J., Ngan, E., Russo, C., Annis, M. G., Muller, W. J., & Siegel, P. M. (2008). Signaling through ShcA is required for transforming growth factor beta- and Neu/ErbB-2-induced breast cancer cell motility and invasion. *Mol Cell Biol, 28*(10), 3162-3176. doi:10.1128/mcb.01734-07

Ozpolat, B., Akar, U., Zorrilla-Calancha, I., Vivas-Mejia, P., Acevedo-Alvarez, M., & Lopez-Berestein, G. (2008). Death-associated protein 5 (DAP5/p97/NAT1) contributes to retinoic acid-induced granulocytic differentiation and arsenic trioxide-induced apoptosis in acute promyelocytic leukemia. *Apoptosis, 13*(7), 915-928. doi:10.1007/s10495-008-0222-9

Pernas, S., & Tolaney, S. M. (2020). Targeting HER2 heterogeneity in early-stage breast cancer. *Current Opinion in Oncology, 32*(6). Retrieved from https://journals.lww.com/co-oncology/Fulltext/2020/11000/Targeting_HER2_heterogeneity_in_early_stage_breast.2.aspx

Pickar-Oliver, A., & Gersbach, C. A. (2019). The next generation of CRISPR-Cas technologies and applications. *Nat Rev Mol Cell Biol, 20*(8), 490-507. doi:10.1038/s41580-019-0131-5

Ravichandran, K. S. (2001). Signaling via Shc family adapter proteins. *Oncogene, 20*(44), 6322-6330. doi:10.1038/sj.onc.1204776

Regad, T. (2015). Targeting RTK Signaling Pathways in Cancer. *Cancers (Basel), 7*(3), 1758-1784. doi:10.3390/cancers7030860

Rocca, A., Braga, L., Volpe, M. C., Maiocchi, S., & Generali, D. (2022). The Predictive and Prognostic Role of RAS-RAF-MEK-ERK Pathway Alterations in Breast Cancer: Revision of the Literature and Comparison with the Analysis of Cancer Genomic Datasets. *Cancers (Basel), 14*(21). doi:10.3390/cancers14215306

Roux, K. J., Kim, D. I., Burke, B., & May, D. G. (2018). BioID: A Screen for Protein-Protein Interactions. *Curr Protoc Protein Sci, 91*, 19.23.11-19.23.15. doi:10.1002/cpps.51

Sain, N., Tiwari, G., & Mohanty, D. (2016). Understanding the molecular basis of substrate binding specificity of PTB domains. *Scientific Reports, 6*(1), 31418. doi:10.1038/srep31418

Sato, N., Fukushima, N., Maitra, A., Iacobuzio-Donahue, C. A., van Heek, N. T., Cameron, J. L., . . . Goggins, M. (2004). Gene Expression Profiling Identifies Genes Associated with Invasive Intraductal Papillary Mucinous Neoplasms of the Pancreas. *The American Journal of Pathology, 164*(3), 903-914. doi:10.1016/S0002-9440(10)63178-1

Seiler, M., Ray-Coquard, I., Melichar, B., Yardley, D. A., Wang, R. X., Dodion, P. F., & Lee, M. A. (2015). Oral Ridaforolimus Plus Trastuzumab for Patients With HER2⁺ Trastuzumab-Refractory Metastatic Breast Cancer. *Clinical Breast Cancer, 15*(1), 60-65. doi:10.1016/j.clbc.2014.07.008

Sharp, M., & LLC, D. (2011). Safety and Tolerability of Different Dose Combinations of Ridaforolimus With MK-2206 or MK-0752 for Participants With Advanced Cancer (MK-8669-049). In: https://ClinicalTrials.gov/show/NCT01295632.

Shen, Y., Wang, Y., Sheng, K., Fei, X., Guo, Q., Larner, J., . . . Mi, J. (2011). Serine/threonine protein phosphatase 6 modulates the radiation sensitivity of glioblastoma. *Cell Death & Disease, 2*(12), e241-e241. doi:10.1038/cddis.2011.126

Sheng, P., Flood, K. A., & Xie, M. (2020). Short Hairpin RNAs for Strand-Specific Small Interfering RNA Production. *Frontiers in Bioengineering and Biotechnology, 8*. doi:10.3389/fbioe.2020.00940

Smirnova, V. V., Shestakova, E. D., Nogina, D. S., Mishchenko, P. A., Prikazchikova, T. A., Zatsepin, T. S., . . . Terenin, I. M. (2022). Ribosomal leaky scanning through a translated uORF requires eIF4G2. *Nucleic Acids Res, 50*(2), 1111-1127. doi:10.1093/nar/gkab1286

Sørlie, T., Perou, C. M., Tibshirani, R., Aas, T., Geisler, S., Johnsen, H., . . . Børresen-Dale, A. L. (2001). Gene expression patterns of breast carcinomas distinguish tumor subclasses with clinical implications. *Proc Natl Acad Sci U S A, 98*(19), 10869-10874. doi:10.1073/pnas.191367098

Thoreen, C. C., Kang, S. A., Chang, J. W., Liu, Q., Zhang, J., Gao, Y., . . . Gray, N. S. (2009). An ATP-competitive mammalian target of rapamycin inhibitor reveals rapamycin-resistant functions of mTORC1. *J Biol Chem, 284*(12), 8023-8032. doi:10.1074/jbc.M900301200

Tomas, A., Futter, C. E., & Eden, E. R. (2014). EGF receptor trafficking: consequences for signaling and cancer. *Trends Cell Biol, 24*(1), 26-34. doi:10.1016/j.tcb.2013.11.002

Totten, S. P., Im, Y. K., Cepeda Cañedo, E., Najyb, O., Nguyen, A., Hébert, S., . . . Ursini-Siegel, J. (2021). STAT1 potentiates oxidative stress revealing a targetable vulnerability that increases phenformin efficacy in breast cancer. *Nat Commun, 12*(1), 3299. doi:10.1038/s41467-021-23396-2

Tsang, J. Y. S., & Tse, G. M. (2020). Molecular Classification of Breast Cancer. *Advances in Anatomic Pathology, 27*(1), 27-35. doi:10.1097/pap.0000000000000232

Uko, N. E., Güner, O. F., Matesic, D. F., & Bowen, J. P. (2020). Akt Pathway Inhibitors. *Curr Top Med Chem, 20*(10), 883-900. doi:10.2174/1568026620666200224101808

Ullah, R., Yin, Q., Snell, A. H., & Wan, L. (2022). RAF-MEK-ERK pathway in cancer evolution and treatment. *Seminars in Cancer Biology, 85*, 123-154. doi:https://doi.org/10.1016/j.semcancer.2021.05.010

University of California, S. F., Sharp, M., & LLC, D. (2011). MK-2206, Paclitaxel and Trastuzumab in Treating Patients With HER2-overexpressing Solid Tumor Malignancies. In: https://ClinicalTrials.gov/show/NCT01235897.

Ursini-Siegel, J., Hardy, W. R., Zuo, D., Lam, S. H., Sanguin-Gendreau, V., Cardiff, R. D., . . . Muller, W. J. (2008). ShcA signalling is essential for tumour progression in mouse models of human breast cancer. *Embo j, 27*(6), 910-920. doi:10.1038/emboj.2008.22

Wang, Z. (2017). ErbB Receptors and Cancer. *Methods Mol Biol, 1652*, 3-35. doi:10.1007/978-1-4939-7219-7_1

Weinberg, F., Peckys, D. B., & de Jonge, N. (2020). EGFR Expression in HER2-Driven Breast Cancer Cells. *Int J Mol Sci, 21*(23). doi:10.3390/ijms21239008

Weingarten-Gabbay, S., Khan, D., Liberman, N., Yoffe, Y., Bialik, S., Das, S., . . . Kimchi, A. (2014). The translation initiation factor DAP5 promotes IRES-driven translation of p53 mRNA. *Oncogene, 33*(5), 611-618. doi:10.1038/onc.2012.626

Wolff, A. C., Hammond, M. E. H., Hicks, D. G., Dowsett, M., McShane, L. M., Allison, K. H., . . . Hayes, D. F. (2013). Recommendations for Human Epidermal Growth Factor Receptor 2 Testing in Breast Cancer: American Society of Clinical Oncology/College of American Pathologists Clinical Practice Guideline Update. *Journal of Clinical Oncology, 31*(31), 3997-4013. doi:10.1200/jco.2013.50.9984

Wright, K. D., Miller, B. S., El-Meanawy, S., Tsaih, S. W., Banerjee, A., Geurts, A. M., . . . Sorokin, A. (2019). The p52 isoform of SHC1 is a key driver of breast cancer initiation. *Breast Cancer Res, 21*(1), 74. doi:10.1186/s13058-019-1155-7

Wu, N., Liu, X., Xu, X., Fan, X., Liu, M., Li, X., . . . Tang, H. (2011). MicroRNA-373, a new regulator of protein phosphatase 6, functions as an oncogene in hepatocellular carcinoma. *The FEBS Journal, 278*(12), 2044-2054. doi:https://doi.org/10.1111/j.1742-4658.2011.08120.x

Xing, Y., Lin, N. U., Maurer, M. A., Chen, H., Mahvash, A., Sahin, A., . . . Meric-Bernstam, F. (2019). Phase II trial of AKT inhibitor MK-2206 in patients with advanced breast cancer who have tumors with PIK3CA or AKT mutations, and/or PTEN loss/PTEN mutation. *Breast Cancer Res, 21*(1), 78. doi:10.1186/s13058-019-1154-8

Xuhong, J. C., Qi, X. W., Zhang, Y., & Jiang, J. (2019). Mechanism, safety and efficacy of three tyrosine kinase inhibitors lapatinib, neratinib and pyrotinib in HER2-positive breast cancer. *Am J Cancer Res, 9*(10), 2103-2119.

Zeiser, R., Andrlová, H., & Meiss, F. (2018). Trametinib (GSK1120212). *Recent Results Cancer Res, 211*, 91-100. doi:10.1007/978-3-319-91442-8_7

Zhang, Y. (2021). The root cause of drug resistance in HER2-positive breast cancer and the therapeutic approaches to overcoming the resistance. *Pharmacol Ther, 218*, 107677. doi:10.1016/j.pharmthera.2020.107677

Zhong, J., Liao, J., Liu, X., Wang, P., Liu, J., Hou, W., . . . Xu, X. (2011). Protein phosphatase PP6 is required for homology-directed repair of DNA double-strand breaks. *Cell Cycle, 10*(9), 1411-1419. doi:10.4161/cc.10.9.15479

COPYRIGHT